NTNU – Trondheim
Norwegian University of
Science and Technology

Development of Rare Earth Metal Iron Oxides as Mixed Ionic and Electronic Conductors

Christine Blom

Chemical Engineering and Biotechnology
Submission date: June 2014
Supervisor: Sverre Magnus Selbach, IMTE
Co-supervisor: Tor Grande, IMTE
Sandra Helen Skjærvø, IMTE

Norwegian University of Science and Technology
Department of Materials Science and Engineering

Problem description

$LuFe_2O_4$ has recently been reported to have a high oxygen storage ability at relatively low temperatures, and is therefore considered as a potential material for use in oxygen permeable membranes. This work seeks to find a new, safer and more convenient powder preparation route for this material, and rare earth RFe_2O_4 materials in general. Both solid state and sol-gel synthesis routes will be explored. The oxygen storage ability will be investigated by TGA, and the structural changes upon heat treatment in different atmospheres examined by XRD and Rietveld refinement. Conductivity and dilatometry measurements will be carried out to study the conductivity and sintering ability of the materials, as well as preliminary studies into the possibility of preparing an oxygen permeable membrane.

Preface

The studies presented in this master thesis have been conducted at the Department of Materials Science and Engineering at the Norwegian University of Science and Technology, NTNU, during spring 2014.

My main supervisor has been Associate Professor Sverre M. Selbach, and my co-supervisors, PhD Candidate Sandra H. Skjærvø and Professor Tor Grande.

The work presented has been performed by the author, except from the dilatometry measurement presented in Figure 4.13, which was performed by Senior Engineer Eli Beate Larsen.

Trondheim, June 16, 2014

Christine Blom

Christine Blom

Acknowledgment

First of all I have to thank my main supervisor Sverre M. Selbach. His enthusiasm for this field of study and the work I have done has been an inspiration ever since I started on my project last fall. His guidance and comments to my work have been of great help, and the small breaks discussing soccer, Strømsgodset and PolyCrystal Palace have given me the chance to process some of the hundreds of ideas that have been planted in my head during our meetings.
I would also like to thank my co-supervisor Sandra H. Skjærvø for her response and questions provided both on my presentations and on my thesis, and for being the type of person that is always willing to help and provide others with encouraging comments.
I am grateful to my co-supervisor Professor Tor Grande for valuable comments on my work and his broad knowledge both in materials science and thermodynamics.
I am also very grateful to the technical staff of the Ceramics group, especially Julian Tolchard, Pei Na Kui and Eli Beate Larsen who have helped me with many practical manners. Especially Jools deserves acknowledgment for his great help with Rietveld refinement.
I also have to thank Ove Paulsen for attributing with his long experience and providing me with insight into the stability of iron oxides under CO_2/CO pressures.
I would also like to thank Tobias Elve for great help with Latex, and for being who you are.
Finally I have to thank my family for believing in me and encouraging me in what I do, and especially my father and grandfather for passing on their interest in chemistry to me. I am also very grateful to my father, Hans Blom, for reading through my thesis and attributing with valuable comments to my work.

Abstract

In recent years there has been an increasing interest in finding a new and less energy demanding alternative to cryogenic distillation in the production of pure oxygen gas. The use of oxygen permeable membranes has been considered a preferable alternative, and extensive studies into candidate materials for use in these membranes, performed. Problems concerning cationic demixing and breakdown of the material structure has been reported for many of these materials were oxygen is transported through oxygen vacancies, usually requiring an operating temperature above 800°C. Lately, an increasing interest in materials that can transport oxygen through oxygen interstitials instead of vacancies has emerged, since oxygen interstitials can be transported at temperatures below 600°C where cationic diffusion is usually prevented. A study of the oxygen storage ability of rare earth ferrites has recently been reported, where an oxygen storage ability of an x=0.5, and a good cycling ability has been found for $LuFe_2O_{4+x}$. A problem with the use of rare earth ferrites for this purpose is that the powder preparation route involves metallic iron as one of the precursors, requiring the use of a glove box in the preparation of the material. In this study, phase pure powder of another rare earth ferrite, $YbFe_2O_4$, has been performed from a conventional solid state synthesis route. Strong indications of the possibility of obtaining the material from a sol-gel synthesis route is also reported. Heat treatment of the material in oxygen atmosphere resulting in an oxygen rich phase, $YbFe_2O_{4.5}$, was quantified from in situ TGA measurements, while an ex. situ heat treatment performed under oxidizing and reducing conditions strongly indicates a good cycling ability of the material. The increase in the oxygen content during heat treatment in oxygen atmosphere took place below 500°C, and is therefore expected to originate from oxygen interstitials being implemented in the structure. A significant change in structure is also observed after heat treatment in oxygen atmosphere, emphasizing this theory. Indications of a p-type conductivity from van der Pauw measurements are also reported. The new and more convenient powder preparation route, significantly increases the potential of rare earth ferrites for use in oxygen permeable membranes, and a further investigation into their reported multiferroic properties. A replacement of Lu with Yb in the material significantly decreases the material cost, and therefore the use of these materials in up-scale production.

Sammendrag

I de senere år har det blitt økende interesse for å finne et nytt og mindre energikrevende alternativ til kryogenisk destillasjon i produksjonen av ren oksygengass. Bruken av oksygenpermeable membraner har vært betraktet som et foretrukket alternativ, og en omfattende undersøkelse av kandidatmaterialer som kan anvendes i slike membraner, har blitt utført. Problemer forbundet med nedbrytning av materialstrukturen som følge av akkumulering av kationer på den oksygenrike og oksygenfattige delen av membranen har blitt rapportert for mange av disse materialene når oksygen transporteres ved hjelp av oksygenvakanser. Denne vakans-diffusjonen krever vanligvis en driftstemperatur på over 800°C. I det siste har det blitt en økende interesse for materialer som kan transportere oksygen ved hjelp av interstitielt oksygen istedenfor vakanser, ettersom interstitielt oksygen kan transporteres ved temperaturer under 600°C, der kationdiffusjon vanligvis er forhindret. En undersøkelse av de oksygenlagrende egenskapene til sjeldne jordartsferitter har nylig blitt rapportert, hvor en oksygenlagrende evne tilsvarende x = 0,5 for $LuFe_2O_{4+x}$, og en god syklingsevne er oppdaget. Et problem ved bruk av sjeldne jordartsferritter til dette formålet er at pulverframstillingen innebærer bruk av metallisk jern som en av forløperne, og krever bruk av en hanskeboks ved framstillingen av materialet. I dette studiet, er faserent pulver av en annen type sjeldent jordartsferitt, $YbFe_2O_4$ framstilt fra en konvensjonell faststoffsyntese. Sterke indikasjoner på at materialet kan framstilles fra en sol-gel synthese er også rapportert. Varmebehandling av det framstilte materialet i oksygenatmosfære resulterte i en oksygenrik fase, $YbFe_2O_{4,5}$, kvantifisert ved bruk av in situ TGA-målinger, mens ex. situ varmebehandling under oksiderende og reduserende betingelser indikerte en god syklingsevne for materialet. Økningen i oksygeninnholdet observert under varmebehandlingen i oksygenatmosfæren fant sted under 500°C, og forventes derfor å skyldes at interstitielt oksygen blir implementert i strukturen. Indikasjoner påp-type ledningsevne er ogsåfunnet ved hjelp av van der Pauw ledningsevnemłinger. Den nye, og mer fordelaktige pulversyntesen, øker i betydelig grad potensialet for sjeldne jordartsferritter for bruk i oksygenpermeable membraner, og en nærmere undersøkelse av deres rapporterte multiferroiske egenskaper. Utskiftningen av Lu med Yb i materialet reduserer materialkostnaden betydelig, og øker mulighetene for bruk av disse materialene i oksygenpermeable membraner.

Contents

1 Introduction

1.1 Background

With coal and natural gas still being the worlds main source of energy, the demand for new technologies that can accommodate the challenges associated with the high CO_2 emissions, is crucial, and production of pure oxygen gas is a vital step in reducing CO_2 emission to an acceptably low level [1]. Pure oxygen gas can be used in many chemical process operations in order to reduce the amount of CO_2 that is either emitted to the atmosphere or that needs to be sequestrated. Chemical process operations that uses oxygen as a feedstock is therefore one of the main reasons for the increasing demand for oxygen production that is expected in upcoming years [2]. One example is the use of oxygen gas as feed in oxyfuel combustion processes [2], as indicated in Figure 1.1(a). By the use of pure oxygen instead of air in the inlet gas, the flue gas produced will contain mainly CO_2 and water. These can be separated, and the volume of CO_2 that needs to be sequestrated will be smaller than if air was used in the feed. Another example is the use of pure oxygen gas in the production of syn gas by partial oxidation of methane. Syn gas is an important intermediate gas in the production of hydrogen gas and the conversion of methane into methanol [3]. Pure oxygen gas is also important in other well established industrial processes as for example steel and glass production, waste water treatment and in the production of pharmaceuticals, as indicated in Figure 1.1(b).

Most of the oxygen production today is performed by cryogenic distillation which is an energy-intensive process [2]. It is therefore desirable to develop a new alternative for use in up-scale oxygen production, requiring a lower energy input and lower cost. [4]. Oxygen permeable membranes are a promising alternative to cryogenic distillation considering production of pure oxygen gas both in terms of cost and up-scale production [5].

Two classes of materials that have been thoroughly investigated for use in oxygen perme-

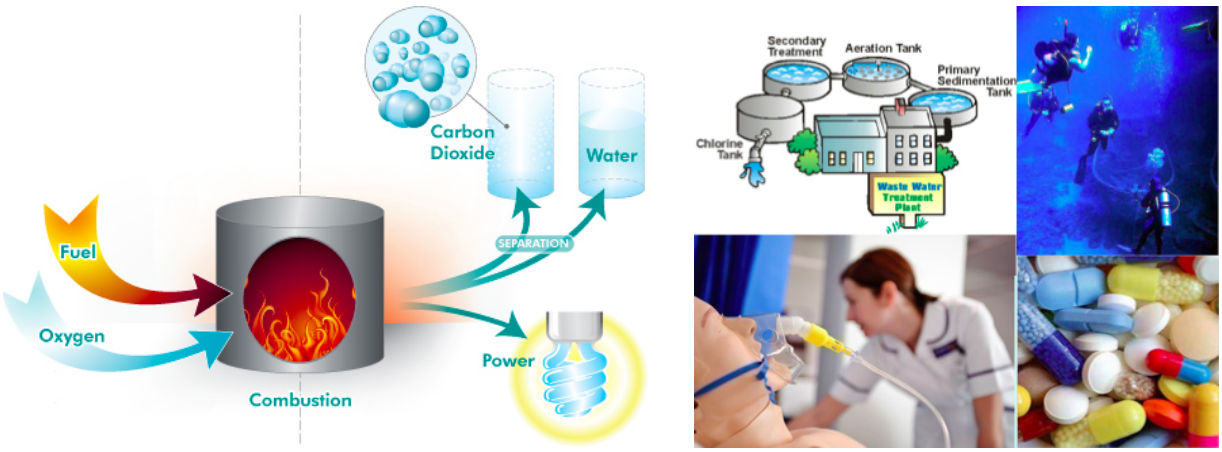

(a) (b)

Figure 1.1: Different areas where pure oxygen is needed. (a) In oxyfuel combustion processes where the use of pure oxygen gas in the feed is an important step in reducing CO_2-emissions[1] and (b) In waste water treatment[2], by scuba divers[3], in medicine[4] and in the production of pharmaceuticals[5]

able membranes are the perovskites ($ABO_{3-\delta}$ and $A_2BO_{4\pm\delta}$) and the fluorites ($A_\delta B_{1-\delta}O_{2-\delta}$ and $A_{2\delta}B_{2-2\delta}O_3$) [6]. Although these materials show many promising features, the high operating temperature leads to problems concerning energy consumption and long term durability of the membranes. One of the reasons for this is that oxygen transport through the membranes is caused mainly by oxygen vacancies. Transport through oxygen vacancies requires an operating temperature of 800 – 900°C. This leads to a high energy demand, and for the process to be energetically favorable in terms of energy penalties, an operating temperature below 700°C is required [6]. The high operating temperature can also result in thermal expansion, as well as cationic demixing, and thereby a reduced durability of the membrane [7], [8].

One possibility to accommodate these problems, is to use materials that can transport oxygen at a lower temperature through oxygen interstitials instead of vacancies. Transport by oxygen interstitials can occur below 600°C, and a decrease in the operating temperature can therefore

[1] http://www.oresomeresources.com/media_centre_view/resource/image_oxyfiring_combustion/category/coal_low_emission/section/media/parent/ (February 2014)
[2] http://cqwastewatertreatment.com.au/how-it-works/ (February 2014)
[3] http://en.wikipedia.org/wiki/File:Scuba-diving.jpg (February 2014)
[4] http://www.usesof.net/uses-of-oxygen.html (February 2014)
[5] http://dmaarson.com/images/pic/4.jpg (February 2014)

be obtained. Below 600°C, cationic diffusion is usually prevented, and the long term durability of these membranes may therefore be increased. Recent publications indicate an increasing interest in this field of research [9], [10], [11], [12]. Remsen et al. [9] and Abughayada et al.[10] have found that $Dy_{1-x}Y_xMnO_{3+\delta}$ ($0 \leq x \leq 1$) has a reversible oxygen uptake at around 200-400°C indicating the presence of oxygen interstitials in these materials. Selbach et al. [11] indicated the presence of oxygen interstitials in $YMnO_3$ and $HoMnO_3$ due to a non-linear electrical conductivity observed under oxidizing conditions. A newly reported finding by Hervieu et al. indicates the presence of oxygen interstitials in $LuFe_2O_{4-x}$ [12]. An oxygen gain starting at approximately 200°C is observed in the material, and the oxygen content increases from x = 0 to an x $\simeq$ to 0.5 around 500°C when heated in a dynamic primary vacuum. By keeping the temperature at 500°C, and switching to reducing atmosphere, the oxygen content starts to decrease, and ends at an x = 0 at room temperature. A cycling ability is also demonstrated, where five cycles are repeated giving the same result. These features show that $LuFe_2O_4$ have promising characteristics in terms of use in oxygen permeable membranes. One drawback is that $LuFe_2O_4$ is an expensive material. Lu is an expensive element, and the total material cost is therefore high. Another limiting factor is the powder preparation route which involves mixing of Lu_2O_3 with Fe_2O_3 and Fe powder sealed in an evacuated silica tube where a glove box is needed in the preparation of the raw powder. The ability to replace Lu in this compound and to find a simpler powder preparation route would therefore be of interest considering its potential for large scale production.

1.2 Objective

The objective of this study is to find a suitable substitution for Lu in the rare earth ferrite $LuFe_2O_4$, to develop a material that has a larger potential for up-scale production of oxygen permeable membranes with the same promising features as those reported by Hervieu et al. [12]. Rare earth ferrites consisting of elements that have approximately the same ionic radii as Lu (Sc, Y, Yb) [13] will be investigated, their crystal structure determined and their oxygen storage ability examined. A new, safer and more convenient powder preparation route will be investigated by the use of general solid state synthesis with heat treatment under inert

and reducing conditions. The materials transport properties will be investigated by van der Pauw conductivity measurements, and preliminary studies with respect to preparation of an asymmetric oxygen permeable membrane will be performed. Preparation of powder from a sol-gel synthesis route in order to make a thin film will be studied, as well as the possibility of making a porous support.

2 Literature survey

2.1 Oxygen permeable membranes

Oxygen permeable membranes have been studied intensively in recent years because of their potential of becoming a viable alternative to cryogenic distillation [2]. The materials that have potential for use in oxygen permeable membranes are non-stoichiometric oxides that can transport oxygen either by oxygen vacancies or oxygen interstitials.

In general, there are two different types of oxygen permeable membranes - ionic conducting membranes and mixed ionic-electronic conducting membranes (MIEC)[6]. In the ionic conducting membranes, oxygen is transported through solid electrolytes while the electrons are transferred through electrodes. In mixed ionic-electronic conductors, both electrons and ions are conducted through the electrolyte. For oxygen transport to occur through the MIEC, there has to exist an oxygen pressure difference across the membrane [6].

For oxygen transport to occur through the membrane material, both ionic and electronic conductivity is necessary, and the factors responsible for electronic and ionic conduction are independent of each other. The electronic conduction is dependent on the electronic band gap, while ionic conduction often is dependent on the crystal structure. Usually, the mobility of electrons and electron holes are larger than the ionic mobility, but will be dependent on the temperature and partial pressure for non-stoichiometric oxides [6]. A general representation of an oxygen permeable membrane is given in Figure 2.1.

There are three steps that are involved in the oxygen transport trough a dense MIEC membrane [6]: (1) The surface-exchange reaction on interface I, (2) The simultaneous bulk-diffusion of charged species and electron/electron holes in the bulk phase, and (3) the surface exchange reaction on interface II, as demonstrated in Figure 2.2. If bulk-diffusion, step number two,

is the rate limiting step, which is the case in most perovskite-based compounds, a reduction of the membrane thickness will increase the oxygen permeation through the membrane since the flux in this case will be inversely proportional to the membrane thickness. One approach to increase the oxygen flux through these membranes have therefore been to prepare an asymmetric membrane consisting of a dense defect-free thin film deposited on a porous support [14]. The porous support enhances the strength of the membrane by applying sufficient mechanical strength. The thin film and the porous support is made from the same material to ensure a similar thermal expansion coefficient for the two components.

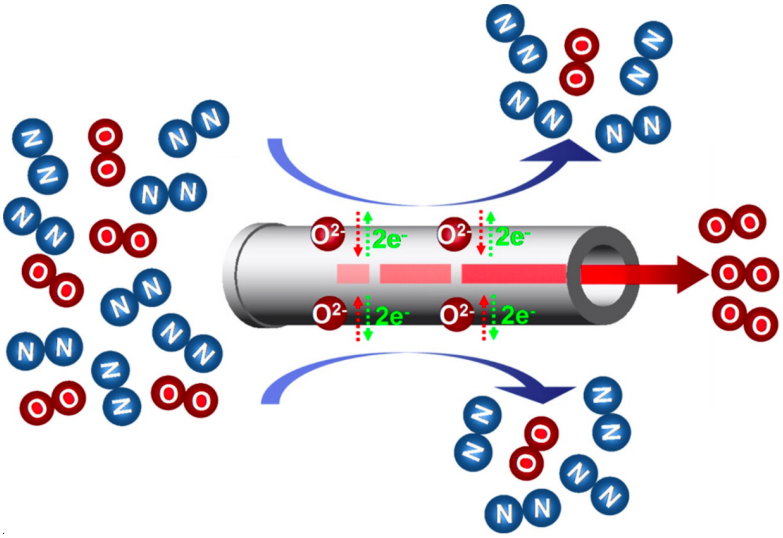

Figure 2.1: A general representation of an oxygen permeable membrane where oxygen is separated and collected on the oxygen depleted side of the membrane. Figure reprinted from Liang et. al. [15].

Two classes of materials that have been studied in detail for use in oxygen permeable membranes are the perovskites and the fluorites. In these materials, oxygen vacancies are the main type of defect. Although these materials show many promising features, there are also some limitations. The most pronounced problems are presented in Figure 2.3.

As can be seen in the figure, many of the major problems associated with the use of oxygen permeable membranes for large scale production, are temperature related. Both chemical and thermal stability and high temperature sealing will be affected by the operating temperature of the membrane. Especially the combination of high temperature and reducing

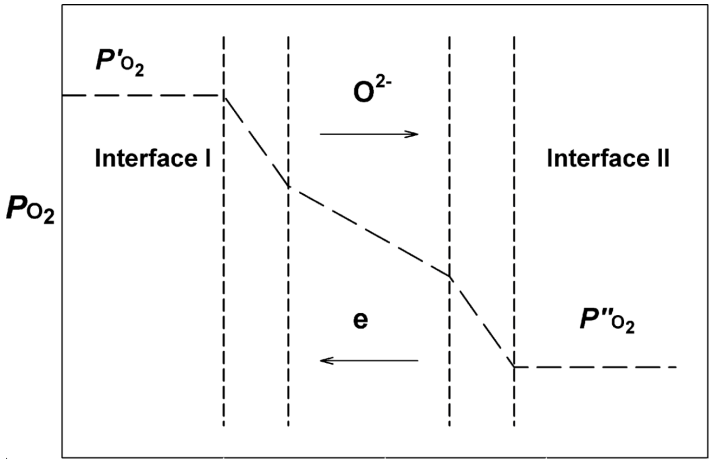

Figure 2.2: The three steps involved in the oxygen transport through a dense MIEC membrane. Figure reprinted from Sunarso et al. [6].

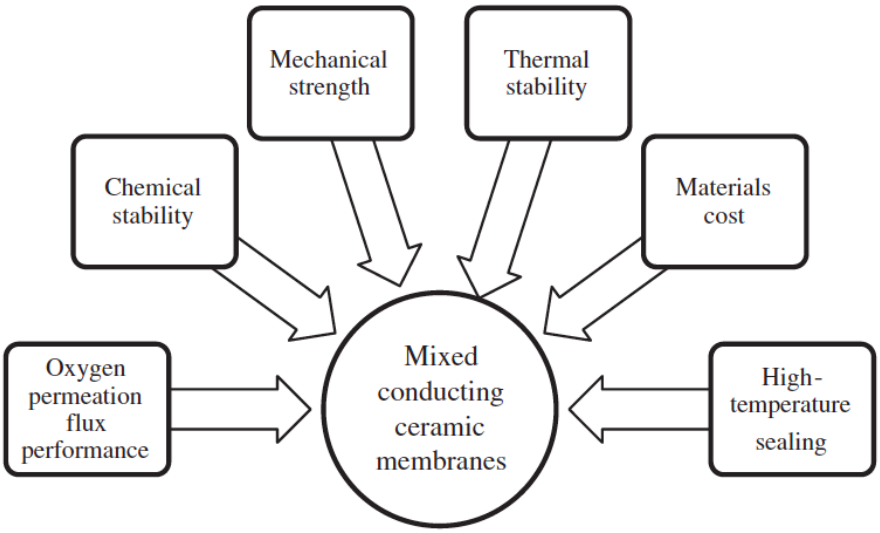

Figure 2.3: The most pronounced challenges associated with oxygen permeable membranes. Figure reprinted from Hashim et al. [2]

atmosphere leads to problems concerning mechanical stability of the membranes. Thermal expansion is affected because an increase in temperature leads to an increase in the ionic motion and thereby an increase in the distance between adjacent atoms or ions. The result is an increase in volume. The chemical stability is affected by the high operating temperature because cationic demixing can occur when the temperature exceeds the threshold temperature for cationic diffusion. In oxygen permeable membranes, oxygen is usually the fastest moving specie, while cation diffusion takes place at elevated temperatures, usually above 800°C. When the oxide consists of both A and B cations, the mobility of the two will differ from each

other, and result in cationic demixing during operation of the membrane. When a potential gradient is created across the membrane caused by the partial pressure difference of oxygen at the two different sides of the membrane, the fastest moving cation will with time be accumulated at the oxygen rich side, while the slowest moving specie will be accumulated at the oxygen depleted side. This will cause the material to become inhomogeneous, and will eventually lead to breakdown of the membrane [8]. The chemical stability will also be influenced by chemical expansion when the oxygen vacancies are transported through the material. At elevated temperatures, the number of oxygen vacancies will be increased. The creation of oxygen vacancies will result in the surrounding ions obtaining a lower valence state and thereby an increase in their ionic radii, leading to an increase in the volume these ions occupy [16]. The result is a chemical expansion that contributes to the thermal expansion, as displayed in Figure 2.4. High temperature sealing is another problem associated with these membranes. As the chemical and thermal expansion increases with increasing temperature, it can be difficult to find a sealing material that is chemically stable under the operating conditions and that has a similar thermal expansion coefficient as the membrane material.

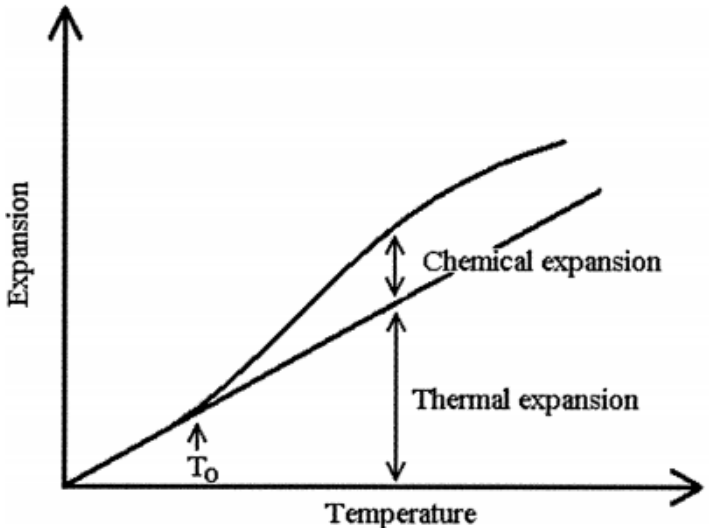

Figure 2.4: The contribution of chemical expansion to the thermal expansion inherent in all mixed-valence materials forming oxygen vacancies by reduction of the cations. Figure reprinted from Lein [17]

A strong correlation between chemical expansion and oxygen partial pressure has been re-

ported by Grande et al [18] for $La_{1-x}Sr_xMnO_{3+\delta}$, where a chemical expansion was found to result in an increase in volume during heat treatment in inert atmosphere, assumed to originate from oxygen vacancies being formed in the material.

One approach to accommodate these challenges is to use materials that can transport oxygen trough oxygen interstitials instead of vacancies. Oxygen interstitials are formed at a lower temperature than oxygen vacancies, and a lower operating temperature can therefore be obtained. Oxygen interstitials are usually formed below 600°C, where cationic diffusion is normally prevented. This may lead to an increase in the the long term stability of the material, by the reduction in temperature hindering cationic movement and thereby cationic demixing of the membrane from taking place. A decrease in the operating temperature will probably also improve the stability in terms of the above-mentioned aspects regarding thermal expansion. A lower energy input will also be required when the temperature is decreased, making the process more energy efficient.

2.2 Structure and properties of RFe_2O_4 (R= La-Lu, Y)

2.2.1 Multiferroism

Rare earth metal iron oxides, with the general formula RFe_2O_4, have been extensively studied at low temperature because of their interesting magnetic and electronic properties caused by the presence of Fe in a mixed valence state [19]. Multiferroism has been reported for this structure when R = Y, Yb, Lu, making these materials promising for use in different electronic devices [20]. Despite the large interest with regard to the low-temperature properties of these materials, investigation of different features expected to occur at elevated temperature, such as oxygen storage and oxygen transport abilities, have not been reported until recently [12]. Due to the interesting material properties reported by Hervieu et. al [12], an investigation of the potential for oxygen storage and transport ability of other rare earth metal iron oxides will be performed in this study.

2.2.2 Structure

All the rare earth metal iron oxides belong to the the same crystal structure with the general formula RFe_2O_4. The space group to which these materials belong, have been a subject of debate. The RFe_2O_4 materials have been reported to belong to a trigonal structure and the space group $R\bar{3}m$ [21], while others have described the structure as monoclinic, represented by the space group $C2/m$ [12]. A representation of the $R\bar{3}m$ structure is given in Figure 2.5, in terms of $LuFe_2O_4$, where Lu is represented by green atoms, Fe by orange atoms, and O by red atoms. As can be seen in Figure 2.5(a), the material has a structure that consist of alternating R, Fe and O layers. Figure 2.5(b) and 2.5(c) shows the structure including its polyhedra and it can be seen that the material has a bilayer of FeO_5 bipyramids alternating with LuO_6 octahedra with edge sharing both inside the FeO_5 bilayers and inside the LuO_6 layers, while they are connected to each other by corner sharing. In this material, Fe is present in two different oxidation states, both Fe^{2+} and Fe^{3+}, and both ions coexist in the triangular Fe-layers. The atomic positions of the different atoms in the structure are taken from Isobe et al. [21] and are given in Table 2.1.

Table 2.1: The atomic positions for $LuFe_2O_4$ in the space group $R\bar{3}m$ with unit cell parameters a = 3.4406 Å and c = 25.28 Å. The data is taken from Isobe et al. [21] for $LuFe_2O_4$.

Site	*x*	*y*	*z*
Lu	0.00000	0.00000	0.00000
Fe1	0.00000	0.00000	0.21518(3)
Fe2	0.00000	0.00000	0.21518(3)
O1	0.00000	0.00000	0.1281(3)
O2	0.00000	0.00000	0.2926(2)

A representation of the monoclinic structure belonging to the space group $C2/m$ is given in Figure 2.6. In this structure, Lu is represented by blue atoms, Fe by purple atoms and O by red atoms. Also in this structure, as can be seen in 2.6(a) there are alternating R, Fe and O layers. From Figure 2.6(b) and 2.6(c) it can be seen that the structure consists of a bilayer of FeO_5 bipyramids alternating with LuO_6 octahedra with edge sharing both inside the FeO_5 bilayers

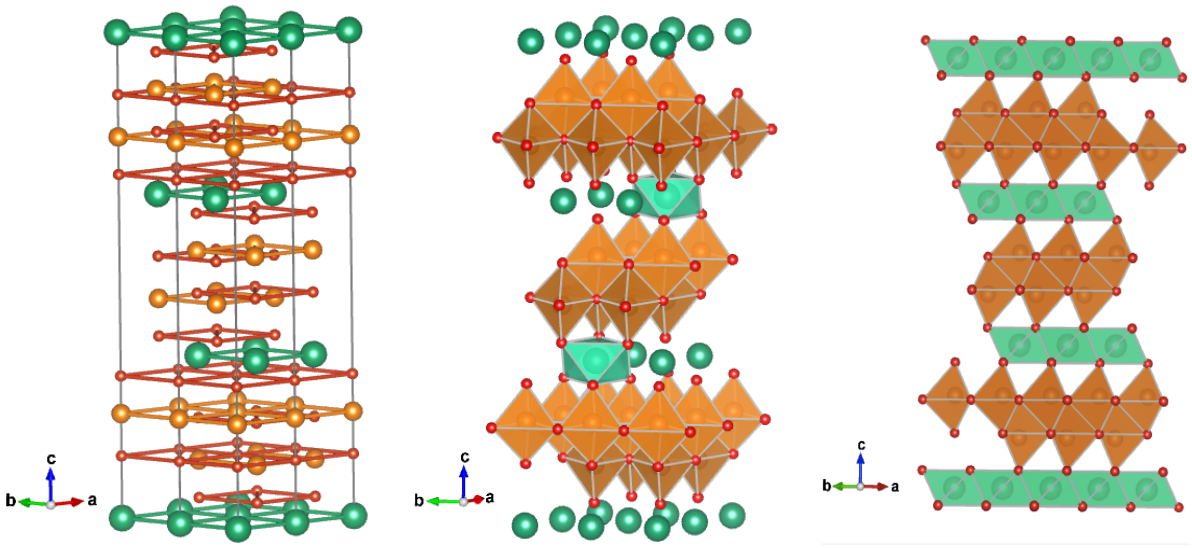

(a) (b) (c)

Figure 2.5: The general structure of RFe_2O_4 represented by $LuFe_2O_4$ within the space group $R\bar{3}m$. In the figure, Lu is represented by green atoms, Fe by orange atoms, and O by red atoms. Both a layered structure (a) and two different structures including the surrounding polyhedra (b), (c) is displayed. [22]

and inside the LuO_6 layers, while they are connected to each other by corner sharing. Fe is also here present in the two different oxidation states, both Fe^{2+} and Fe^{3+}. The atomic positions of the different atoms in the structure is given in Table 2.2. Compared to the $R\bar{3}m$ structure, the C2/m unit cell is smaller, and has a lower symmetry.

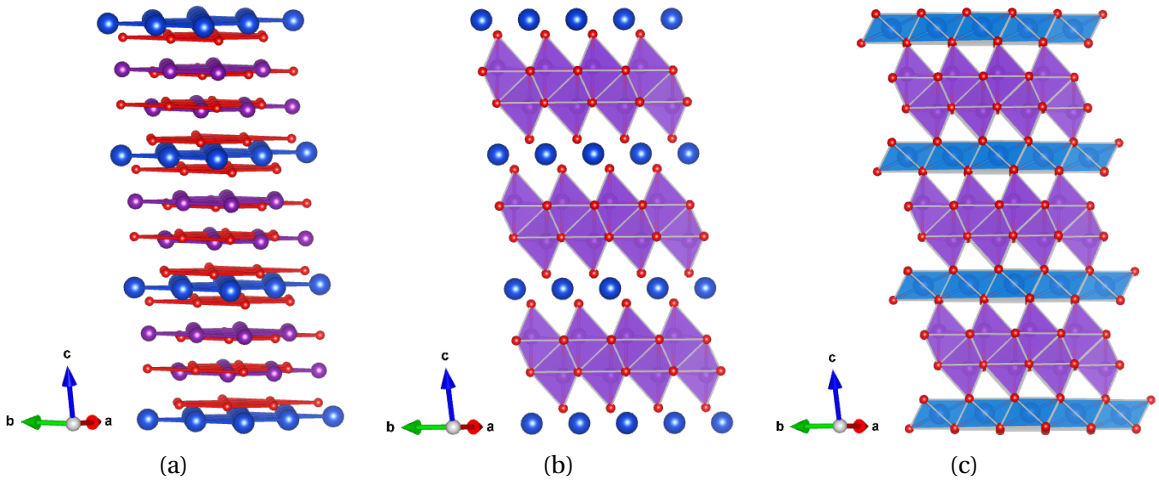

(a) (b) (c)

Figure 2.6: The general structure of RFe_2O_4 represented by $LuFe_2O_4$ within the $C2/m$ space group, demonstrated as a layered structure (a) and with the surrounding polyhedra (b), (c). [22]

Table 2.2: The atomic positions for $LuFe_2O_4$ within the space group $C2/m$ with unit cell parameters a=5.95548 Å, b=343645 Å and c=8.64181 Å, β = 103.2505 °. Data reprinted from Bourgeois [23].

Site	*x*	*y*	*z*
Lu	0.00000	0.00000	0.00000
Fe	0.2145(9)	0.00000	0.6467(1)
O1	0.302(4)	0.00000	0.8877(5)
O2	0.109(2)	0.00000	0.3825(4)

2.2.3 Phase stability

The preparation of RFe_2O_4 can be a challenging task because iron is present in two different oxidation states. As can be seen from the predominance phase diagram given in Figure 2.7, Fe^{3+} is observed to be the most stable oxidation state under ambient conditions, while high temperature combined with reducing atmosphere is required to form Fe^{2+}. To obtain a compound that contains a 1:1 ratio of Fe^{3+} and Fe^{2+}, a precisely controlled temperature and atmosphere program is required. The stability of the different iron compounds is also indicated in Figure 2.8 where the stability is given relative to the partial pressure of CO_2/CO, the partial oxygen pressure and temperature.

In the preparation of rare earth ferrites, witch are all represented by a tree component system, the stability of the different phases is expected to be altered to some extent relative to the two component systems given in Figure 2.7 and 2.8. Despite this altering, the difficulty of obtaining the desired 1:1 ratio of Fe^{3+} and Fe^{2+} is expected to depend strongly on the oxygen partial pressure also in the three component system.

The phase stability of the rare earth metal iron oxides have been studied by Kimizuka et al. [26, 27] at 1200°C under different oxygen partial pressures. In these studies, different stable phases were obtained for the different rare earth ferrites when heat treated at 1200°C in different atmospheres. The different stable phases obtained for the different compounds are given in Table 2.3. From this table it can be seen that four stable phases were obtained when

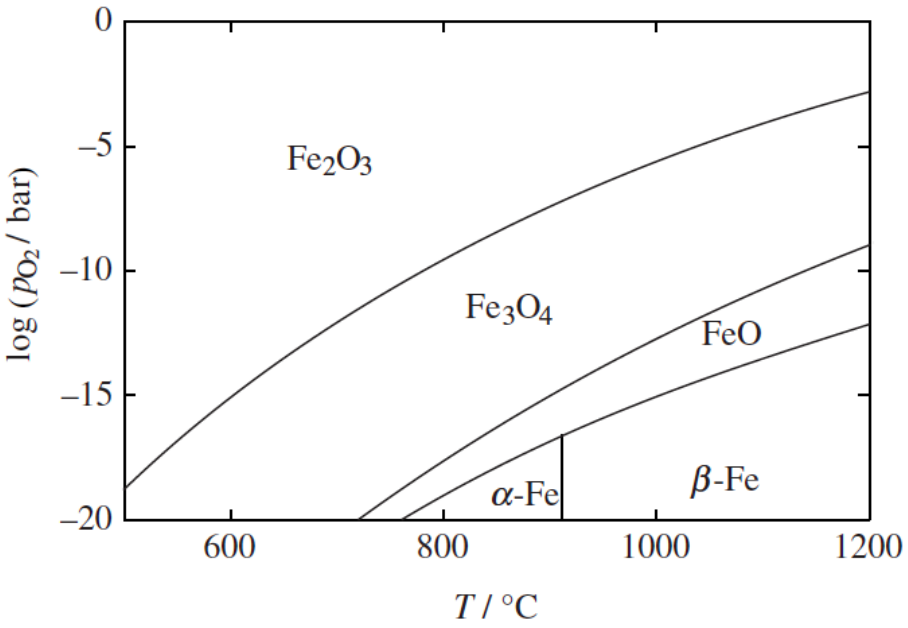

Figure 2.7: Predominance phase diagram for the Fe-O system. Figure reprinted from Stølen and Grande [24].

the precursors were Yb_2O_3 and Lu_2O_3, while only one phase is reported when the precursors were La_2O_3 and Nd_2O_3.

Table 2.3: The classification of the Fe-Fe_2O_3-Ln_2O_3 system. Data obtained from Kimizuka et al. [27]

Type	*Stable ternary compounds*	*Lanthanoid sesquioxide*
A	$LnFeO_3$	La_2O_3, Nd_2O_3
B	$LnFeO_3$, $LnFeO_3$	Sm_2O_3, Eu_2O_3, Gd_2O_3, Tb_2O_3, Dy_2O_3
C	$LnFeO_3$, $LnFeO_3$, $LnFe_2O_4$	Ho_2O_3, Er_2O_3, Tm_2O_3, (Y_2O_3)
D	$LnFeO_3$, $LnFeO_3$, $LnFe_2O_4$, $Ln_2Fe_3O_7$	Yb_2O_3, Lu_2O_3

In the literature, many different preparation routes are reported for the preparation of RFe_2O_4 [28, 29, 30, 31]. For RFe_2O_4 compounds to become viable alternatives for use in large scale production of oxygen permeable membranes, a safe, economical and environmentally friendly preparation route is required. It is therefore desirable to avoid the use of CO and CO_2 in the preparation of these compounds, and in terms of improving the probability for up-scale production, the use of Fe powder, a glove box and evacuated silica tubes should be avoided. A more conventional preparation route will therefore be investigated in this study.

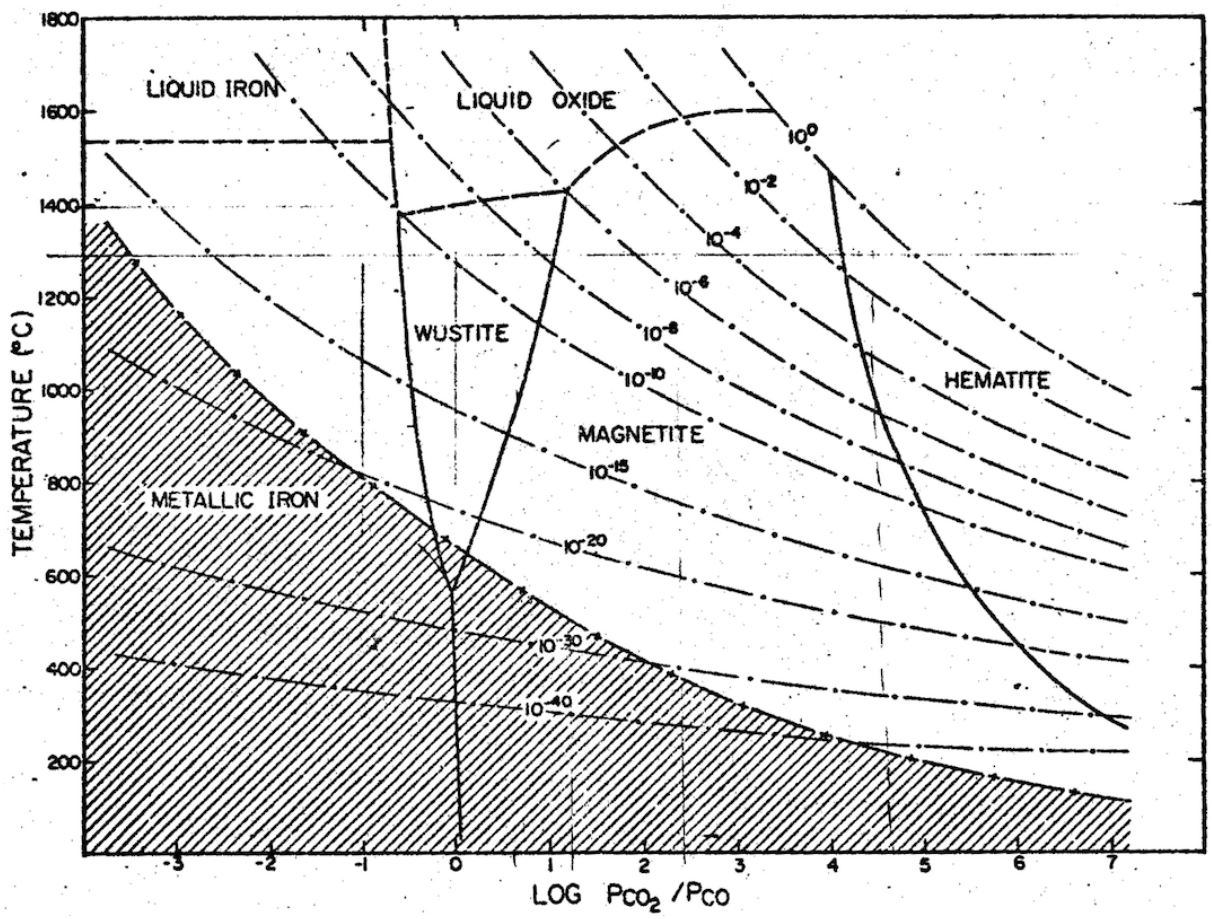

Figure 2.8: Stability relations among metallic iron and iron oxides, as a function of CO_2/CO ratios and temperature, at the total pressure of 1 atm. The dash-cross curve represents the equilibrium between the gas phase and carbon (graphite), and dash-dot lines are oxygen isobars. Figure reprinted from Muan and Osborn [25].

2.2.4 Conductivity

Since rare earth metal iron oxides mainly have been studied at low temperature due to their interesting magnetic and electronic properties, conductivity measurements in terms of ionic motion of these materials have not been reported in the literature. In general, for ionic conduction to occur, there has to exist either vacant sites in the crystal structure were adjacent ions can move, or ions at interstitial positions that have the ability to move to other interstitial positions that are located in close vicinity [32]. Ionic conductivity usually increases with increasing temperature, and in most cases follow the Arrhenius relationship given in equation 2.1. In this equation, A is the pre-exponential factor, E the activation energy for ion motion, R

is the gas constant and T the absolute temperature.

$$\sigma = Aexp(\frac{-E}{RT}) \tag{2.1}$$

In rare earth metal iron oxides, oxygen transport is governed either by the creation of oxygen vacancies or oxygen interstitials. To reach the goal of decreasing the operating temperature below 700°C to make the oxygen production process energetically favorable, the creation of oxygen interstitials is the preferred alternative. Oxygen interstitials can be created in RFe_2O_4 in accordance with Equation 2.2 where the formation of Fe^{3+} from Fe^{2+} can be expressed as Fe^{2+} plus a hole in accordance with Equation 2.3. Since $LuFe_2O_4$ has been found to absorb oxygen at low temperature (< 500°C) [12], the conductivity in this material is assumed to be p-type in accordance with Equation 2.2 and 2.3.

$$\frac{O_2}{2} + 2Fe^x_{Fe^{2+}} \rightarrow O_i^{''} + 2Fe^{\bullet}_{Fe^{2+}} \tag{2.2}$$

$$Fe^{\bullet}_{Fe^{2+}} \rightarrow Fe^x_{Fe^{2+}} + h^{\bullet} \tag{2.3}$$

2.3 $LuFe_2O_4$

Of the rare earth metal iron oxides, $LuFe_2O_4$ and $TmFe_2O_4$ are the only materials where an investigation of the oxygen storage ability has been reported in the literature [12]. Hervieu et al. found that $LuFe_2O_{4+x}$ has an oxygen storage ability of x = 0.5 as can be seen in Figure 2.9(a), and $TmFe_2O_4$ an oxygen storage ability of x = 0.17. For $LuFe_2O_4$, the oxygen content increases when the material is heated in oxygen atmosphere, forming a new state corresponding to an increase in oxygen content of x = 0.5. This new state is retained during cooling in the same atmosphere, and remains stable when coming back to ambient conditions. $LuFe_2O_4$ was also found to have a good cycling ability as depicted in Figure 2.9(b). When heated to 500°C in a dynamic primary vacuum, the oxygen content increased from an x = 0 to a value of x = 0.5. By changing the atmosphere to Ar/H_2, ensuring reducing conditions, the oxygen excess decrease back down to x = 0. The same result was obtained when running four more cycles.

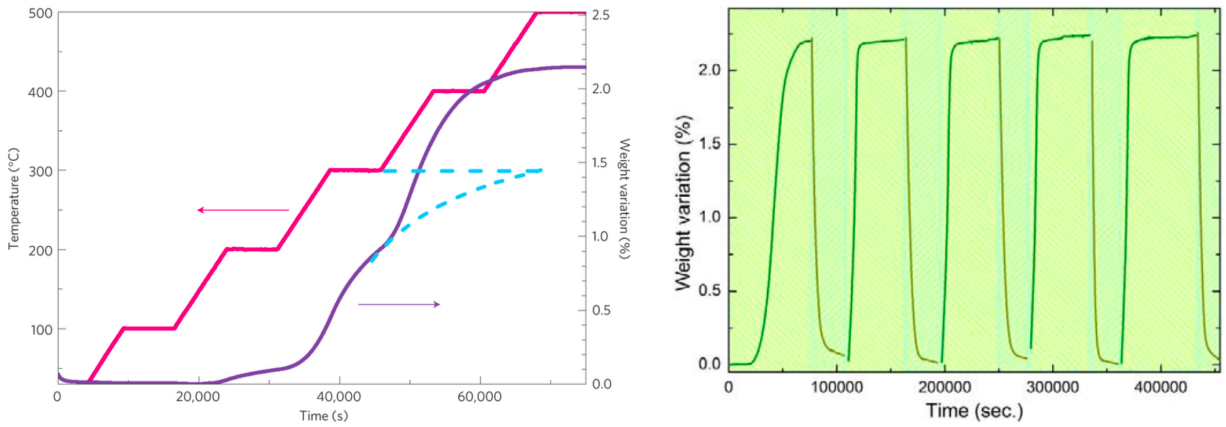

(a) (b)

Figure 2.9: (a) TGA results displaying the mass loss, temperature profile and time interval for $LuFe_2O_4$ heated to 500°C in dynamic primary vacuum. (b) TGA curve displaying the cycling ability of $LuFe_2O_4$. The sample was heated from room temperature to 500°C in dynamic primary vacuum, where a high temperature phase, $LuFe_2O_{4.5}$, was obtained. The temperature was held at 500°C and the atmosphere changed to Ar/H_2 resulting in a decrease in the oxygen excess back to the stoichiometric sample, $LuFe_2O_4$. This process was repeated resulting in a total of five cycles. Figures reprinted from Hervieu et al. [12]

The crystal structure is also observed to change during the oxidation of the material. Hervieu et al. [12], use three different structures to describe the transition that occur when going from the stoichiometric sample, $LuFe_2O_4$, to the oxygen rich state, $LuFe_2O_{4.5}$. A representation of the three different structures are given in Figure 2.10. Hervieu et al [12] defines the material to belong to the space group $C2/m$, and the room temperature cell is therefore described as monoclinic (M) as indicated in Figure 2.10(a). When heating the material under oxidizing conditions the structure changes into a rhombohedral structure, Figure 2.10(b). Further oxidation introduces a new monoclinic cell labelled (M'), and the structure obtained is given in Figure 2.10(c).

In Figure 2.11, the changes taking place in the structure during heat treatments in different atmospheres are displayed with regards to the cycling of the material. The XRD diffractograms are here represented in the 2θ range. It can be seen in the figure that the stoichiometric sample, M, changes into an oxygen rich phase, M', when the material is heated in oxygen atmosphere. When the atmosphere is changed to H_2/Ar atmosphere, the original structure, M, is

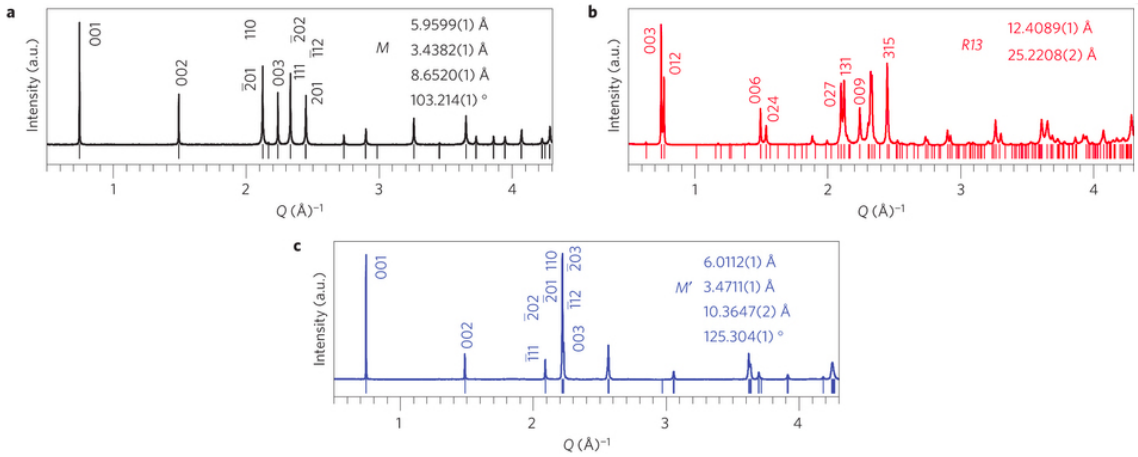

Figure 2.10: The three different cells used to describe the different oxidation states during heat treatment in oxygen atmosphere for $LuFe_2O_4$. Figure reprinted from Hervieu et. al [12].

retained with only slight changes in structure. When oxygen is introduced a second time, the oxygen rich phase M' is obtained once more.

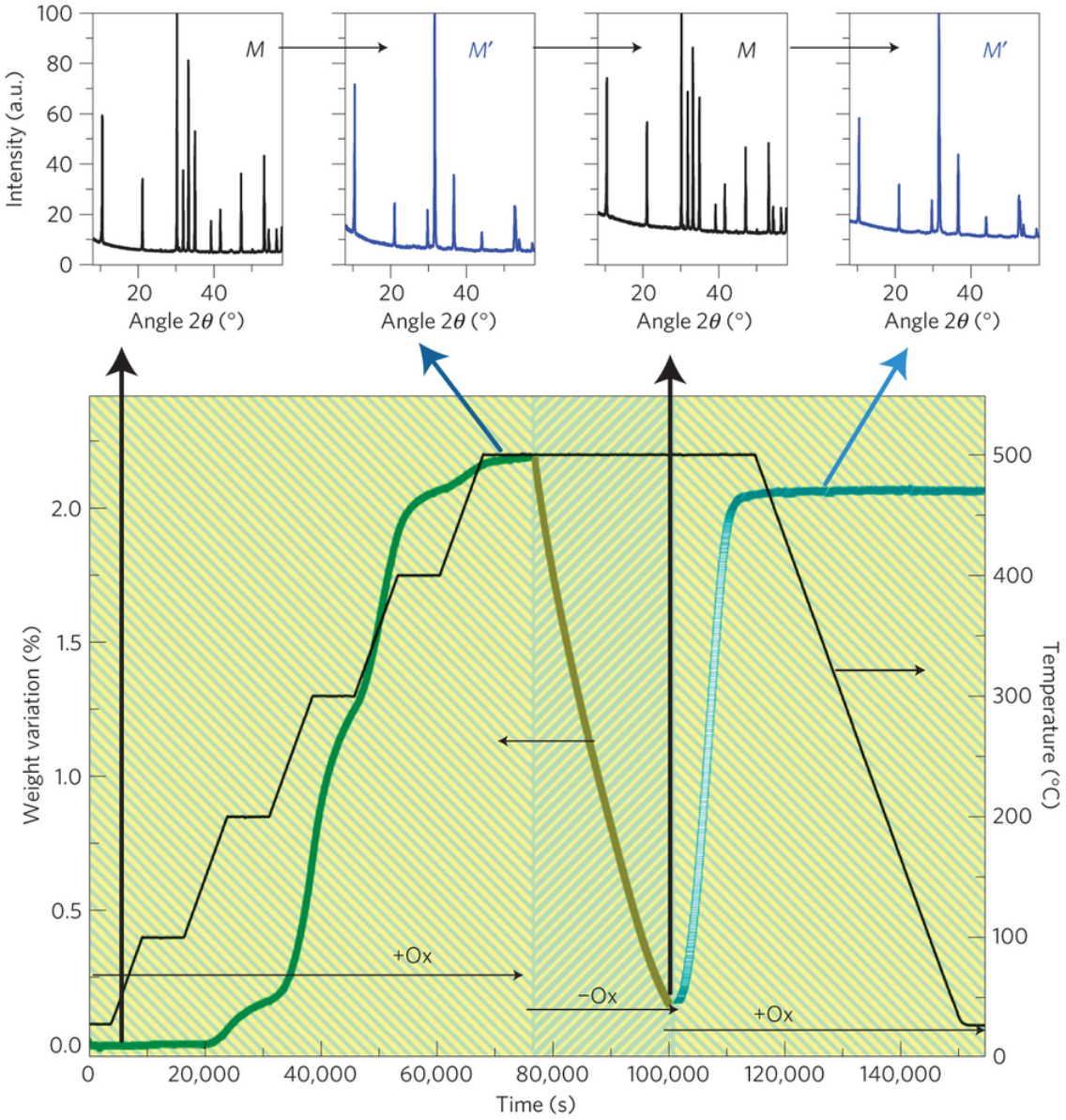

Figure 2.11: The changes taking place in the $LuFe_2O_4$ XRD diffractograms as a result of the cycling performed under heat treatment in different atmospheres. The stoichiometric sample with structure M changes into an oxygen rich phase, M', when the material is heated in oxygen atmosphere. When the atmosphere is changed to H_2/Ar atmosphere, the original structure, M, is retained with only slight visible changes in the structure. When oxygen is introduced a second time, the oxygen rich phase M' is obtained once more. Figure reprinted from Hervieu et. al [12].

2.3.1 Substitutions

In an attempt to taylor the different magnetic properties of the rare earth metal iron oxides, substitutions on both the A and B cation sites have been performed in previous studies [33], [34]. As described above, only $LuFe_2O_4$ and $TmFe_2O_4$ have been reported for investigation considering oxygen storage ability. Since both these materials have shown promising features in this regard, it is likely that other similar materials may have the same potential, and an investigation of other rare earth metal iron oxides in terms of oxygen storage ability will here be performed.

2.4 Solid state synthesis

Solid state synthesis is an old and simple method that is widely used for mixing powder reactants into desired ceramic products [32]. For preparation of small amounts of powder, stoichiometric amounts of the reactants are often mixed and grind by the use of a mortar and a pestle, and then pressed either uniaxial or isostatic and heated at high temperature to ensure mixing at the atomic level. A temperature of at least two thirds of the melting temperature is often required to achieve the desired product [6]. For larger amounts of powder, the reactants are often milled before pressed to obtain a small and uniform particle size, and a good mixing of the different precursor oxides. By pressing the powder into pellets, the number of contact points between the particles increases, hence the reaction rate increases. It is often necessary to grind, press and fire the pellets several times to obtain complete mixing of powders and thereby phase pure samples. Secondary grinding and pressing introduces new contact points between the particles, and the reaction rate increases. By annealing the pellets in different atmospheres, the valence state of the different ions can be tailored. Oxidizing atmospheres result in high valence states, while reducing atmospheres results in a low valence states [35].

2.5 The Pechini process

The Pechini process is a wet chemical synthesis route where the precursors are prepared from alkoxides, oxides, hydrated oxides or carbonates [36]. An alpha-hydroxycarboxylic acid is added to the solution for complexation of the cations and chelating effect. A polyhydroxy alcohol is added for esterification. The solution is stirred and heated on a hotplate until water has evaporated and a raw powder is formed. Powder prepared from the Pechini process has high purity, and the particles are often small (20-50nm) and have a high surface area.

In a modified Pechini process, the precursor solutions are prepared from metal nitrates. Citric acid and ethylene glycol are used as the alpha-hydroxycarboxylic acid and polyhydroxy alcohol, respectively. By preparation of powder from the Pechini process, a lower temperature can be used compared to the more simple solid state synthesis route. For the preparation of a thin film deposit, a small particle size is necessary, and the wet chemical synthesis route is the preferred alternative in comparison to the solid state synthesis route given above. The decrease in the crystallite size also increases the reactivity of the crystallites due to an increasing surface to volume ratio obtained when the crystallite size is decreased [36].

3 Experimental

3.1 Chemicals

The chemicals used in this study are listed in Table 3.1

Table 3.1: A list of the different chemicals used in this study

Compound	*Chemical formula*	*Manufactorer*	*Quality*
Iron(II) oxide	FeO	Aldrich Chemistry	99.9%
Iron(III) oxide	Fe_2O_3	Aldrich Chemistry	99.995%
Scandium(III) oxide	Sc_2O_3	Aldrich Cemistry	99.999%
Ytterbium(III) oxide	Yb_2O_3	Aldrich Chemistry	99.9%
Yttrium(III) oxide	Y_2O_3	Aldrich Chemistry	99.9%
Isopropanol	C_3H_8O	VWR Chemicals	100%
Ytterbium(III) nitrate	$Yb(NO_3)_3$ x $5H_2O$	Aldrich Chemistry	99.9%
Iron(III) nitrate	$Fe(NO_3)_3$ x $9H_2O$	Aldrich Chemistry	98%
Citric acid	$C_6H_8O_7$	MERCK	≥ 99%
Ethylene glycol	$C_2H_6O_2$	EMSURE®	≥ 99.5 %
Charcoal activated	C	MERCK	-

3.2 Preparation of powder by solid state synthesis

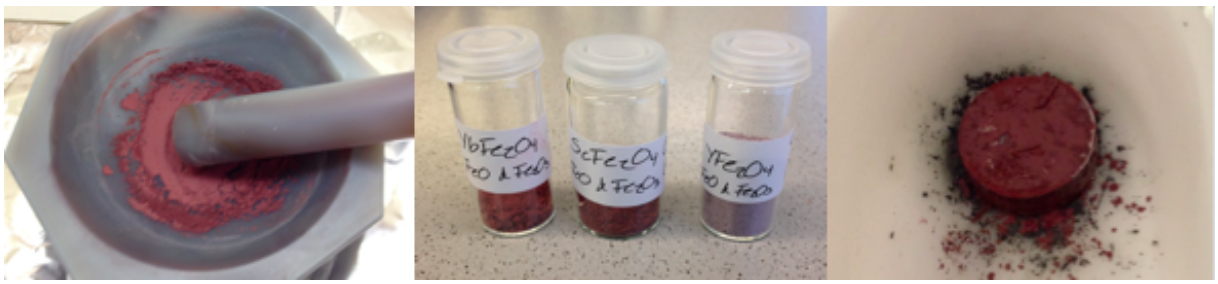

Figure 3.1: Preparation of powder by solid state synthesis.

3.2.1 Preparation of powder from R_2O_3 and Fe_2O_3 (Route 1)

For preparation of YFe_2O_4, $YbFe_2O_4$ and $ScFe_2O_4$, stoichiometric amounts of Fe_2O_3 and R_2O_3 (R=Y, Yb, Sc) in a ratio 2:1 in accordance with Equation 3.1 were weighted after drying the powders at 700°C for 6 hours. The oxides were retrieved from the furnace when the temperature was approximately 200°C, and weighted shortly thereafter. The oxides were mixed and grind in an agate mortar by addition of isopropanol to form a slurry to ensure sufficient mixing of the powders. After the isopropanol had evaporated, the resulting powders were pressed into pellets with a diameter of 10 mm.

$$2Fe_2O_3 + R_2O_3 \rightarrow 2RFe_2O_4 + \frac{1}{2}O_2 \tag{3.1}$$

3.2.2 Preparation of powder from R_2O_3, Fe_2O_3 and FeO (Route 2)

Preparation of powder was also performed from the same route as described above, but by the use of a mixture of both Fe_2O_3 and FeO as iron precursors. The FeO was not dried before mixing to prevent oxidation of iron in the compound. A combination of FeO and Fe_2O_3 as iron precursors were used to ensure a powder mixture where a stoichiometric amount of Fe^{2+} and Fe^{3+} was present from the start, before annealing the powders in different reducing atmospheres. The three different precursors FeO, Fe_2O_3 and R_2O_3 were added in a ratio 2:1:1 in accordance with Equation 3.2, and the resulting powders were pressed into pellets with 10 mm in diameter as described in the previous section. A schematic overview of the two different preparation routes are given in Figure 3.2

$$2FeO + Fe_2O_3 + R_2O_3 \rightarrow 2RFe_2O_4 \tag{3.2}$$

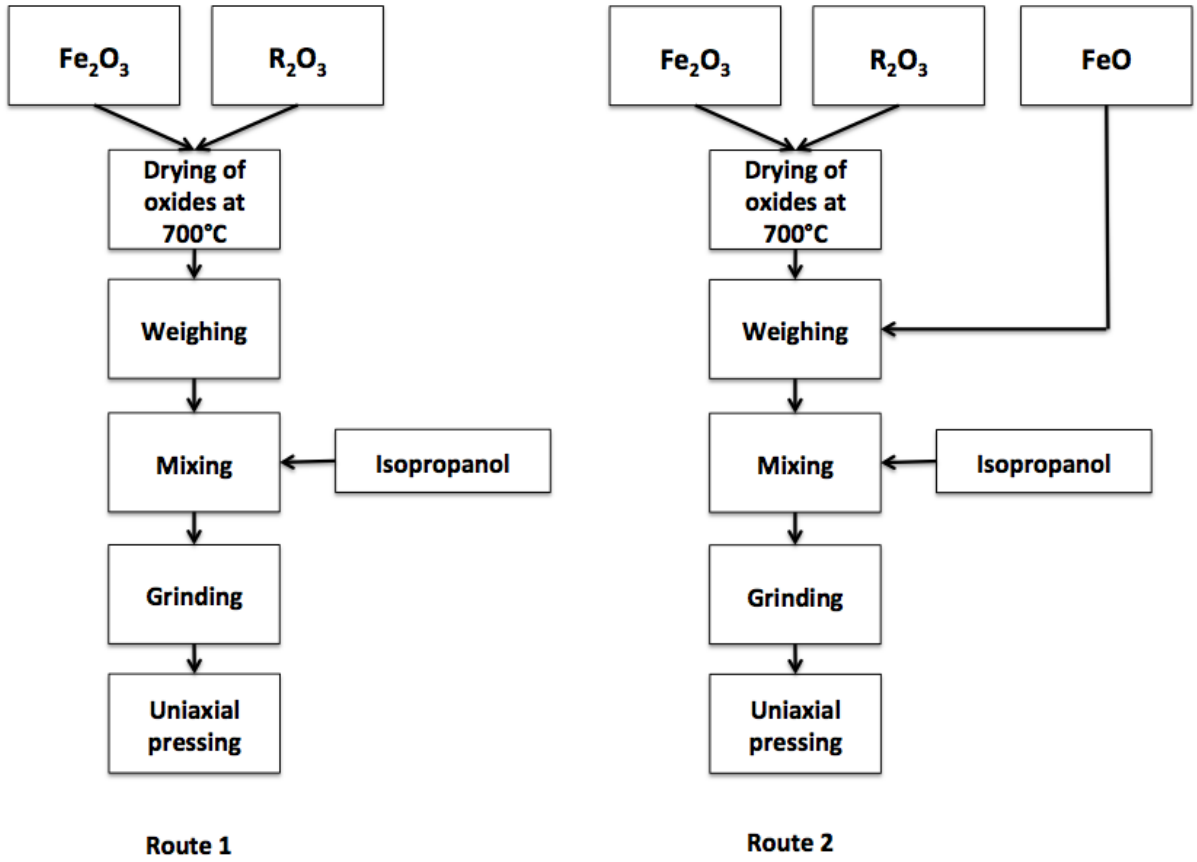

Figure 3.2: Powder prepared from two different preparation routes by solid state synthesis. (R = Y, Yb, Sc)

3.2.3 Annealing of powders in different atmospheres

Heat treatment of powders obtained from preparation route 1

In order to obtain RFe_2O_4 with a 1:1 ratio of Fe^{2+} : Fe^{3+}, the powders were heat treated both in inert and two different reducing atmospheres to investigate under which conditions the desired ratio could be obtained. Both annealing in N_2, 5 %H_2/Ar and 3 %H_2/Ar atmospheres were tested for the powders obtained from preparation route 1, and the temperature programs used for powders prepared from this route are given in Figure 3.3.

Heat treatment of powders obtained from preparation route 2

The powders prepared from preparation route 2 were annealed only in N_2 atmosphere at three different temperatures, including 1200, 1275 and 1300°C, as indicated in Figure 3.12.

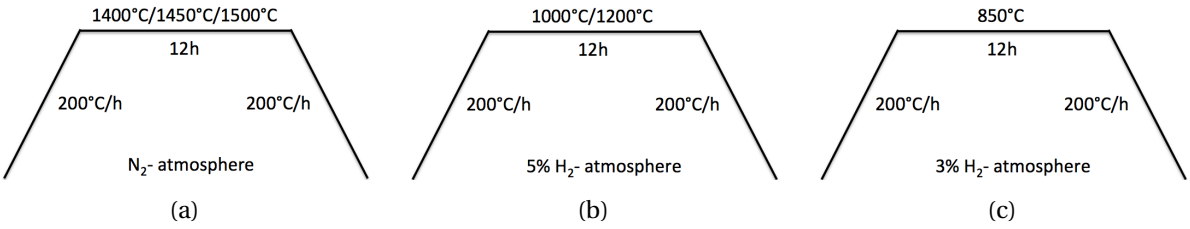

Figure 3.3: The temperature programs used for powders prepared from preparation route 1. (a) Annealing at three different temperatures in N_2-atmosphere, (b) annealing at two different temperatures in 5% H_2/Ar-atmosphere and (c) annealing in 3% H_2/Ar-atmosphere.

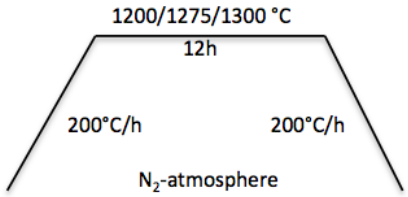

Figure 3.4: The heat treatment program used for annealing of RFe_2O_4 (R=Y, Yb, Sc) powder prepared from solid synthesis (Route 2). The powder was heat treated at three different temperatures, 1200, 1275 and 1300 °C in N_2 atmosphere.

$YbFe_2O_4$ powder obtained from preparation route 2 annealed at 1300 °C gave a phase pure powder, and the further investigation of the oxygen storage ability and the structure parameters of RFe_2O_4 compounds were therefore confined to an investigation of the properties of $YbFe_2O_4$.

3.2.4 Preparation of $YbFe_2O_4$ for investigation of material properties

In order to prepare $YbFe_2O_4$ powder that could be used in the investigation of the oxygen storage ability and structure parameters of the material, as well as the preparation of a porous support, powders were prepared in five new batches. All five were prepared from the same powder preparation route as described in section 3.2.2, and the raw powders annealed at 1300°C in N_2 atmosphere. The amount of powder prepared differed between the different batches, and the amount prepared in each, as well as the amount of powder used to prepare the different pellets from each batch, is given in Table 3.2. Batch 1 represents the batch prepared when the phase pure powder was initially obtained. In this preparation, a 10 mm pellet was prepared, as described in section 3.2.2, while for pellets prepared from batch 2-6, a 15

mm pressing tool was used.

Table 3.2: Powder preparation of $YbFe_2O_4$ from six different batches

Batch	*Powder prepared [g]*	*Powder per pellet [g]*
1	3	2
2	6	3
3	20	4
4	20	4
5	12	4
6	6	3

After annealing of the pellets, they were all grinded by the use of a mortar and a pestle, and the obtained powder examined in terms of phase purity by x-ray diffraction. Some of the pellets were also pressed and annealed a second time in order to improve the phase purity of the powders obtained.

3.2.5 Annealing of powders in oxidizing and reducing atmospheres

Heat treatment of as prepared powder of $YbFe_2O_4$ in oxygen atmosphere

Phase pure $YbFe_2O_4$ powders obtained from preparation route 2 annealed at 1300°C in N_2 atmosphere, were annealed in O_2-atmosphere at both 500°C and 600°C to study if this would result in an increase in the oxygen content in the material, obtaining $YbFe_2O_{4+\delta}$. The temperature programs used to study this are given in Figure 3.5.

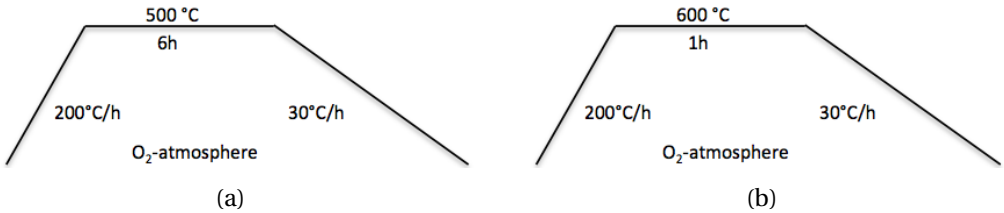

(a) (b)

Figure 3.5: The two different temperature programs used in heat treatment of as prepared $YbFe_2O_4$ powder obtained from solid state synthesis (Route 2) annealed in N_2 atmosphere at 1300 °C. The two different heat treatments in O_2 atmosphere were performed to study the change in crystal structure as a result of heat treatment under oxidizing conditions

Heat treatment of as prepared powder of $YbFe_2O_4$ in hydrogen atmosphere

After the heat treatment of as prepared $YbFe_2O_4$ in oxygen atmosphere, the possibility of reducing the oxygen rich powder obtained, back to the stoichiometric compound was investigated. The oxygen rich powder was heated in 10%H_2/Ar atmosphere to ensure reducing conditions. The two different temperature programs used in the investigation are given in Figure 3.6.

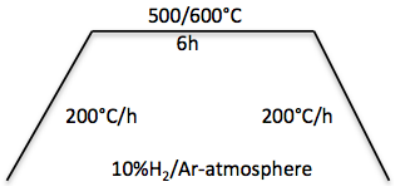

Figure 3.6: The two different temperature programs used in the attempt of reducing the oxygen rich powder, $YbFe_2O_{4+\delta}$, back to the original stoichiometric sample, $YbFe_2O_4$.

3.3 Preparation of powder by sol-gel synthesis

Figure 3.7: An illustration of the different stages in the process of obtaining a raw powder of $YbFe_2O_4$ from sol-gel synthesis .

3.3.1 Preparation of raw powder

$YbFe_2O_4$ was also prepared from a sol-gel synthesis route by a modified pechini process. An illustration of the different stages in this process is given in Figure 3.7, while a more thorough representation of the synthesis route is given in Figure 3.8. As can be seen in this figure, the

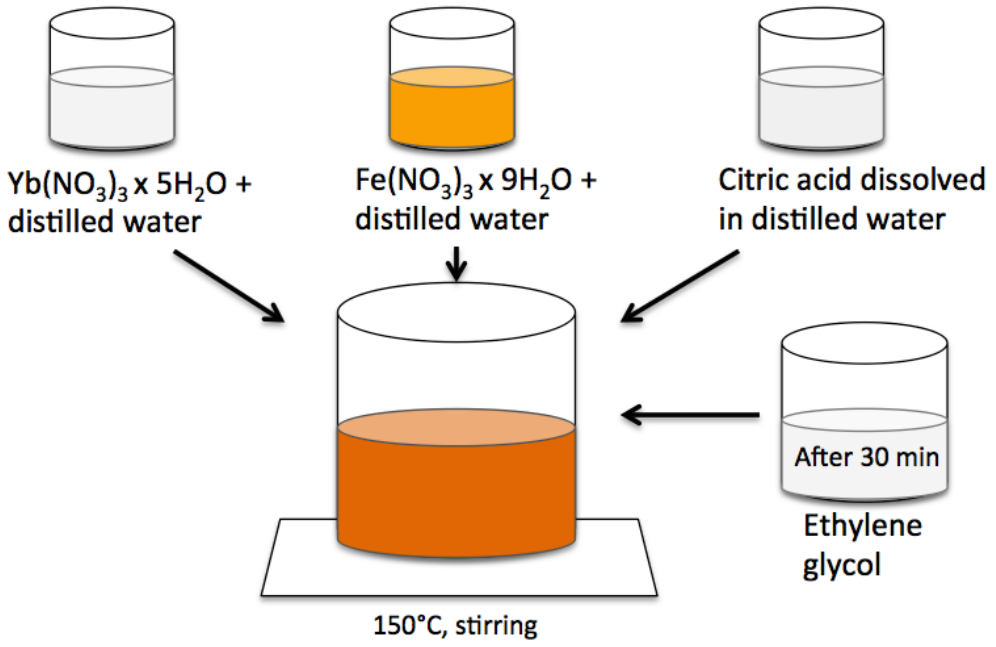

Figure 3.8: A schematic of the preparation route of the sol-gel synthesis of $YbFe_2O_4$ where the precursors were $Yb(NO_3)_3$ x $5H_2O$ and $Fe(NO_3)_3$ x $9H_2O$. Citric acid and ethylene glycol were added for complexation and esterification, respectively.

precursors were $Yb(NO_3)_3$ x $5H_2O$ and $Fe(NO_3)_3$ x $9H_2O$. In the preparation of the sol, both salts were dissolved in distilled water, and then added to a beaker. Citric acid and ethylene glycol were added for complexation of the cations and esterification, respectively. The cation to citric acid and ethylene glycol ratio was 1:2:2. The solution was stirred and heated on a hotplate holding a temperature of 150°C until a raw powder was formed.

3.3.2 Calcination of raw powder

The raw powder was then heated in a regular calcination furnace at 500°C in air for two hours to remove the residual organic compounds. Two different calcination routes were afterwards performed in the attempt of preparing a powder containing a 1:1 ratio of Fe^{2+} and Fe^{3+}. Both routes involved heat treatment in a tube furnace under reducing conditions, and the different temperature programs are given in Figure 3.9, where the preceding heat treatments in air are included.

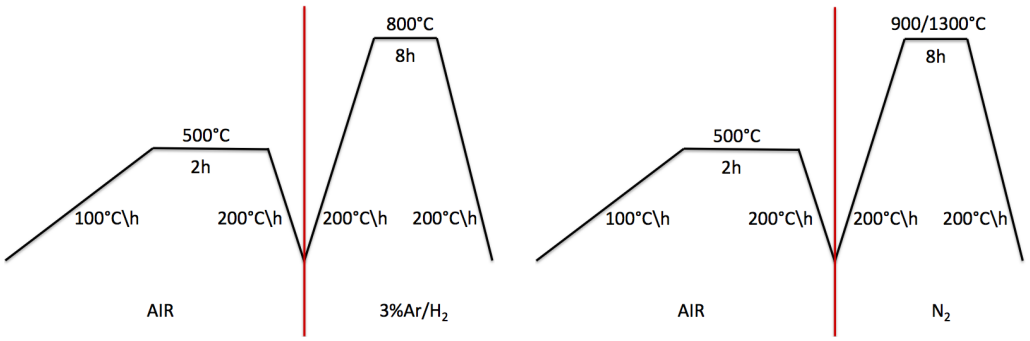

(a) (b)

Figure 3.9: The temperature programs used in the calcination of raw powder obtained in the sol-gel synthesis of $YbFe_2O_4$. (a) In air and 3%H_2/Ar-atmosphere and (b) in air and N_2-atmosphere

3.4 Preparation of porous support

In order to investigate the possibility of preparing an oxygen permeable membrane from $YbFe_2O_4$, a preparation of a porous support was performed by ball milling $YbFe_2O_4$ obtained by solid state synthesis (Route 2) with 20 vol% charcoal activated. The mixture was placed in a 100 mL plastic bottle, and milled together with milling balls and 96% ethanol for one hour at a speed of approximately 40 rpm in order to mix the two powders without destroying the texture of the charcoal activated. The ethanol was removed by the use of a rotavapor after milling, and the milling balls rinsed and removed. The obtained powder was uniaxially pressed into pellets that were 30 mm in diameter. The pellets were afterwards sintered in accordance with the temperature program given in Figure 3.10. The first step involved dissipation of charcoal activated to ensure pore formation, while the second step was performed as a sintering step to ensure sufficient mechanical strength for use in the asymmetric oxygen permeable membrane.

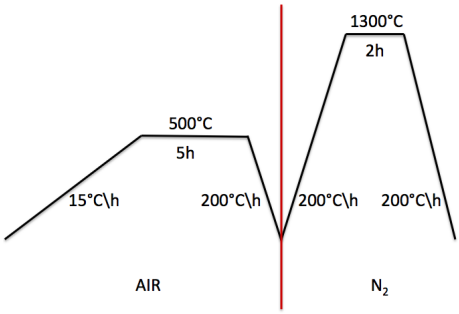

Figure 3.10: The sintering program used for the preparation of a porous support in the preliminary studies of making a membrane prototype.

3.5 General overview of the characterization methods performed on the different powders

A general overview of the different powders obtained in this study, and the characterization performed on each of them, is given in Figure 3.11.

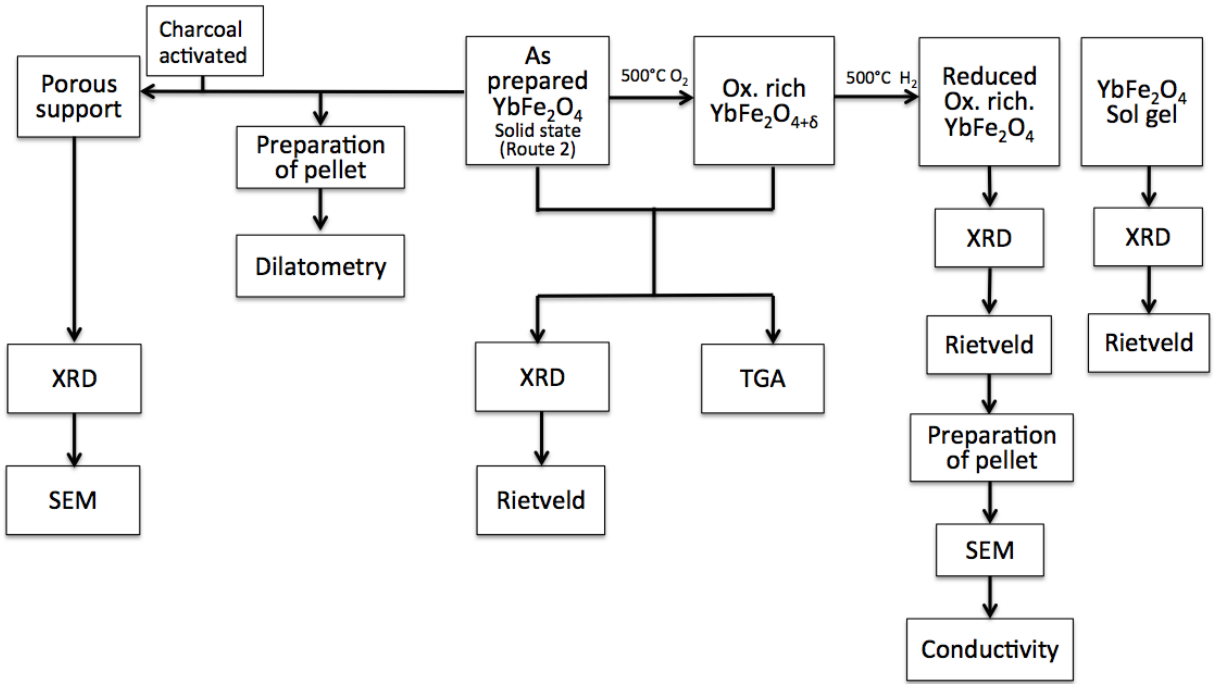

Figure 3.11: A general overview of the different characterization methods performed on the different powders obtained in this study.

3.6 Characterization of powder

3.6.1 X-ray diffraction, (XRD)

The XRD data were collected using a Bruker Focus D8 diffractometer with Cu Kα radiation. The data collection time was five hours, the step size 0.013 and counting time 2.5 seconds per step. The 2θ range was 7 - 100 °. Phase purity of the different powders obtained in the different powder preparation routes were investigated by comparing the diffractograms to PDF cards obtained from the DIFFRAC.EVA V3.0 software. The different PDF cards used in the study of

the different powders are given in Table 3.3.

Table 3.3: An investigation of the phase purity of the different powders obtained in this study were performed by the use of different DIFFRAC.EVA V3.0 pdf cards

Powder	*Preparation route*	*DIFFRAC.EVA V3.0 pdf card*
As prepared powder	Solid state synthesis (Route 2)	(04-088-3888)
Oxygen rich powder	Solid state synthesis (Route 2)	(00-044-1066)
Reduced powder	Solid state synthesis (Route 2)	(04-088-3888)
As prepared powder	sol-gel synthesis	(04-088-3888), (04-001-2438)
Porous support	solid state synthesis (Route 2)	(00-023-7030)

3.6.2 Rietveld refinement

Rietveld analysis by Bruker AXS Topas academic software version 4.2 was performed on the four different powders obtained in this study, to investigate the structures in more detail. An overview of the specific instrumental settings used in the refinement of the different powders is given in Table 3.4, while the atomic positions used in the refinement are given in Table 3.5 and 3.6, respectively. The as prepared powder prepared from solid state synthesis was observed to be highly crystalline, and tube tails were therefore used in the refinement to improve the fit to this diffractogram. The oxygen rich phase was refined by the use of an hkl phase, because the atomic positions in the structure were difficult to obtain. Three peak phases were also added in the refinement due to an uneven background obtained in the diffractogram during the XRD scan. A peak phase was also added in the refinement of the reduced oxygen rich phase, to avoid background irregularities to influence the refinement. A peak phase was also added in the refinement of the powder prepared from the sol-gel synthesis route to adjust for the impurity that could not be identified from the DIFFRAC.EVA V3.0 software. The refinement of the reduced oxygen rich powder had to be performed with the use of the sample spill parameter since the diffractogram was collected using an Si holder with cavity. The use of a holder with cavity introduces differences in the powder volume being detected during the measurement, and an adjustment for this was therefore performed.

Table 3.4: Rietveld refinement instrumental settings

As prepared powder, solid state		**Oxygen rich powder**	
Parameter	*Value*	*Parameter*	*Value*
Primary/secondary radius	280	Primary/secondary radius	280
Source Width (mm)	0.04	Divergence	4.1
Z1	-1.997133	Filament length	12
Z2	2.238379	Sample length	15
Fraction	0.00075612	Recieving slit length	12
Simple axial model (mm)	8.986324	Primary/secondary solle	2.5
–	–	LP factor	0
Background	10	Background	7
Sample displacement	-0.04927(41)	Sample displacement	0.0103(12)
–	–	Peak phase	26.29
–	–	Peak phase	29.57
–	–	Peak phase	61.39
Reduced oxygen rich powder		**As prepared powder, sol-gel**	
Parameter	*Value*	*Parameter*	*Value*
Primary/secondary radius	280	Primary/secondary radius	280
Divergence	4.1	Divergence	4.1
Slit	0.26	Slit	0.26
Filament length	12	Filament length	12
Sample length	15	Sample length	15
Recieving slit length	12	Recieving slit length	12
Primary/secondary solle	2.5	Primary/secondary solle	2.5
LP factor	0	LP factor	0
Pref. orient. dir 1, 001	0.4083(41)	Pref. orient. 001	1.0712(15)
Pref. orient. dir 2, 110	0.8032(48)	–	–
Fraction of direction 1	0.2027(62)	–	–
Background	7	Background	9
Sample displacement	-0.09208(59)	Sample displacement	-0.06643 (72)
Beam spill	5.624(30)	–	–
Peak phase	13.23	Peak phase	44.65

Table 3.5: The atomic positions used in the Rietveld refinement within the $C2/m$ space group with unit cell parameters a = 5.95532 Å, b = 3.43656Å, c = 8.64175Å and β = 103.2493 ° for powders obtained in this study. The parameters are obtained from Bourgeois [23].

Site	*Np*	*x*	*y*	*z*
Yb	2	0.00000	0.00000	0.00000
Fe	4	0.214	0.00000	0.6467
O1	4	0.321	0.00000	0.8842
O2	4	0.103	0.00000	0.3849

Table 3.6: The atomic positions for Yb_2O_3 within the $Ia3$ space group used in the Rietveld refinement of the as prepared powder obtained from sol-gel synthesis containing a secondary phase. The structure parameters are taken from Schleid et al. [37] where the unit cell parameters were reported to be a = b = c = 10.4342 Å

Site	*Np*	*x*	*y*	*z*
Yb1	2	0.25000	0.25000	0.25000
Yb2	4	0.96866(41)	0.00000	0.25000
O	4	0.0915(36)	0.1114(37)	0.3474(38)

3.6.3 Thermogravimetric analysis, (TGA)

To investigate the mass gain in the different materials during heat treatment in oxygen atmosphere in order to quantify the amount of oxygen going into the structure, TGA was carried out using a Jupiter Netzsch STA 449C. TGA measurements were performed on both the as prepared powder and oxygen rich powder prepared from the solid state synthesis route. The temperature program used in these measurements is given in Table 3.7.

Table 3.7: Temperature program used in all six TGA measurements

Step	*Start temperature* [°C]	*Ramp* [°C/min]	*End temperature* [°C]	*Dwell* [min]	*Atmosphere*	*Flow* [ml/min]
1	30	1	600	5	O_2	30-40
2	600	1	30	5	O_2	30-40
3	30	1	600	5	O_2	30-40
4	600	10	30	1	O_2	30-40

3.6.4 Dilatometry

Dilatometry was performed by the use of a Netzsch DIL 402C to obtain a better insight into the preferable sintering temperature of the material. The measurement was performed on a uniaxially pressed 5 mm pellet made from as prepared powder obtained from solid state synthesis. The temperature program used in the measurement is given in Table 3.8.

Table 3.8: Temperature program used in the dilatometry measurements

Step	*Start temperature* [°C]	*Ramp* [°C/min]	*End temperature* [°C]	*Dwell* [min]	*Atmosphere*	*Flow* [ml/min]
1	30	1	1250	1	N_2	20-30

Density measurements

The density of the different pellets obtained in this study were investigated by the use of a caliper to study the volume of the pellets, while weight measurements were performed by the use of a standard four digit balance.

3.6.5 SEM

SEM studies of the surface of the pellet used in the conductivity measurements described in section 3.7 and the porous supports described in section 3.4 were conducted with the use of a Hitachi LV S-3400N. The data were collected by the use of a 15kV accelerating voltage and secondary electrons.

3.7 Conductivity measurements

A conductivity measurement was performed to study how the conductivity of $YbFe_2O_4$ responded to a change in atmospheres. The measurement was performed by the use of an in-house built van der Pauw setup, as demonstrated in Figure 3.12. The setup illustrated, consists of four platinum contact points where current is forced between two adjacent electrodes, and the voltage drop is measured between the other two. A thin bulk sample made from phase pure reduced oxygen rich powder from solid state synthesis was used in the experiment. A 15 mm pellet was uniaxially pressed and sintered in nitrogen atmosphere according to the temperature program given in Figure 3.13 The pellet was attached to the van der Pauw setup by placing it on top of the four platinum electrodes and stabilizing it by the use of the clamp. The whole setup was then placed in a quartz container and inserted in the electrical conductivity furnace. The measurement was conducted with a voltage of 2.0 V. The temperature program used in the measurement, including heating rates and atmospheres applied is given in Table 3.9

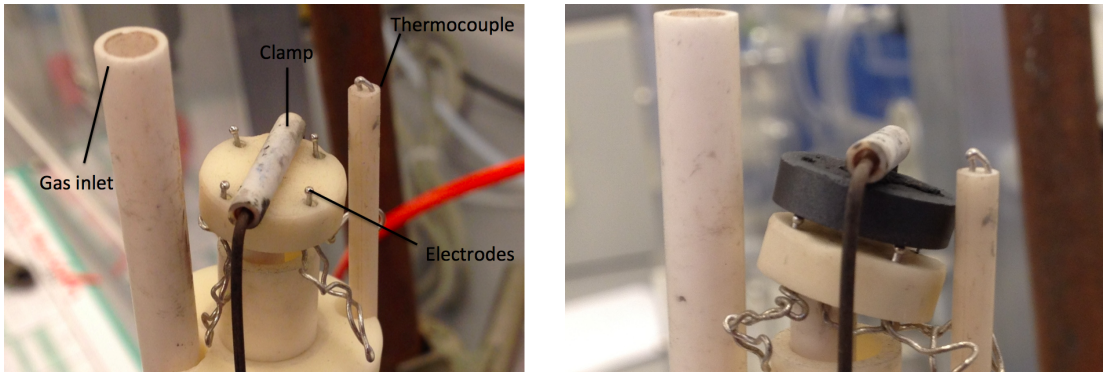

(a) (b)

Figure 3.12: A representation of the van der Pauw setup used in the conductivity measurement. (a) The general setup. (b) The setup included a pellet placed on top of the four platinum electrodes, stabilized by the clamp.

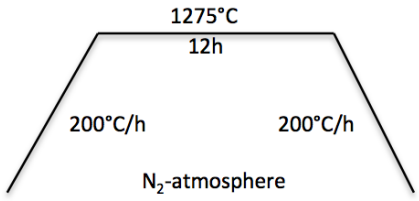

Figure 3.13: The temperature program used in the sintering step of a 15mm pellet for use in conductivity measurements.

Table 3.9: The measurement specifications used in the conductivity measurement performed on a 15mm sample uniaxially pressed from reduced oxygen rich powder obtained from solid state synthesis (Route 2).

Step	*Type* [°C]	*Start temperature* [°C/min]	*Ramp* [°C]	*End temperature* [h]	*Atmosphere*	*Flow* [ml/min]
1	dynamic	30	60	500	N_2	50
2	isostatic	-	-	-	N_2	50
3	isostatic	-	-	-	O_2	50
4	isostatic	-	-	-	N_2	50
5	isostatic	-	-	-	O_2	50
6	dynamic	500	60	500	O_2	50

4 Results

4.1 Powder preparation

4.1.1 Preparation of $YbFe_2O_4$ by solid state synthesis

Preparation of $YbFe_2O_4$ from solid state synthesis (Route 2), as described in section 3.2.2, gave a phase pure powder when annealed at 1300°C in N_2 atmosphere. The further investigation of the oxygen storage and cycling ability of rare earth ferrites was therefore concentrated on a study of the properties of $YbFe_2O_4$. The structural details of the material was also investigated, and how these parameters changed upon heat treatment in different atmospheres.

The attempt of obtaining $YbFe_2O_4$ from preparation route 1 was not successful. The powder prepared from heat treatment at 1400 and 1450°C in N_2 atmosphere resulted in a combination of $YbFeO_3$ and Fe_3O_4 by a comparison to the DIFFRAC.EVA V3.0 pdf cards (04-006-8312) and (04-015-9120), respectively. When heated to 1500°C in the same atmosphere, a decomposition of the material took place, before a reduction into the desired compound containing a 1:1 ratio of Fe^{2+} and Fe^{3+} was obtained. Heat treatment of the powder obtained from preparation route 1 annealed in 3%H_2/Ar and 5%H_2/Ar, as described in section 3.2.3, resulted in a reduction into metallic iron indicating too reducing conditions.

The preparation of YFe_2O_4 and $ScFe_2O_4$ was neither successful, and the results obtained in the attempts of preparing these materials are given in section A.

4.1.2 Phase pure $YbFe_2O_4$ obtained from solid state synthesis (Route 2)

$YbFe_2O_4$ prepared from solid state synthesis (Route 2), as described above, gave a phase pure powder when annealed at 1300°C in N_2 atmosphere for 12 hours. The XRD diffractogram obtained for this powder is given in Figure 4.1 where the diffractogram is compared to the

DIFFRAC.EVA V3.0 PDF card (04-088-3888). The powder was observed to be highly crystalline.

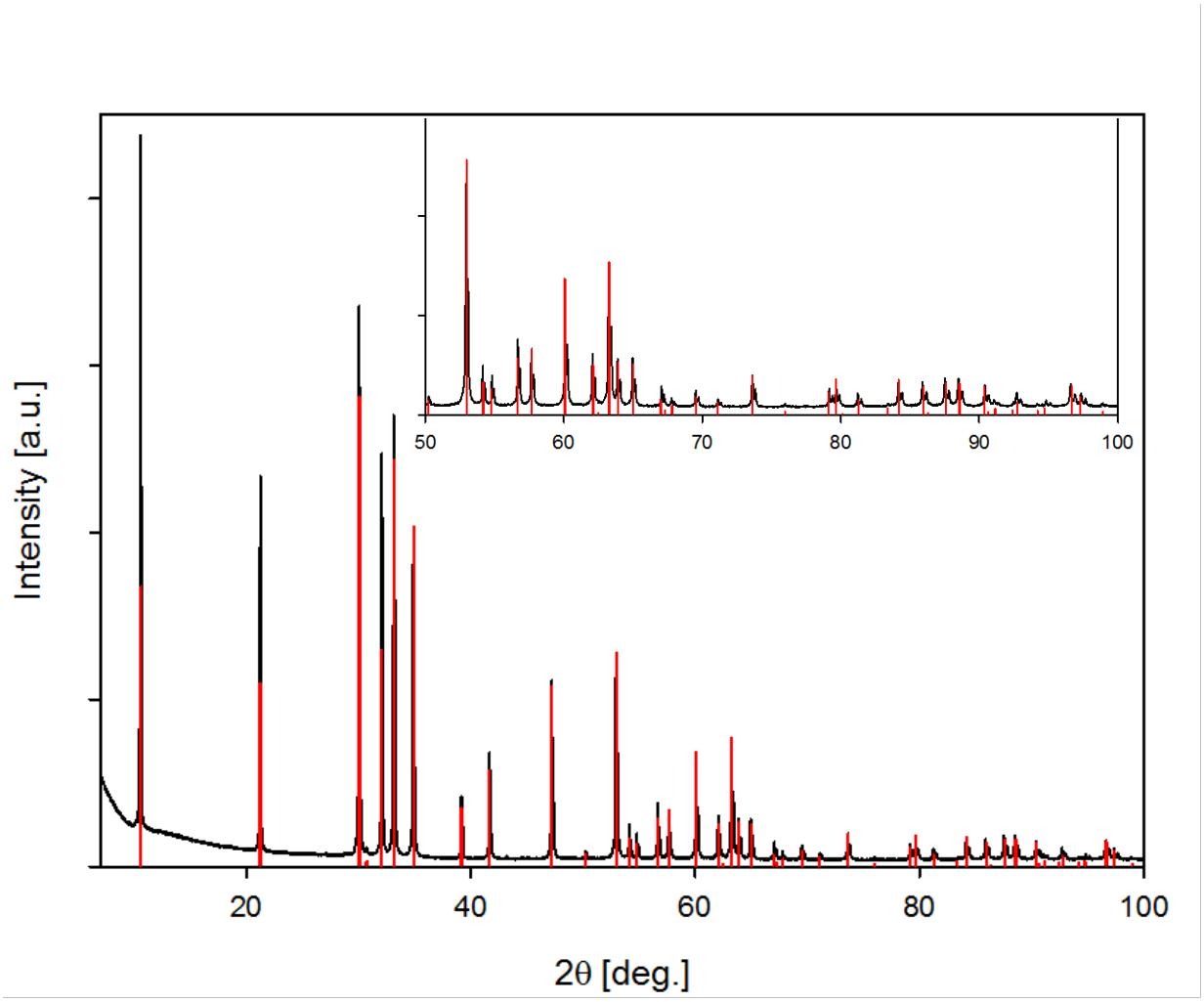

Figure 4.1: Phase pure $YbFe_2O_4$ powder prepared from solid state synthesis (Route 2) annealed at 1300°C in N_2 atmosphere. The diffractogram is compared to the DIFFRAC.EVA V3.0 pdf card (04-088-3888).

Although phase pure powder of $YbFe_2O_4$ was obtained from solid state synthesis, the result proved difficult to reproduce. Phase pure powder was only obtained for three out of 20 pellets, all prepared from reparation route 2, annealed at 1300°C. The raw powders used, were prepared from six different batches, as represented in Table 3.2, all following the preparation route described in section 3.2.2. For one of the 20 pellets, traces indicating peritectic decomposition on the surface of the pellet was also observed.

The phase pure powder of $YbFe_2O_4$ was obtained by annealing one of the pellets from batch 1, and both pellets prepared from batch 2, at 1300°C in N_2 atmosphere. The second pellet prepared from batch 1 was observed to have traces of a peritectic decomposition on the surface. $YbFe_2O_4$ was later prepared from four additional batches (3-6), where the same phase pure powder was not obtained. All these powders were observed to contain a secondary phase, and the secondary phase did not disappear after a second heat treatment at 1300°C in N_2 atmosphere.

In Figure 4.2, powder resulting from one pellet from each batch is displayed. The phase pure powder obtained from batch 1 and 2 are represented in the figure with the powder obtained from one of the two pellets obtained from batch 2.

From the results shown in this figure, it can be seen that the amount of secondary phase present, correlates with the amount of powder prepared in each batch.

The amount of secondary phase present in the $YbFe_2O_4$ materials, was also observed to differ between powders produced from the same batch, but not annealed simultaneously in the furnace. The results obtained for four different pellets prepared from the same batch, annealed in two different cycles are given in Figure 4.3 where pellet 1 and pellet 2 were annealed simultaneously. Pellet 3 and 4 were also annealed simultaneously, but at a different time than 1 and 2. Clear differences can be observed regarding the amount of secondary phase present in the different powders obtained. The secondary phase present is indicated by the black bullets.

The secondary phase present was found to be $Yb_2Fe_3O_7$ by the use of the DIFFEAC EVA V3.0 software, and is indicated in Figure C.1 for powder prepared from batch 5, used in the dilatometry measurement.

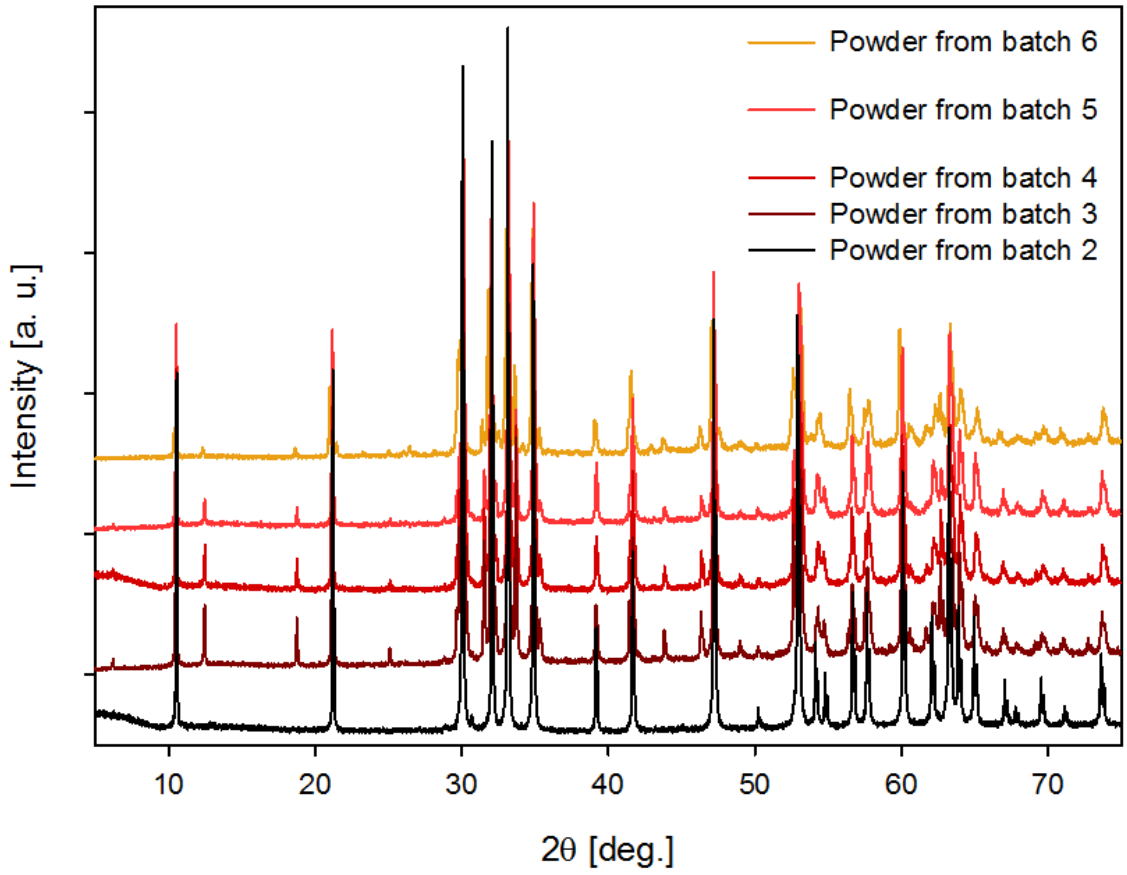

Figure 4.2: XRD diffractograms obtained for pellets prepared from the six different batches of $YbFe_2O_4$. The degree of phase purity of the powders obtained from the different pellets is displayed. Preparation of powder from batch 5 and 6 both gave a phase pure powders and are therefore represented with the diffractogram obtained from batch 6.

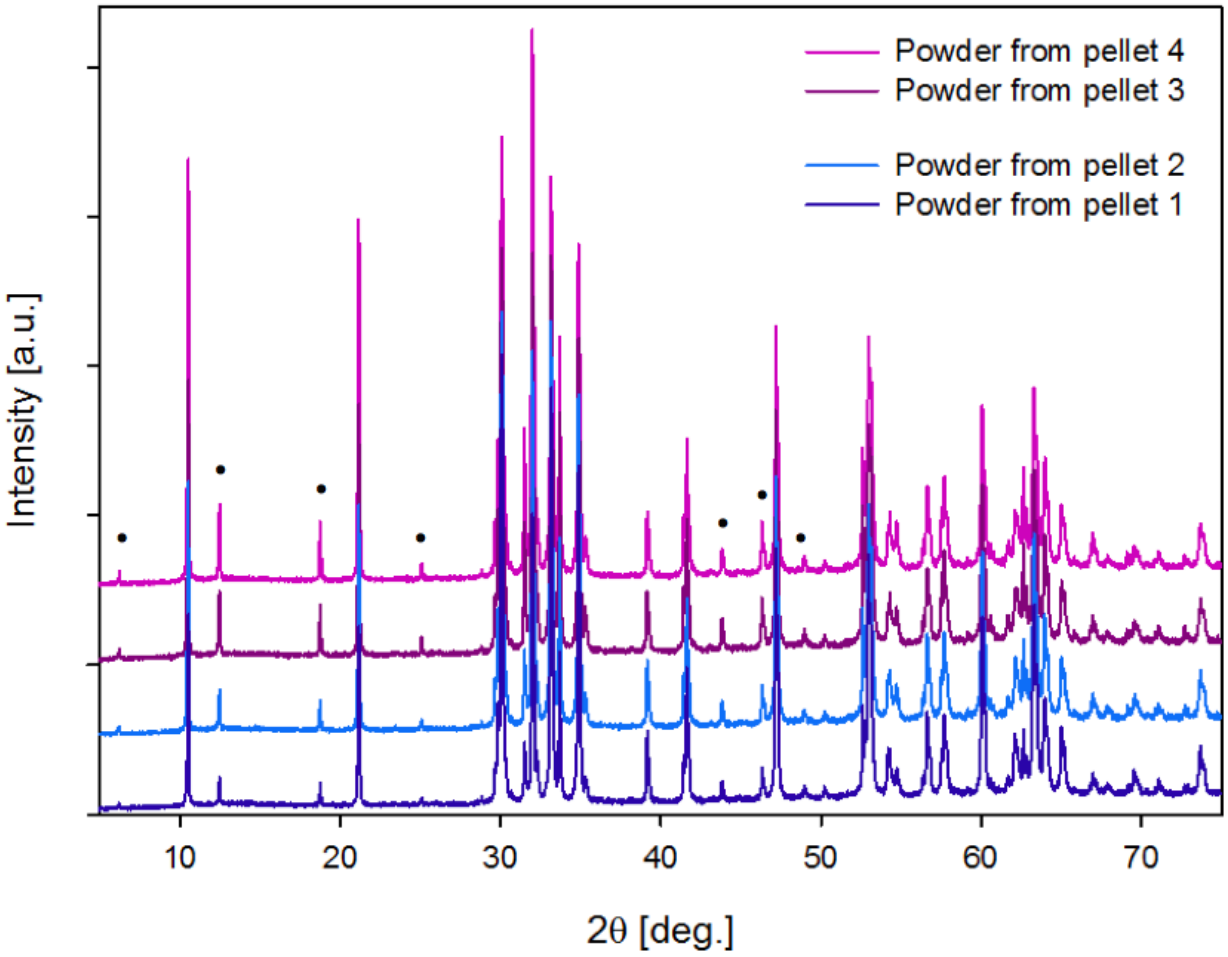

Figure 4.3: XRD diffractograms of powders obtained for pellets prepared from the same batch annealed at 1300°C in N_2 atmosphere. Pellet 1 and 2 were annealed simultaneously in the furnace. Pellet 3 and 4 were also annealed simultaneously, but at a different time than 1 and 2. The most pronounced reflections indicating the presence of the secondary phase, is given by the black bullets.

4.1.3 Preparation of $YbFe_2O_4$ by sol-gel synthesis

In order to study the possibility of making a thin film for preparation of an asymmetric oxygen permeable membrane consistent of a thin film and a porous support, a sol-gel synthesis was performed to investigate if this could result in phase pure $YbFe_2O_4$ powder. Some of the steps involved in this process is given in Figure 3.7, and the detailed information about the synthesis and different heat treatments is given in section 3.3.1. The raw powder obtained was first annealed in air followed by annealing in 3% H_2/Ar atmosphere as given in Figure 3.9(a), resulting in a powder containing metallic iron, indicating too reducing conditions. Annealing of the powder in air followed by annealing at 1300 °C in N_2, Figure 3.9(b), resulted in decomposition of the material indicating that the temperature was too high. Annealing in air followed by annealing at 900°C in N_2 atmosphere resulted in a powder that was almost completely phase pure. The XRD diffractogram of this powder is given in Figure 4.4 together with the phase pure powder obtained from the solid state synthesis route discussed in section 4.1.2. The impurity observed in the sol-gel powder was found to be Yb_2O_3 by the use of the DIFFRAC.EVA V3.0 PDF card (00-043-1037), and the peak positions of the secondary phase are indicated in the diffractogram. The amount of the secondary phase present was found to be 7.95% by an investigation of this phase by rietveld refinement. The additional reflection observed at a 2θ angle of 44.65 was not found to originate from the Yb_2O_3 structure, and could not be identified from the DIFFRAC.EVA V3.0 software.

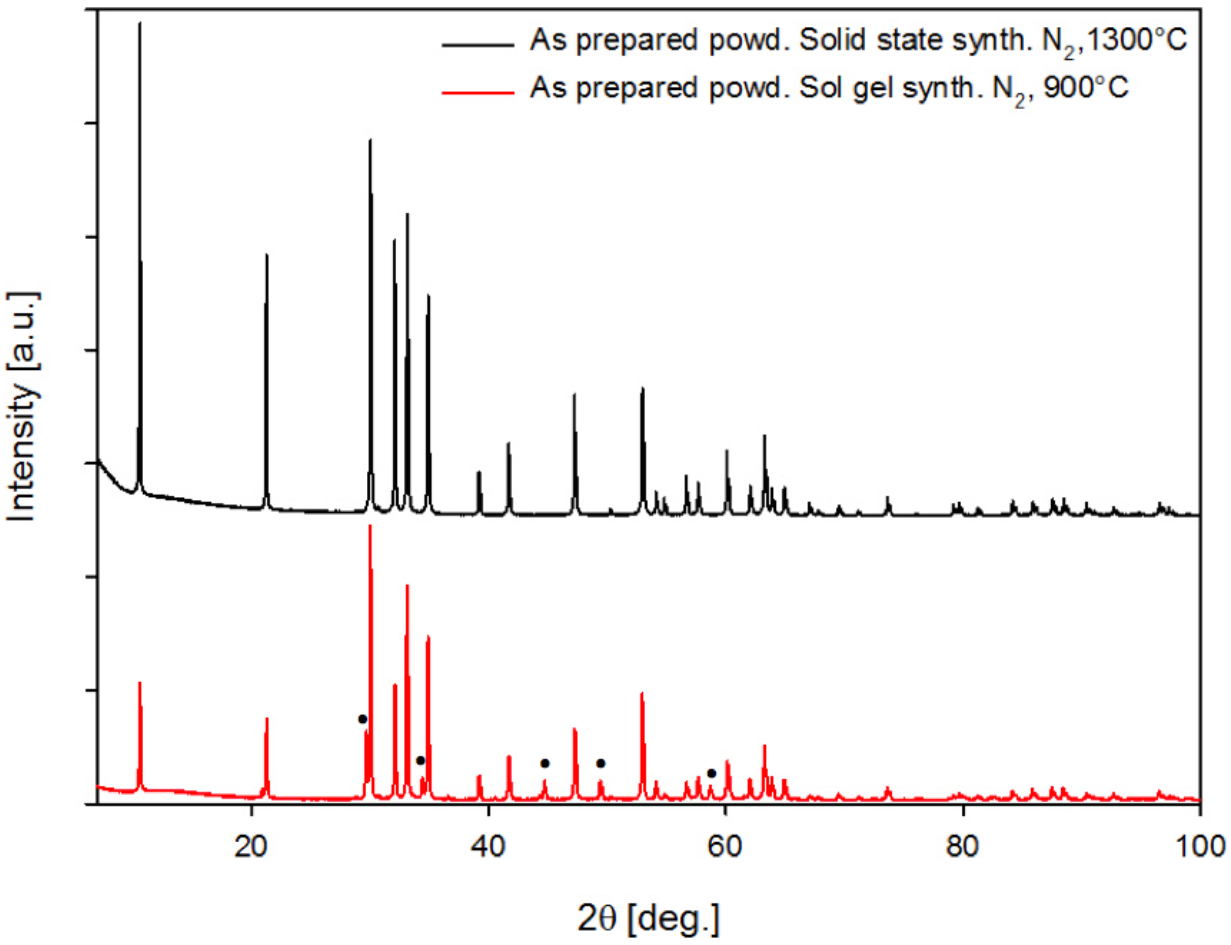

Figure 4.4: Almost completely phase pure $YbFe_2O_4$ powder obtained by sol-gel synthesis calcined at 900°C in N_2 atmosphere, compared to the phase pure as prepared powder obtained from solid state synthesis. The impurities observed in the as prepared powder obtained by sol-gel synthesis, indicated by the black bullets, was found to be Yb_2O_3 by comparing the diffractogram to the DIFFRAC.EVA V3.0 pdf card (04-001-2438). The impurity observed at a 2θ angle of 44.65 could not be identified by the software.

4.2 Structural changes under heat treatment in different atmospheres

In order to study the structural changes upon heat treatment under oxidizing conditions, phase pure powder of $YbFe_2O_4$ was heat treated in oxygen atmosphere at two different temperatures, as reported in section 3.2.5. The two different heat treatments resulted in two identical XRD diffractograms, and are therefore represented in Figure 4.5 with the diffractogram obtained from the heat treatment at 500°C. The phase pure as prepared powder obtained by solid state synthesis is also given in the figure. When heat treated in oxygen atmosphere, a significant change in structure is observed. It can be seen that the number of reflections significantly decreases, and that the four most pronounced reflections at the 2θ range between 28 and 36 are drawn close together.

After heat treatment in oxygen atmosphere, the possibility of reducing the powder back to its original structure was investigated by heating the oxygen rich powder obtained, under reducing conditions. The powder was heat treated in 10% H_2/Ar atmosphere as described in section 3.2.5. The heat treatment of the oxygen rich structure at 600°C resulted in a powder containing metallic iron, indicating that the temperature used was too high. By reducing the temperature to 500°C, a reduction back to the original structure was observed. The XRD diffractogram obtained after this reduction is given in Figure 4.5 together with the as prepared powder obtained by solid state synthesis, and the oxygen rich powder obtained from heat treatment in oxygen atmosphere. The reduced powder is observed to obtain the same structure as the original as prepared powder, although some differences can be observed when comparing with this diffractogram. Especially the intensity of the four most pronounced reflections in the 28-36 2θ range is observed to be altered to some extent.

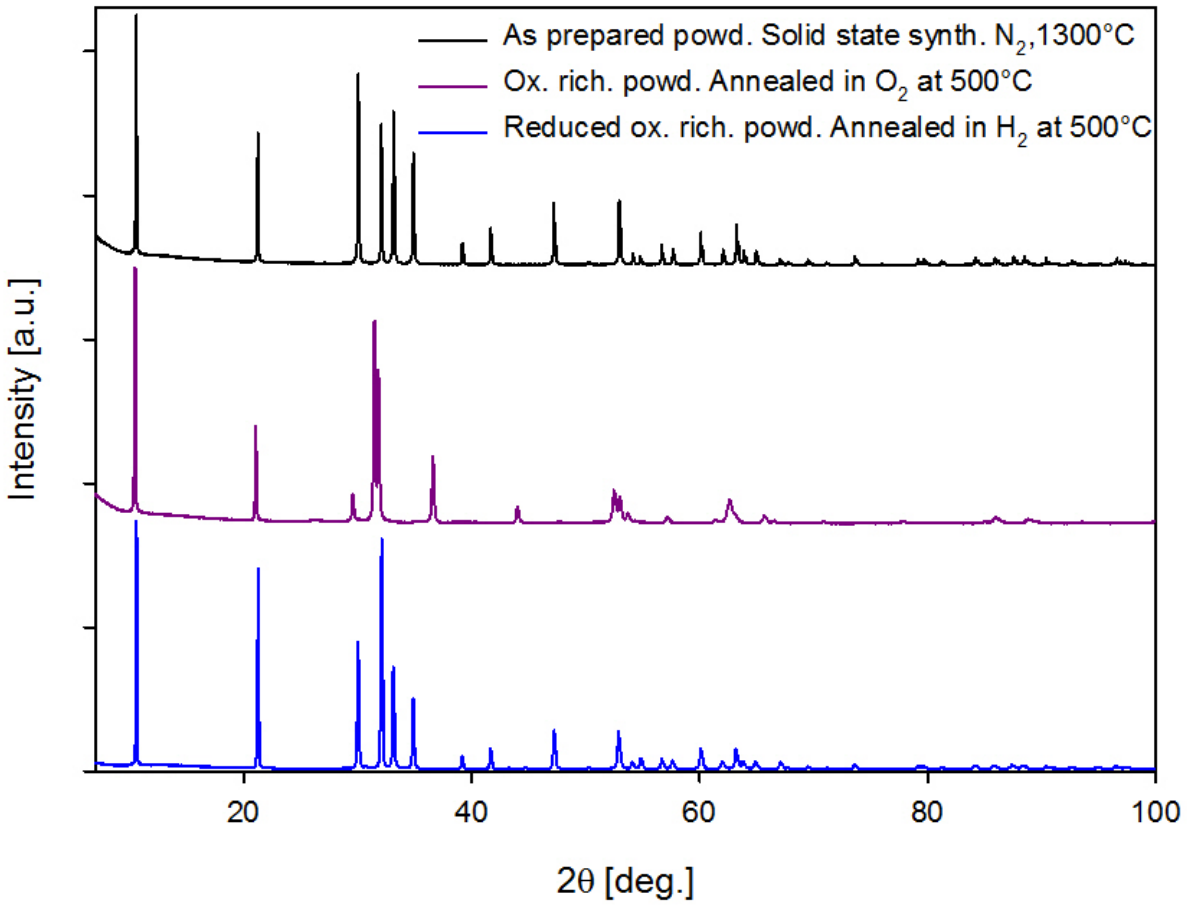

Figure 4.5: A representation of the differences in XRD diffractograms obtained after heat treatment of the as prepared powder from solid state synthesis in different atmospheres.

4.3 Structure parameters obtained from Rietveld refinement

In order to investigate the structure in more detail, Rietveld refinement was performed on both the as prepared powder and reduced powder obtained from solid state synthesis, as well as the as prepared powder obtained by sol-gel synthesis. The oxygen rich powder was refined by the use of an hkl phase as the atomic positions are not previously known for this phase, neither for $YbFe_2O_4$, nor the other rare earth ferrites. The instrumental details used in the refinement are given in section 3.6.2.

The results from the Rietveld refinement of the as prepared powder obtained by solid state synthesis, the oxygen rich powder and the reduced oxygen rich powder are given in Figure 4.6, Figure 4.7 and Figure 4.8, respectively, while the results from the Rietveld refinement of the as prepared powder obtained from sol-gel synthesis is given in Figure 4.9. It can be seen in these figures that by refining the diffractograms obtained from the different powders with the instrumental settings given in section 3.6.2, a good correlation was found. All the structure parameters obtained in the refinement are given in Table 4.1, while all the atomic positions are given in Table 4.2.

The as prepared powder obtained from the sol-gel synthesis route contained a secondary phase which was found to be Yb_2O_3. The refinement of this powder was therefore conducted by the use of both the $YbFe_2O_4$ structure within the $C2/m$ space group, and Yb_2O_3 within the $Ia3$ space group. In the refinement, the amount of Yb_2O_3 present in the sample was found to be 7.95%

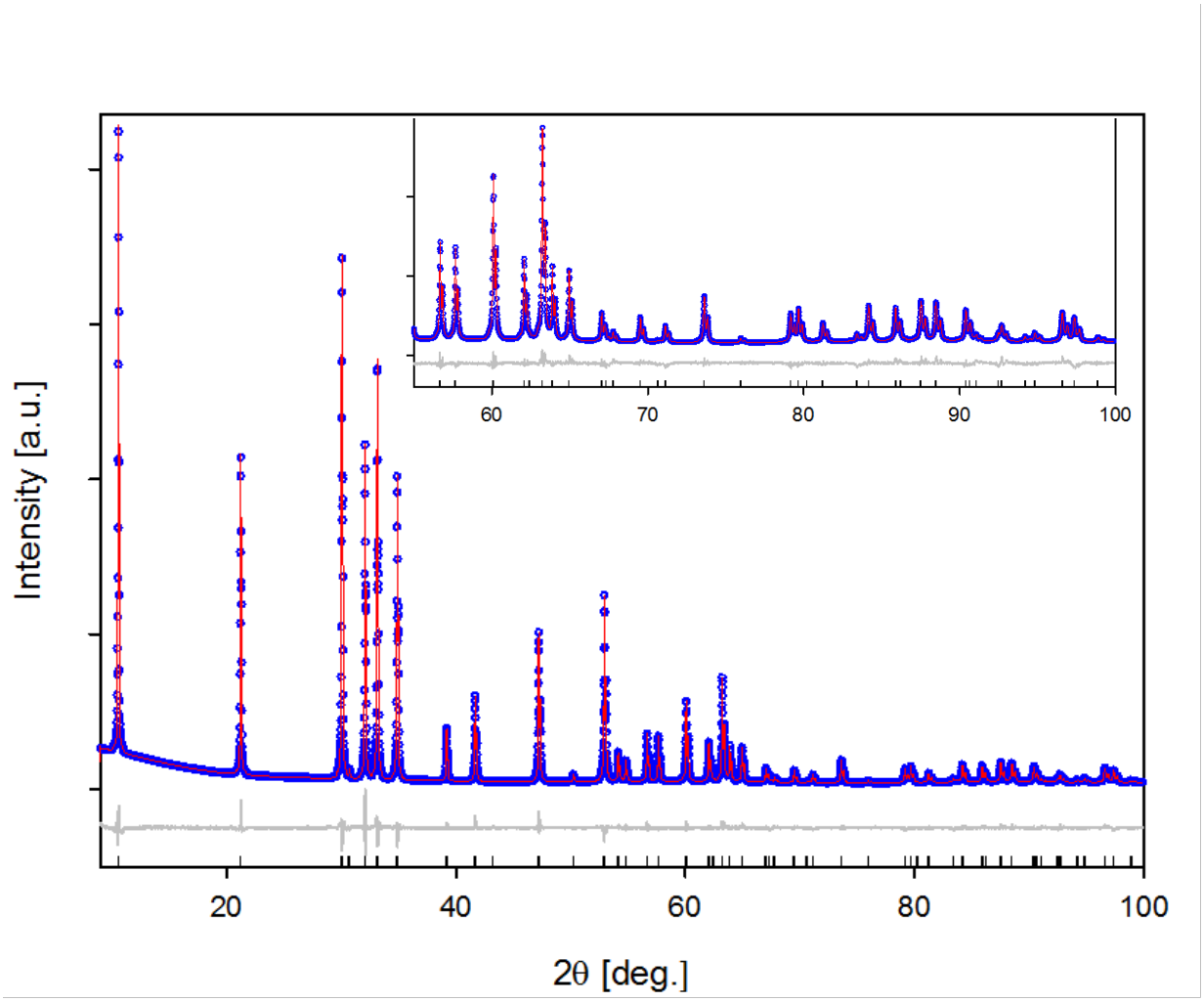

Figure 4.6: Rietveld refinement of the as prepared powder obtained from solid state synthesis. The refinement was performed within the space group $C2/m$ with structural details taken from Bourgeois [23].

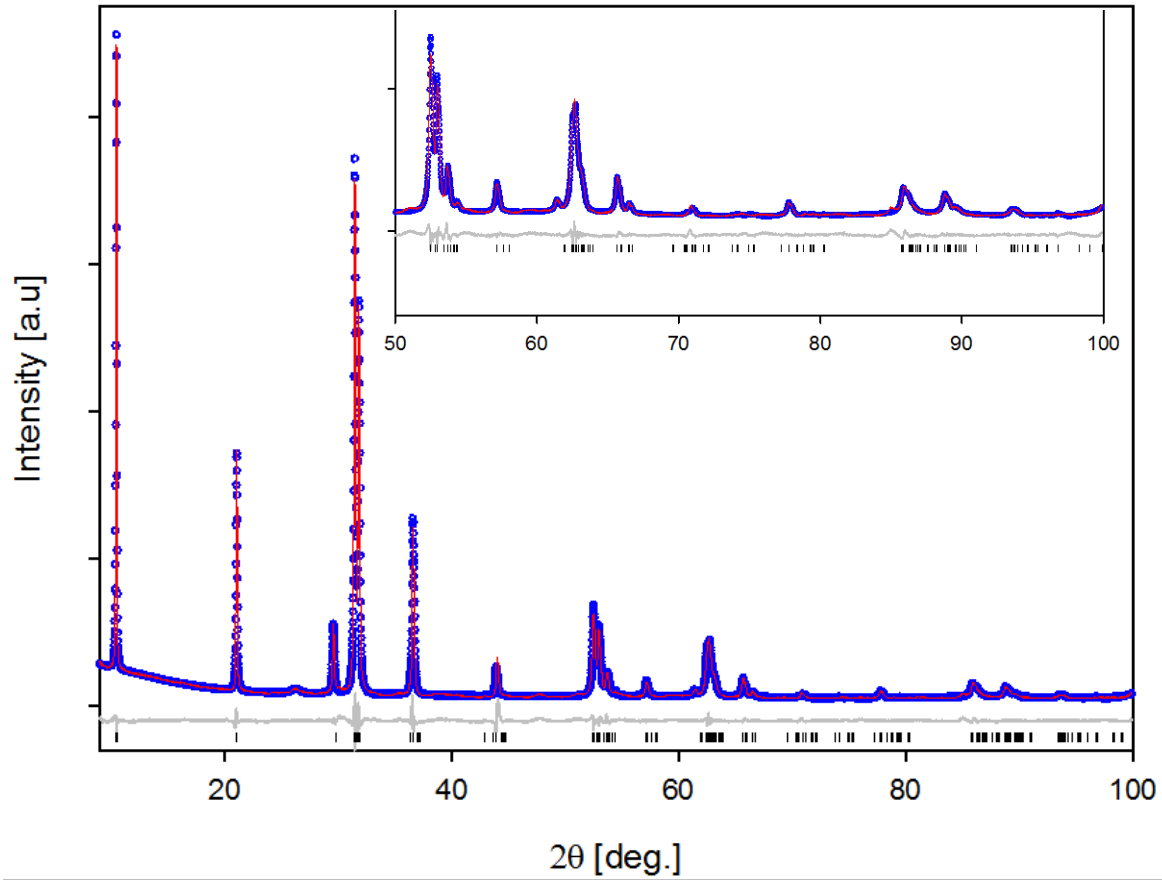

Figure 4.7: Rietveld refinement of the oxygen rich powder. The refinement was performed within the $C2/m$ space group with structural details taken from Hervieu et al.[12]. The diffractogram was fitted using an hkl phase as the atomic positions were difficult to obtain for the oxygen rich phase.

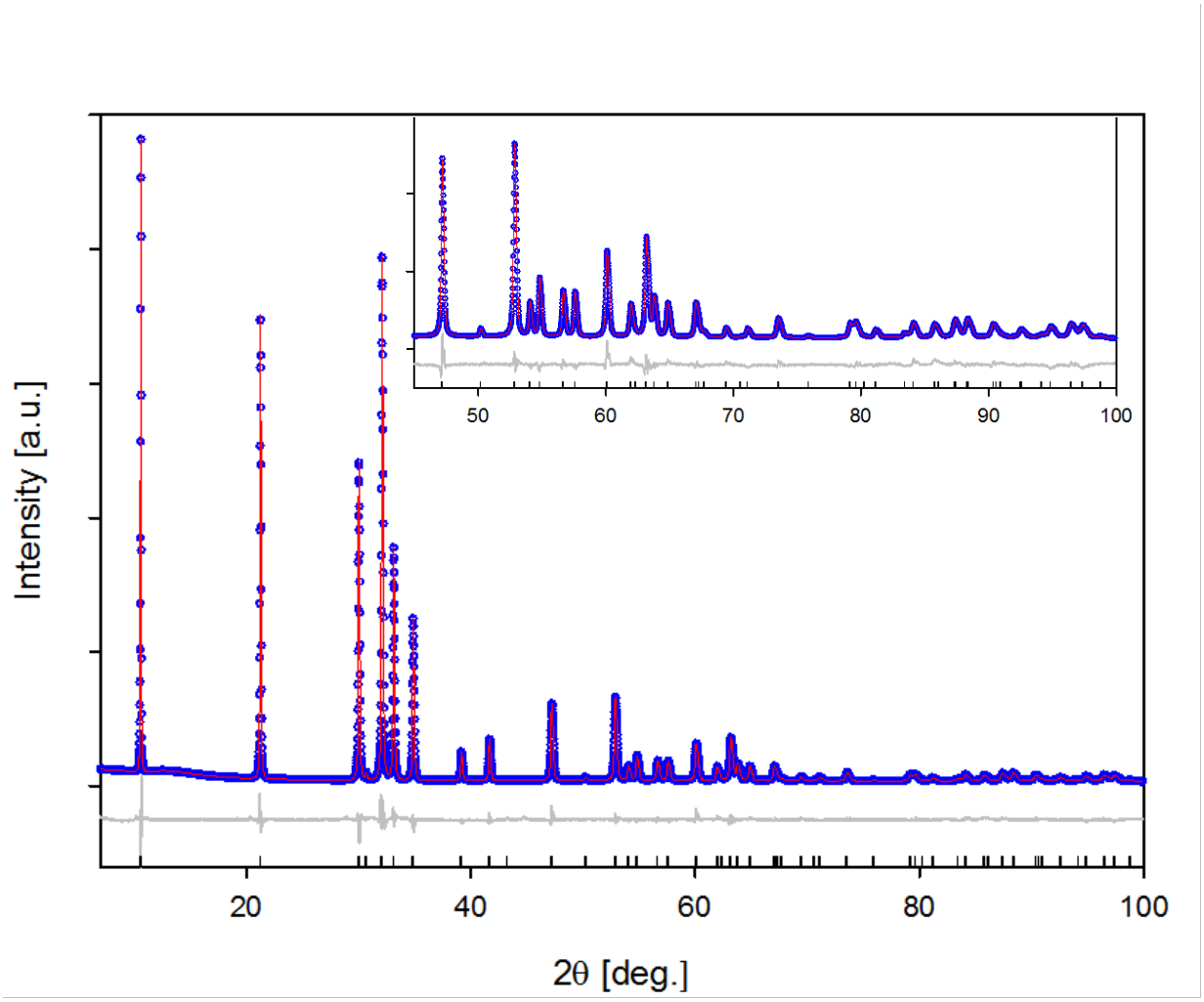

Figure 4.8: Rietveld refinement of the reduced oxygen rich powder. The refinement was performed within the $C2/m$ space group with structural details taken from Bourgeois [23].

Table 4.1: The different structure parameters obtained in the Rietveld refinement of the four different powders obtained in this study. The as prepared powder obtained from sol-gel synthesis was refined within the *C*2/*m* and the *Ia*3 space group since a secondary phase of Yb_2O_3 was found in this powder.

As prepared powder, solid state		**Oxygen rich powder**	
Structure parameter	*Value*	*Structure parameter*	*Value*
a[Å]	5.989(5)	a[Å]	5.98(8)
b[Å]	3.457(7)	b[Å]	3.455(4)
c[Å]	8.605(4)	c[Å]	10.23(0)
β [°]	103.4(1)	β [°]	124.50(4)
V[Å^3]	173.36(5)	V[Å^3]	174.4(5)
Lorentzian strain	0.1(1)	Lorentzian strain	0.1(1)
Lorentzian crystal size [nm]	640 ± 110	Lorentzian crystal size [nm]	640 ± 110
R_{wp}	5.00	R_{wp}	6.971

Reduced oxygen rich powder	
Structure parameter	*Value*
a[Å]	5.99(5)
b[Å]	3.46(4)
c[Å]	8.604(6)
β [°]	103.4(2)
V[Å^3]	173.(8)
Lorentzian strain	0.2(4)
Lorentzian crystal size [nm]	-
R_{wp}	7.513

As prepared powder, sol-gel, *C*2/*m*		**As prepared powder, sol-gel, *Ia*3**	
Structure parameter	*Value*	*Structure parameter*	*Value*
a[Å]	5.99(2)	a[Å]	10.432(6)
b[Å]	3.459(6)	b[Å]	10.432(6)
c[Å]	8.59(9)	c[Å]	10.432(6)
β [°]	103.36(2)	–	–
V[Å^3]	173.4(3)	V[Å^3]	1135.(4)
Lorentzian strain	0.02(2)	Lorentzian strain	–
Lorentzian crystal size [nm]	195.2 ± 3.7	Lorentzian crystal size [nm]	117.1 ± 2.5
R_{wp}	8,196	R_{wp}	8,196

Table 4.2: The atomic positions obtained for the as prepared powder from solid state synthesis, the reduced oxygen rich powder and the as prepared powder from sol-gel synthesis. The refinement of the as prepared powder obtained from sol-gel synthesis was refined both within the *C*2/*m* and the *Ia*3 space group since a secondary phase of Yb_2O_3 was found in this powder. A refinement of the atomic positions in the oxygen rich powder could not be performed because input data could not be obtain.

As prepared powder, solid state

Site	*Np*	*x*	*y*	*z*	*Occupancy*	*Beq*
Yb	2	0.00000	0.00000	0.00000	1	0.732 ± 0.023
Fe	4	0.23(3)	0.00000	0.645(7)	1	0.358 ± 0.049
O1	4	0.3(2)	0.00000	0.88(6)	1	0.96 ± 0.15
O2	4	0.1(6)	0.00000	0.38(4)	1	0.65 ± 0.17

Reduced oxygen rich powder

Site	*Np*	*x*	*y*	*z*	*Occupancy*	*Beq*
Yb	2	0.00000	0.00000	0.00000	1	0.916 ± 0.032
Fe	4	0.2(2)	0.00000	0.64(4)	1	0.698 ± 0.046
O1	4	0.3(1)	0.00000	0.88(5)	1	0.698 ± 0.046
O2	4	0.08(1)	0.00000	0.38(1)	1	0.698 ± 0.046

As prepared powder, sol-gel, $YbFe_2O_4$, *C*2/*m*

Site	*Np*	*x*	*y*	*z*	*Occupancy*	*Beq*
Yb	2	0.00000	0.00000	0.00000	1	1.636 ± 0.032
Fe	4	0.21(4)	0.00000	0.644(5)	1	1.030 ± 0.043
O1	4	0.2(9)	0.00000	0.87(9)	1	1.030 ± 0.043
O2	4	0.08(2)	0.00000	0.38(5)	1	1.030 ± 0.043

As prepared powder, sol-gel, Yb_2O_3, *Ia*3

Site	*Np*	*x*	*y*	*z*	*Occupancy*	*Beq*
Yb1	2	0.25000	0.25000	0.25000	1	1.10± 0.11
Yb2	4	0.96(8)	0.00000	0.25000	1	1.10 ± 0.11
O	4	0.09(1)	0.1(1)	0.3(4)	1	1.10 ± 0.11

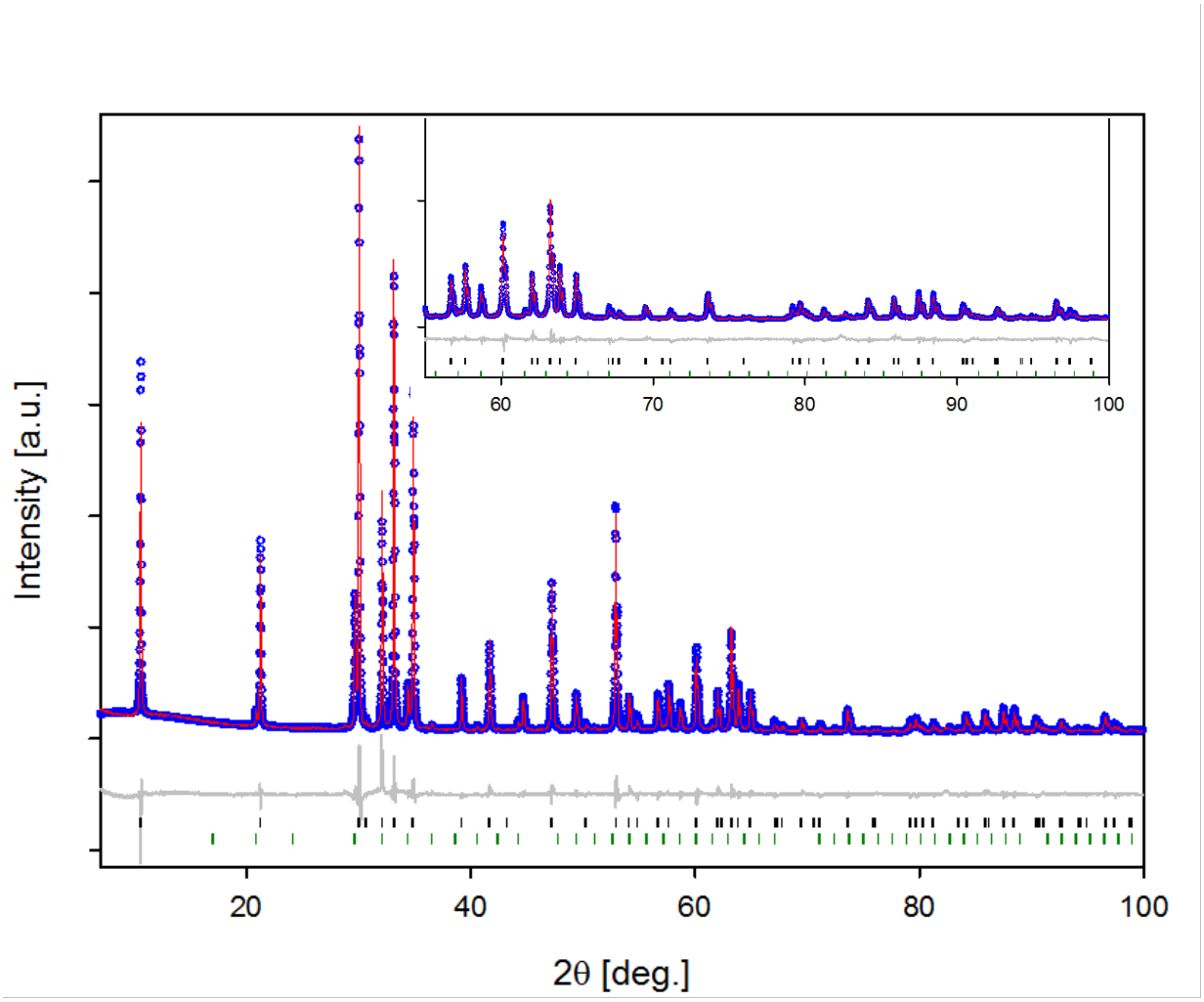

Figure 4.9: Rietveld refinement of the as prepared powder obtained from sol-gel synthesis. The refinement was performed for $YbFe_2O_4$ within the $C2/m$ space group with structural details taken from Bourgeois [23] and for Yb_2O_3 within the $Ia3$ space group with structural details taken from Schleid et al. [37].

4.3.1 Changes in lattice parameters after heat treatment in O_2 atmosphere

The difference in the lattice parameters as a result of heat treatment of $YbFe_2O_4$ in O_2 and 10%H_2/Ar atmosphere is given in Figure 4.10. In the figure it is observed that the a and b lattice parameters remain relatively stable when the material is heat treated in different atmospheres. The unit cell volume is also observed to remain relatively stable, while a large increase in the c-axis and the β angle is observed after heat treatment in O_2 atmosphere. After heat treatment in reducing atmosphere, both the c-axis and the β angle is observed to retain to their original values.

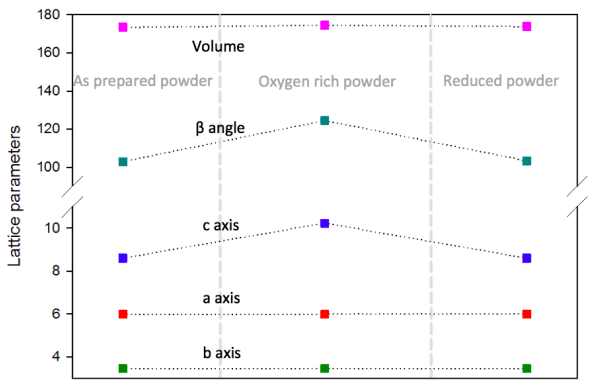

(a) Overview

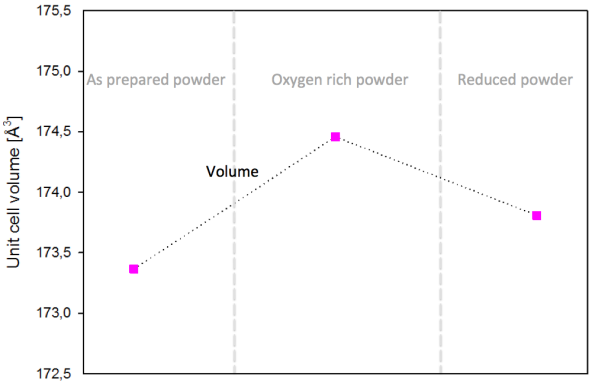

(b) Unit cell volume

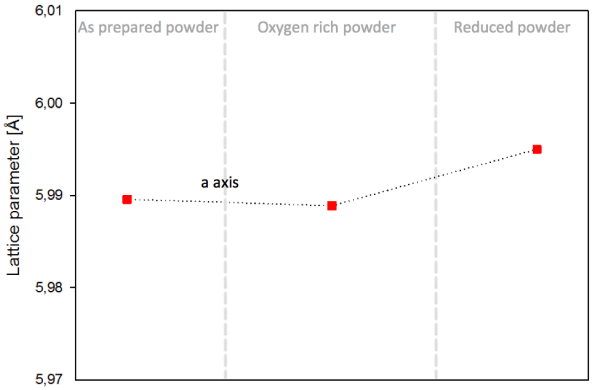

(c) a-axis parameter

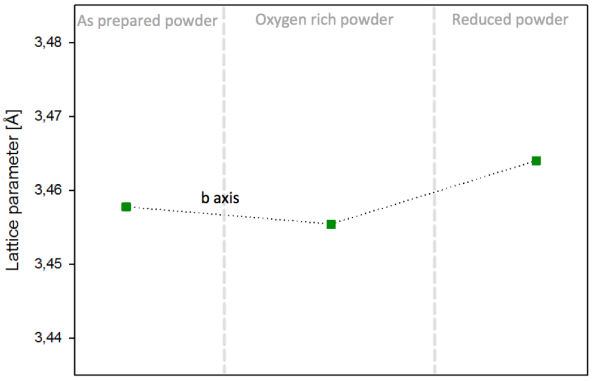

(d) b-axis parameter

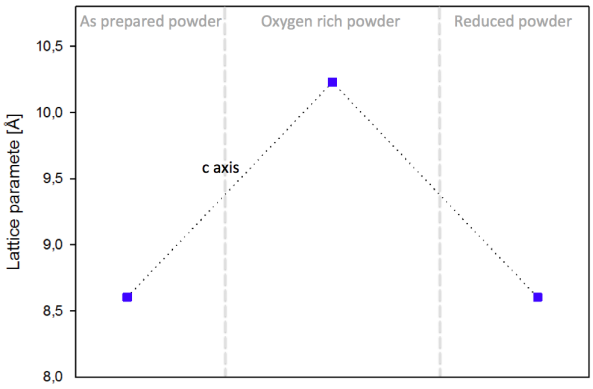

(e) c-axis parameter

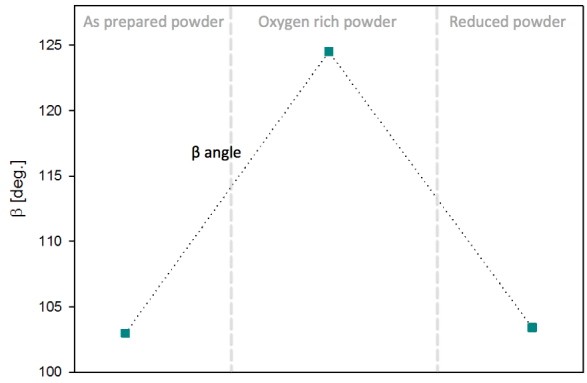

(f) β angle

Figure 4.10: A representation of the changes in lattice parameters obtained after heat treatment of as prepared powder obtained from solid state synthesis in different atmospheres. The structure parameters are obtained from the Rietveld refinement of the different powders. An overview of the changes observed in all the different lattice parameters is given in (a), while the changes observed in each of the parameters individually, are given in (b)-(f).

4.4 Oxygen storage ability

TGA measurements of both the as prepared powder and the oxygen rich sample obtained from solid state synthesis were performed in O_2 atmosphere in accordance with the temperature program given in Table 3.7. The objective was to quantify the mass gain during heat treatment in oxygen rich atmosphere.

4.4.1 Oxygen storage ability of as prepared powder from solid state synthesis

The TGA results for the as prepared powder are given in Figure 4.11. As can be seen in this figure, the mass increases significantly when the material is heated from room temperature to 600°C. An increase in mass of close to 2.5 percent is observed, and the oxygen rich phase obtained, remains stable both during cooling back to room temperature, and a second heating and cooling cycle.

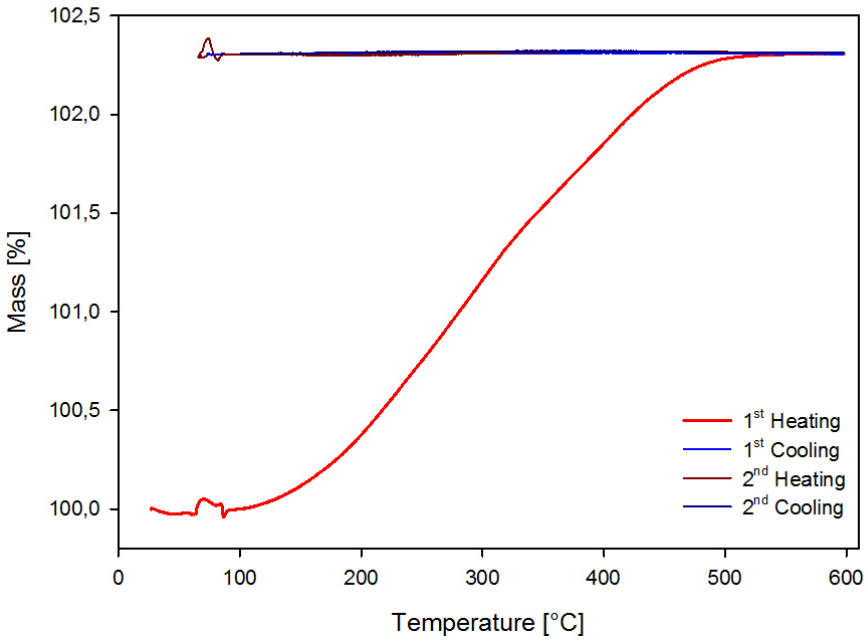

Figure 4.11: The results obtained from the TGA measurement of the as prepared powder obtained from solid state synthesis performed in O_2 atmosphere. An increase inn mass of approximately 2.5 % is observed during the first heating, while the material remains stable during cooling back to room temperature and a second heating and cooling cycle.

4.4.2 Oxygen storage ability of oxygen rich powder

The results obtained from the TGA measurement performed on the oxygen rich powder obtained by heat treatment of the as prepared powder from solid state synthesis at 500°C in O_2 atmosphere is given in Figure 4.12. It can be seen that the mass decreases slightly during the first heating, while it remains steady during cooling back to room temperature and the second cycle. The mass loss observed during the first heat treatment is assumed to originate from evaporation of water or other impurities adsorbed to the crucible, and the oxygen rich powder is therefore assumed to be stable during the whole measurement performed in oxygen atmosphere in accordance with the results displayed in Figure 4.11.

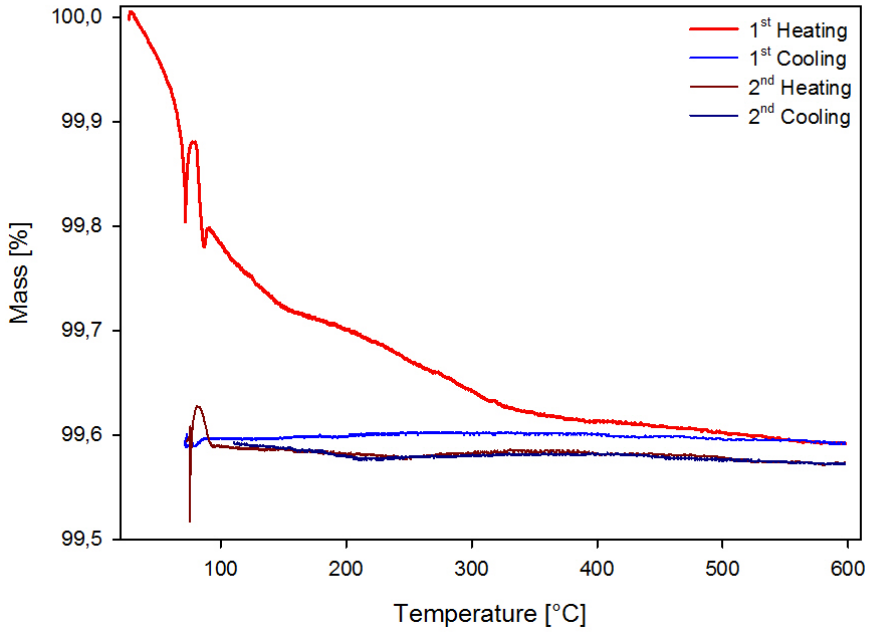

Figure 4.12: The results obtained from the TGA measurement of the oxygen rich powder performed in O_2 atmosphere. A decrease in mass is observed when the material is heated in oxygen atmosphere. This is assumed to originate from water or other impurities evaporating from the crucible, and the powder therefore assumed to be stable during the entire measurement.

4.5 Dilatometry

The results obtained from the dilatometry measurement of $YbFe_2O_4$ are given in Figure 4.13. The measurement was performed in N_2 atmosphere on a 5 mm pellet of $YbFe_2O_4$ prepared from solid state synthesis with the temperature program given in Table 3.8. The powder used in the dilatometry measurement was not completely phase pure, and the XRD diffractogram of the powder used in the preparation of the pellet is given in Figure C.1, where a secondary phase of $Yb_2Fe_3O_7$ was observed. The data show an unexpected behavior up to approximately 750°C, where the material expands upon heating. A sudden decrease follow, before a more familiar curve where a decrease in volume appears when heating above 900°C, as indicated by the red box. The slope indicating a sudden shrinkage in volume around 50°C is expected to be a measurement artifact.

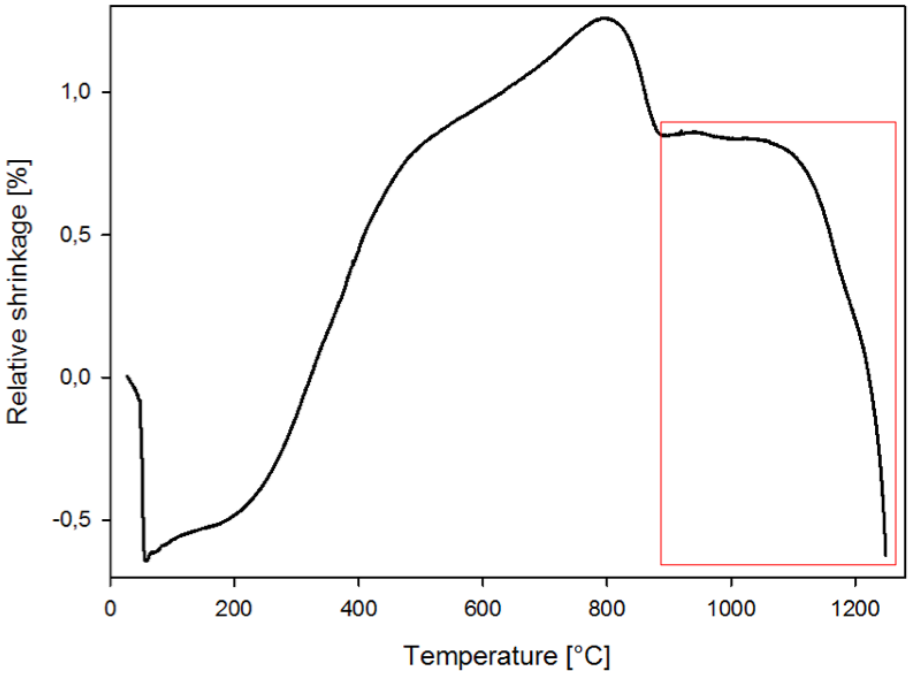

Figure 4.13: The results obtained from the dilatometry measurement performed in N_2 atmosphere on a 5 mm pellet prepared from as prepared $YbFe_2O_4$ made from solid state synthesis. An unexpected expansion of the material is observed when the powder is heated in N_2 atmosphere. A sudden decrease follows before a more expected behavior is observed when the temperature exceeds 900°C, indicated by the red box.

4.5.1 Density measurements

By the use of the unit cell volume obtained in the Rietveld refinement of the as prepared powder of $YbFe_2O_4$, the theoretical density of the material was found to be 6.68 g/cm^3. By calculating the density of the different pellets prepared in this study, an average density of 4.76 g/cm^3 was obtained. This is consistent with an average density of 71.2% of theoretical density. This density was determined from three different pellets prepared from the same batch heat treated simultaneously, and are therefore assumed to have experienced the same pO_2 pressure and temperature. The pellets were all annealed in nitrogen atmosphere in accordance with Figure 3.12, at 1300°C.

4.6 Conductivity

In order to investigate the conductivity of $YbFe_2O_4$, measurements by the use of a van der Pauw setup was performed. A 15 mm pellet was uniaxially pressed and sintered as described in section 3.7, and the measurement performed with the temperature program given in Table 3.9.

In Figure 4.14, the surface of the pellet used in the conductivity measurement is displayed. The surface is observed to consist of large grains and to be relatively dense, with only small indications of pore formation along some of the grain boundaries. The density of the pellet was found to be 91.6% of the theoretical density. During the conductivity measurement, contact problems were a recurring issue, and the data is occasionally affected by heavy noise. An overview of the total response obtained in the measurement is given in Figure B.1.

A more detailed representation of the response obtained when the atmosphere was changed from oxygen to nitrogen, and later back to oxygen is given in Figure 4.15. A change in temperature is observed when a change in atmosphere takes place, as well as a change in conductivity. Both the temperature and the conductivity is observed to decrease when the atmosphere changes from O_2 to N_2 atmosphere, while the opposite is observed when changing from N_2 to O_2 atmosphere.

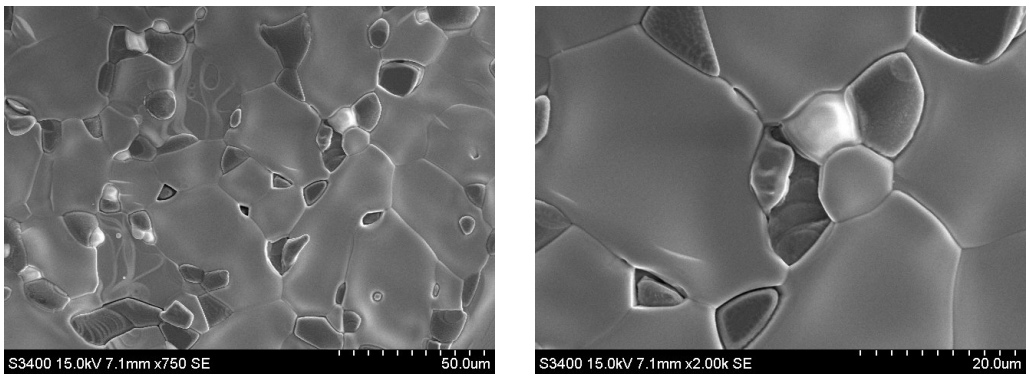

(a) (b)

Figure 4.14: (a) SEM images displaying the surface of the pellet used in the conductivity measurement.

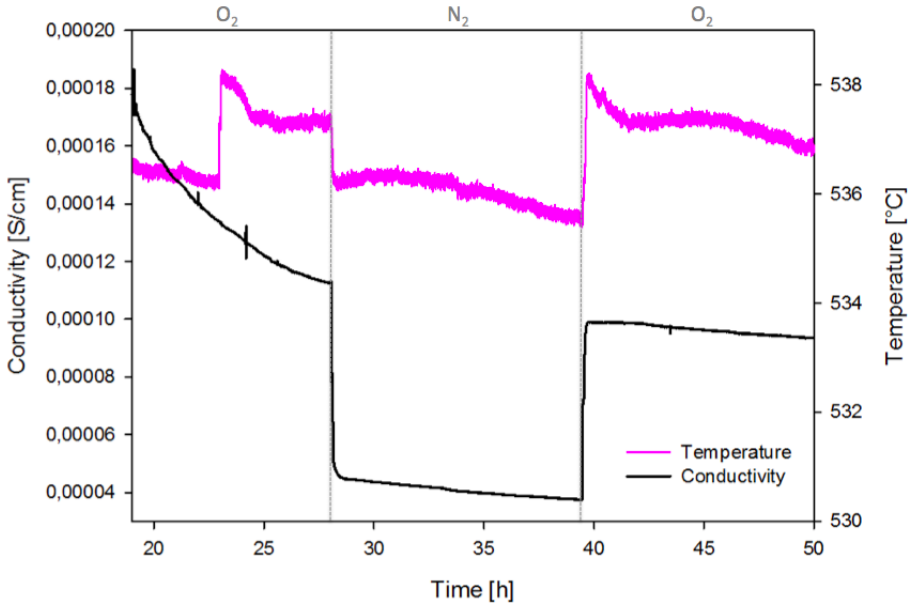

Figure 4.15: An overview of the data response obtained during the conductivity measurement performed in alternating N_2 and O_2 atmosphere. A decrease in conductivity,as well as a decrease in temperature is observed when changing from O_2 to N_2 atmosphere. When changing back to O_2 atmosphere, an increase in conductivity, as well as an increase in temperature is observed.

A closer inspection of the increase and decrease in conductivity and temperature as a response to the changes in atmosphere is given in Figure 4.16. In Figure 4.16(a) the decrease in conductivity is observed when changing from O_2 to N_2, as well as a decrease in temperature, while an increase in both is displayed when going from N_2 to O_2, as given in Figure 4.16(b).

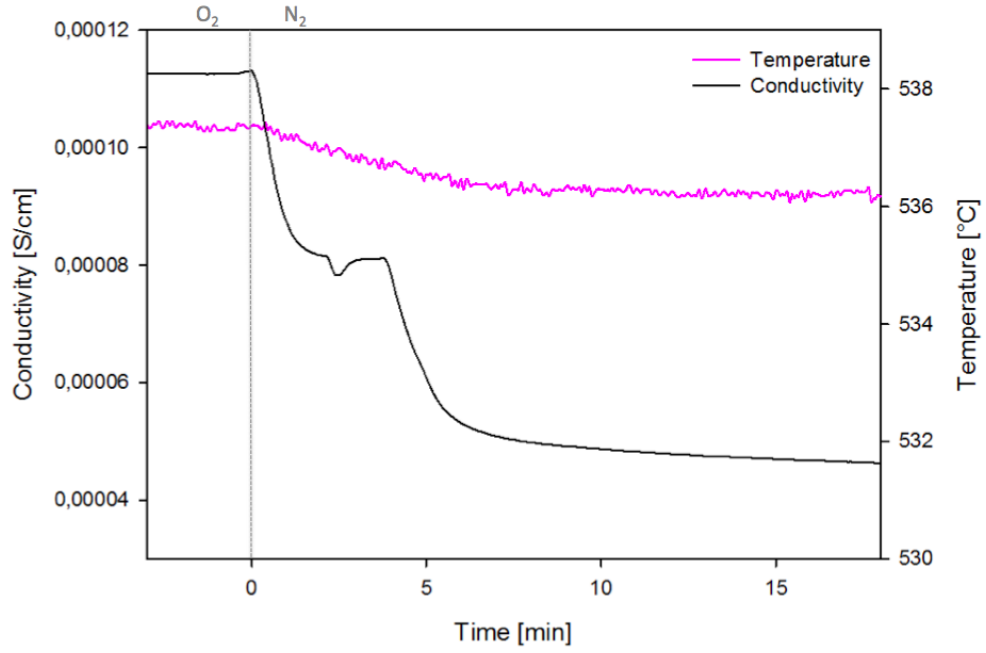

(a)

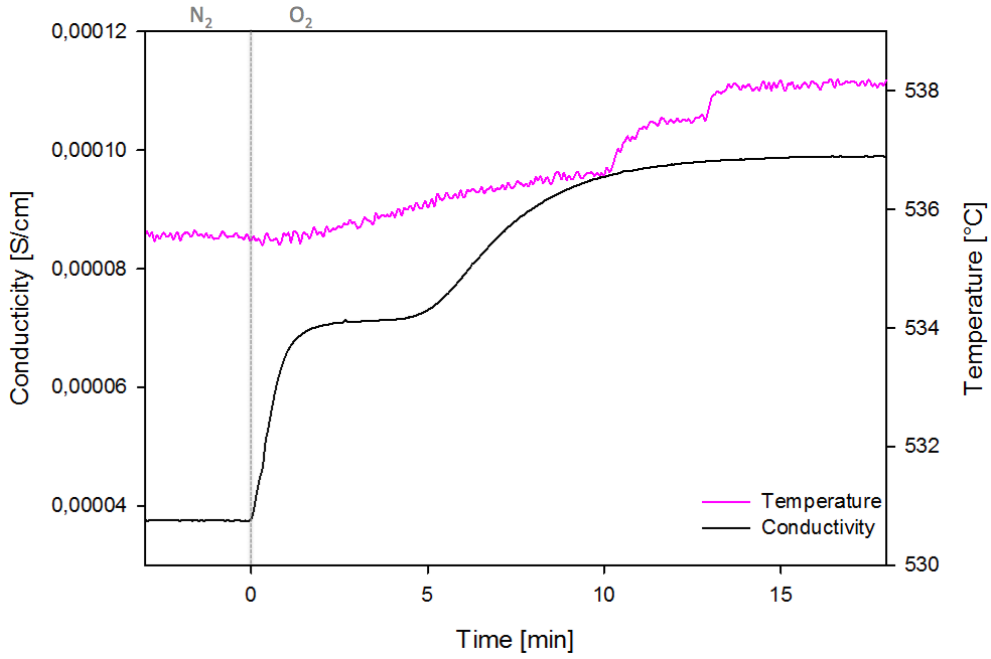

(b)

Figure 4.16: A more detailed representation of the changes in conductivity observed when the atmosphere is altered between O_2 and N_2 atmosphere. The change observed when changing from O_2 to N_2 is given in (a), while the change in conductivity taking place when changing from N_2 to O_2 is given in (b).

4.7 Porous support

Porous supports were prepared from the preparation route described in section 3.4. When the supports were heat treated in air to remove the charcoal activated followed by a sintering step in N_2 atmosphere in accordance with the temperature program given in 3.10, the original structure of the as prepared powder was not retained. A representation of the obtained structure after sintering in nitrogen atmosphere is given in Figure 4.17.

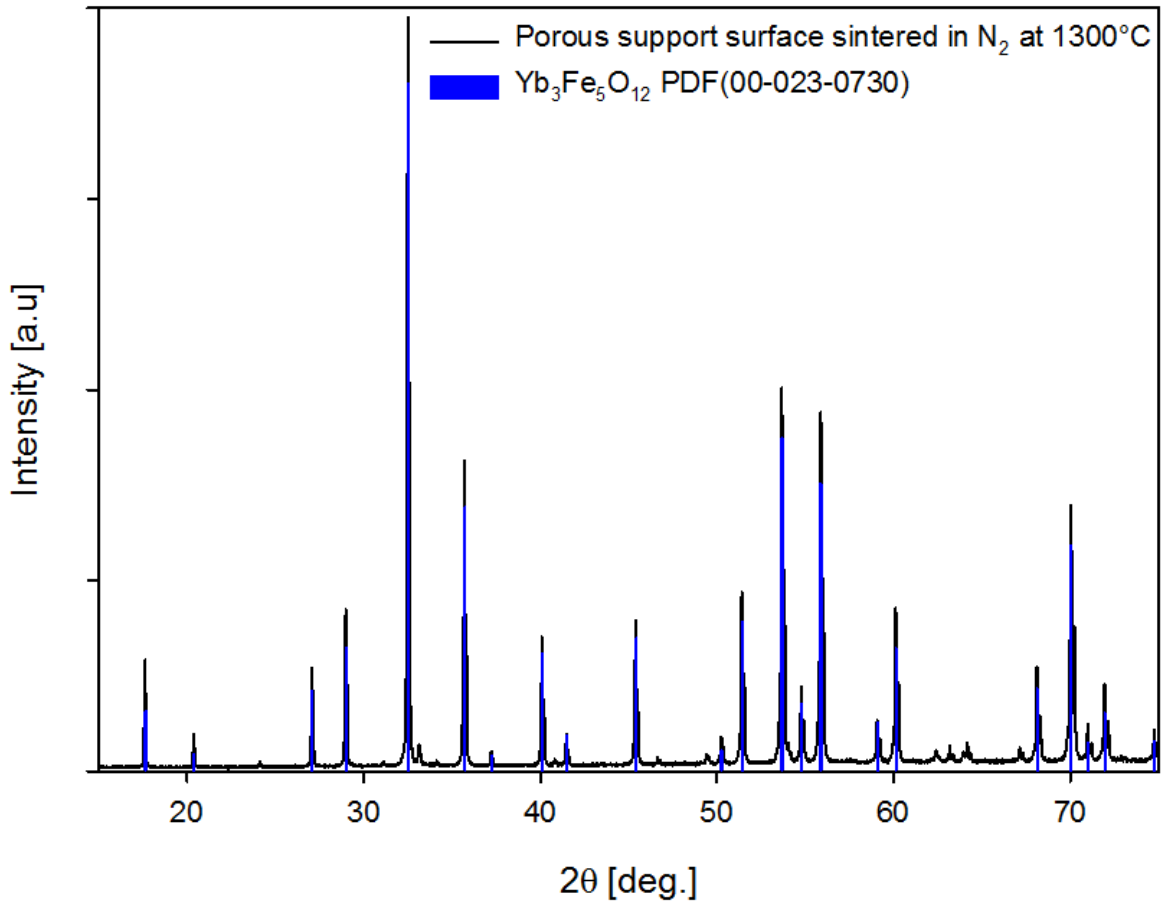

Figure 4.17: The XRD diffractogram obtained from sintering the porous support in N_2 atmosphere at 1300°C after heat treatment in air at 500°C in order to remove the charcoal activated added for preparation of a porous material. The XRD diffractogram obtained is matched with a DIFFRAC.EVA V3.0 pdf card (00-023-7030) for the $Yb_3Fe_5O_{12}$ phase.

5 Discussion

5.1 The preparation of $YbFe_2O_4$, and its potential for up-scale production

In the preparation of $YbFe_2O_4$, phase pure powder was obtained by annealing powder prepared by solid state synthesis at 1300°C in N_2 atmosphere as described in section 3.2.2. Although the preparation of phase pure powder was obtained following this route, the result proved difficult to reproduce. Phase pure powder was only obtained for powder prepared from three out of 20 pellets made from the same preparation route. For one of the 20 pellets, peritectic decomposition of the surface of the pellet was also observed. By studying the results reported in Figure 4.2 and 4.3, both an extensive mixing of the raw powders and a very precisely controlled partial pressure of oxygen is assumed to be necessary to obtain phase pure $YbFe_2O_4$ powder. The amount of secondary phase present was observed to increase when the volume of powder prepared in each batch increased, assumed to originate from the difficulty of obtaining sufficiently mixing of the powders as the volume increases. Differences between powders obtained from pellets prepared within the same batch, prepared in different heat treatments, were also observed to contain different amounts of secondary phase, indicating that phase pure powder is obtainable only if the partial pressure of oxygen is very precisely controlled in the process. The indication of the peritectic decomposition taking place when annealed at 1300°C in N_2 atmosphere also indicates that $YbFe_2O_4$ is accessable by this preparation route only within a narrow temperature and pressure regime, since the temperature required to reach the desired phase is on the borderline of the decomposition temperature of the material when it is heat treated in inert atmosphere.

The secondary phase present in the powders prepared from batch 3-6 from preparation route 2, was found to be $Yb_2Fe_3O_7$. This is consistent with the results obtained by Kimizuka et al.

[26, 27] as indicated in Table 2.3 where an $Yb_2Fe_3O_7$ phase was obtained when powders were prepared from Yb_2O_3 or Lu_2O_3 heat treated at 1200°C in different oxygen partial pressures. The $Yb_2Fe_3O_7$ secondary phase obtained, contains iron present both as Fe^{2+} and Fe^{3+} in contrast to the other stable phases, $LnFeO_3$ and $LnFeO_3$, given in the table, which only contains iron in the state of Fe^{3+}. A phase where iron is present both as Fe^{2+} and Fe^{3+} is expected to compete with the desired $YbFe_2O_4$ phase to a larger extent than phases that only contains iron present as Fe^{3+} if the oxygen partial pressure is not extremely precisely controlled. The presence of $Yb_2Fe_3O_7$ as the secondary phase in this preparation therefore enhances the theory predicted in terms of the oxygen partial pressure not being sufficiently controlled in the furnace during the annealing of the pellets. Since a stoichiometric amount of oxygen is present from start when the powder is prepared from preparation route 2, as indicated in equation 5.1, the larger amount of Fe^{3+} present in this compound is assumed to result from a reaction of the powder with oxygen in the atmosphere surrounding the pellet.

$$2FeO + Fe_2O_3 + R_2O_3 \rightarrow 2RFe_2O_4 \tag{5.1}$$

This means that for this preparation route to be upscalable, a better understanding of the exact temperature and flow rate of nitrogen should be investigated and obtained. If able to determine this precisely, the above mentioned preparation route would be preferable in comparison to earlier reported preparation routes [28, 29, 30, 31] both in terms of simplicity, environmental impact and safety. Solid state synthesis is a simple powder preparation route that involves mixing of oxides and heat treating them at high temperatures where the use of Fe powder and evacuated silica tubes are avoided. The use of nitrogen atmosphere is favored compared to a combination of CO_2/CO, both in terms of environmental impact and safety.

$YbFe_2O_4$ was also prepared from a sol-gel synthesis route by a modified pechini process as described in section 3.3.1. The powder obtained in this preparation route was found to be nearly phase pure when calcined at 900°C in N_2 atmosphere. In the preparation of this powder, a standardization of the precursor solutions was not performed, since the motivation was to do a quick test to investigate the possibility of preparing $YbFe_2O_4$ from a sol-gel synthesis route with a 1:1 ratio between Fe^{2+} and Fe^{2+}. Since almost completely phase pure powder was

obtained in this test, with Yb_2O_3 as the impurity, a sol-gel synthesis where a standardization of the precursors is performed, is expected to give a completely phase pure powder. In a standardization, the molality of the precursor solutions can be precisely controlled, and therefore also the Yb^{3+} to Fe^{3+} ratio obtained in the final product. The impurity observed at a 2θ angle of 44.65 could not be identified by the DIFFRAC.EVA V3.0 software, but is expected to originate from an impurity present in some of the equipment used in the preparation of the sol.

The preparation of powder from the sol-gel synthesis route was obtained by heat treatment in N_2 atmosphere at 900°C. This is consistent with a decrease in the calcination temperature of 400°C compared to the solid state synthesis route. This, in addition to the difficulty of reproducing the phase pure powder obtained by solid state synthesis, makes sol-gel synthesis the most promising preparation route in terms of both lab scale and large scale production of $YbFe_2O_4$, and possibly also for rare earth ferrites in general. If rare earth ferrites are to be used in large scale production of oxygen permeable membranes, both the preparation of the membrane material and the operating temperature of the membrane must be favorable both in terms of energy penalties and cost, and a decrease in the calcination temperature in the preparation of the material is therefore of great importance. The material cost is greatly decreased when going from $LuFe_2O_4$ to $YbFe_2O_4$, but the material cost of $YbFe_2O_4$ is still high. But a successful attempt of making $YbFe_2O_4$ from a sol-gel synthesis route, makes it interesting to study if the use of this preparation route can be used in the preparation of other rare earth ferrites that can be more cost-effective. One example is the preparation of YFe_2O_4.

The new and simpler powder preparation route obtained also increases the potential of these materials in terms of further investigation into other desirable properties. Some of the rare earth ferrites have been reported to be multiferroic, and the potential for the use of these materials in sensors and catalysts are therefore also improved by the new and more convenient powder preparation route, since the use of a glow box and evacuated silica tubes are avoided in the preparation of the raw powder.

Also in the the more practical aspect in terms of preparing an oxygen permeable membrane

prototype is the preparation of powder from a sol-gel synthesis necessary. In order to make an asymmetric membrane consistent of a porous support and a thin film, a powder consisting of small particles is necessary. The preparation of a thin film results in strict requirements in terms of thickness and density, and a powder containing small crystallite sizes is therefore necessary, and a sol-gel synthesis route is therefore required.

5.2 Successful reduction into desirable phase obtained by reduction in crystallite size

In the first attempt of preparing phase pure $YbFe_2O_4$ powder from the solid state synthesis route, the precursors were Yb_2O_3 and Fe_2O_3 as described in section 3.2.1, which means that only iron in the form of Fe^{3+} was present from start. In this attempt, the material was heated to 1400, 1450 and 1500°C in N_2 atmosphere where a decomposition of the material had taken place at 1500°C, while a combination of Fe_3O_4 and $YbFeO_3$ was found when a heat treatment at 1400 and 1450°C was performed. These results indicate that the atmosphere was not sufficiently reducing to obtain the desired phase containing a 1:1 ratio of Fe^{3+} and Fe^{2+} before a decomposition of the material took place. By the preparation of powder from synthesis route 2 on the other hand, containing the desired 1:1 ratio of Fe^{2+} and Fe^{3+} from start, phase pure material was prepared after heat treatment at 1300°C in N_2 atmosphere. This means that the stable phase of $YbFe_2O_4$ is obtainable at a lower temperature in N_2 atmosphere than what the results after heat treatment of powder prepared from solid state synthesis route 1 indicated. The reason for why a reduction into the desirable phase could not be obtained by heat treatment of powder prepared from preparation route 1 in N_2 atmosphere, may be caused by either the cationic diffusion in the material not being sufficiently rapid, or the transport of oxygen out of the material being too slow, or both. In accordance with equation 3.1, oxygen must be transported out of the oxide mixture in order to prepare the desired compound containing a 1:1 ratio of Fe^{3+} and Fe^{2+}. If the oxygen transport in the material is not sufficiently high, the material can obtain a phase that has an increased oxygen content and therefore stabilize in a local energy minima, hindering the more thermodynamically favored phase of being formed.

In the sol-gel synthesis route on the other hand, almost completely phase pure powder was obtained when the precursors were $Fe(NO_3)_3$ and $Yb(NO_3)_3$, and the raw powder obtained, calcined at 900°C. This indicates that by the use of a sol-gel synthesis route, the desired phase containing a 1:1 ratio of Fe^{3+} and Fe^{2+} can be obtained in inert atmosphere at 900°C even though the iron precursor consists of iron pressent only as Fe^{3+}. Preparation of $YbFe_2O_4$ by a sol-gel synthesis route is expected to occur at a lower temperature than by preparation from solid state synthesis, since the particles are mixed at the atomic level. This means that the particles obtained from a sol-gel synthesis route are smaller, and have a higher surface to bulk ratio than particles obtained in the solid state preparation route, as described in section 2.5. This increases the surface area of the particles and thereby also their surface free energy. This increases the reaction rate of these particles compared to the larger particles obtained in solid state synthesis, and a phase transition is therefore expected to take place at a lower temperature.

5.2.1 Possible improvement of the solid state preparation route

Improvement by pO_2 stabilization

In order to prepare phase pure $YbFe_2O_4$ powder from the solid state synthesis route described in section 3.2.2, a precisely controlled temperature and pO_2 regime is necessary. Since the pO_2 in the heat treatment process of preparing $YbFe_2O_4$ is expected to not be sufficiently controlled, phase pure powder was only obtained for three out of 20 pellets prepared. To improve the pO_2 control by the use of the equipment available in the lab, an oxygen getter could be utilized to decrease the partial pressure of oxygen in the heat treatment process of the pellets. The use of an oxygen getter has been reported by Karppinen et al [38], where FeO powder was used as an oxygen getter in the preparation of $BaYMn_2O_5$ from a solid state preparation route. An illustration of a possible way of decreasing the partial pressure of oxygen in the preparation of $YbFe_2O_4$ is given in Figure 5.1 where an Fe or FeO foil is proposed as a possible oxygen getter material. The idea of this setup is that the Fe or FeO foil is oxidized in the heat treatment process, decreasing the O_2 partial pressure in the environment surrounding the pellet. The sacrificial powder acts as an additional barrier, preventing the small amount of O_2 present in

reacting with the powder. To increase the pO_2 stabilization in the heat treatment process, the sacrificial powder could also be replaced by FeO or Fe powder surrounding the pellet.

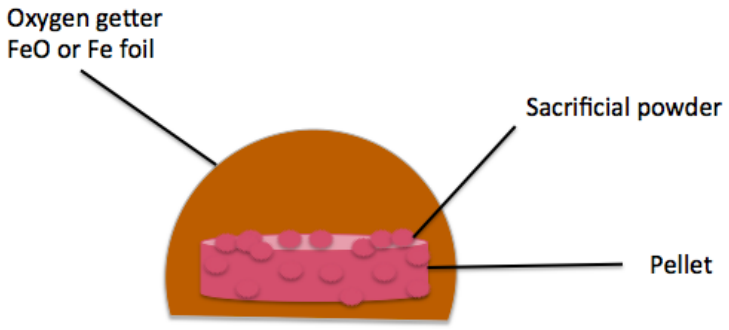

Figure 5.1: An illustration of how an oxygen getter can be used to decrease the partial pressure of oxygen during heat treatment in N_2 atmosphere of raw powder obtained by solid state synthesis.

Improvement by the use of ball milling in the mixing of precursor oxides

Another alternative for improvement of the solid state powder preparation route can be to use ball milling in the preparation of raw powder in order to improve the mixing of the different precursor oxides. The results given in Figure 4.2 indicates that the amount of secondary phase present increased when the volume of the batch increased, despite extensively grinding of raw powder performed in this study. Both cationic and oxygen diffusion appears to be slow in the $YbFe_2O_4$ preparation, and a thoroughly mixing of the precursor oxides, by the use of ball milling, is therefore expected to improve the solid state preparation route.

5.3 Sintering ability of $YbFe_2O_4$

In the results from the dilatometry measurement given in Figure 4.13 it is observed that an increase in volume takes place when the material is heated to approximately 750°C in N_2 atmosphere. At this temperature, the volume is observed to start to decrease, and a more typical sintering behavior is observed when a temperature of approximately 900°C is reached, where the volume decreases with a further increase in temperature. The material used in

the dilatometry measurement was not completely phase pure, and the material might therefor behave differently than if completely phase pure powder was used. In the measurement, the material was heated to 1250°C, not 1300°C, to ensure that the material did not decompose during the measurement, since a peritectic decomposition was observed for some of the pellets heated to 1300°C in N_2 atmosphere. The material is observed to have the steepest decrease in volume at 1250°C, the maximum temperature used in the measurement. A further increase in slope is expected when approaching 1300°C until a decomposition of the material takes place. A sintering temperature of 1275°C is therefore expected to be optimal to obtain a sufficient sintering of the material, while avoiding a decomposition of taking place when the material is sintered in an inert atmosphere. The average density of 71.2% of theoretical density for pellets heat treated at 1300°C for 12 hours is consistent with the dilatometry result, and indicates that the sintering of the material is relatively slow.

5.4 Structural changes upon heat treatment in different atmospheres

From the XRD diffractograms obtained after heat treatment of the as prepared powder from solid state synthesis in both oxidizing and reducing atmosphere, as indicated in Figure 4.5, a large change in structure is observed. By comparing these results to the XRD diffractograms reported for $LuFe_2O_4$ in Figure 2.10 and 2.11, a large similarity between the diffractograms is observed. Both the as prepared powder of $LuFe_2O_4$, indicated by phase M, and the oxygen rich powder indicated M', can be observed to be almost identical to the diffractograms obtained in this study for the as prepared powder of $YbFe_2O_4$, and the oxygen rich powder. For both materials, significant structural changes have taken place after heat treatment in oxygen atmosphere. The four most pronounced reflections in the 2θ range between 28 and 36 are drawn closer together, and in general there are fewer reflections present in the diffractogram obtained for the oxygen rich phase.

In the results obtained in this study, the diffractogram obtained after heat treatment in 10% H_2/Ar atmosphere during the ex. situ cycling is observed to have obtained some small struc-

tural changes compared to the as prepared powder. The intensities of the four most pronounced reflections are altered, and the intensities of the reflections are in general less pronounced for the reduced oxygen rich powder. These results are consistent with the results reported for $LuFe_2O_4$, where the diffractogram reported for the reduced phase is observed to be altered to some extent, mainly in terms of the four most pronounced reflections, after cycling of the material as can be seen in Figure 2.11. From the results obtained in the rietveld refinement of this powder, a preferred orientation for both the 110 and the 001 direction was found, indicating that the differences observed in the reduced powder may result from texture in the material caused by asymmetrical grains.

From the structure parameters obtained in the Rietveld refinement, it can also be seen that a large increase in the c-axis is observed after heat treatment of the as prepared powder from solid state synthesis at 500°C in O_2 atmosphere. The β angle is also observed to increase, from 103.4 for the as prepared powder to 124.5 for the oxygen rich powder, while the size of the a and b-axes remain relatively constant, although some outermost small differences can be observed in Figure 4.10(c) and 4.10(d). The change in volume observed after heat treatment in different atmospheres is observed to have a small increase after heat treatment in oxygen atmosphere, and the volume obtained after reduction in 10%H_2/Ar atmosphere is somewhat higher than the volume of the as prepared powder. These results are consistent with the results reported by Hervieu et al. [12] for $LuFe_2O_4$, where the c-axis was found to increase from 8.625Å to 10.29Å and the β angle from 103.2 to $\cong$ 125 after heat treatment in oxygen atmosphere, while the a and b axis were found to remain relatively unchanged after the oxidation. An explanation for why this change occurs is proposed in section 5.5.2.

5.5 Oxygen non-stoichiometry

5.5.1 Oxygen storage ability, $YbFe_2O_{4+\delta}$

The data obtained from the TGA measurements conducted in O_2 atmosphere for stoichiometric as prepared powder obtained by solid state synthesis and the oxygen rich phase obtained

after heat treatment i oxygen atmosphere, show that a huge mass gain takes place during heating of the as prepared powder in O_2 atmosphere, while the material remains stable during further heat treatments in the same atmosphere. The mass loss observed during the first heating of the oxygen rich powder, as shown in Figure 4.12, is assumed to result from evaporation of water or other impurities adsorbed to the crucible, and the oxygen rich powder therefore considered stable during the whole measurement. The increase in mass observed during the first heat treatment of the stoichiometric as prepared powder of $YbFe_2O_4$ is assumed to be caused by an increase in the oxygen content in the material, in consistence with equation 5.2, indicating the implementation of oxygen interstitials in the structure by the oxidation of Fe^{2+} into Fe^{3+}. In Figure 5.2(a), the increase in mass obtained during the first heating of the as prepared powder is calculated in terms of oxygen excess, δ. It can be seen that an increase in the oxygen content of $\delta \cong 0.5$ is obtained, resulting in an oxygen rich powder $YbFe_2O_{4.5}$ produced, indicating complete oxidation of iron in the material. These results show that the same oxygen storage ability is obtained for $YbFe_2O_4$ as the one reported for $LuFe_2O_4$ by Hervieu et al. [12], and reported in section 2.3. The p-type conductivity observed in Figure 5.2(b) also indicate the presence of oxygen interstitials in the material due to the increase in conductivity observed under oxidizing conditions, compared to inert atmosphere. The large change in structure observed after heat treatment in O_2 atmosphere indicates that a large structural change takes place, as indicated in Figure 5.2(c). This is also assumed to originate from oxygen interstitials being introduced into the structure.

$$\frac{1}{2}O_2 + 2Fe^{2+} \rightarrow O_i'' + 2Fe^{3+} \tag{5.2}$$

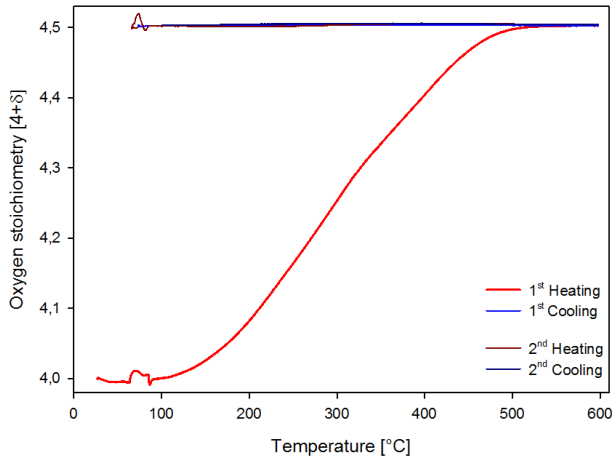

(a) TGA, Oxygen excess, δ

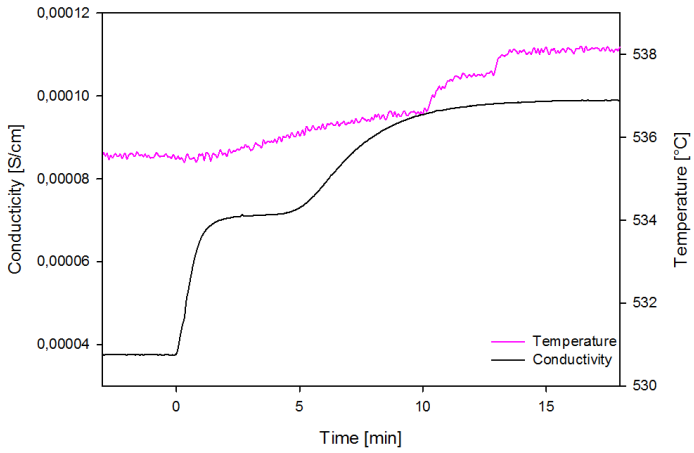

(b) Van der Pauw, Increased conductivity in O_2

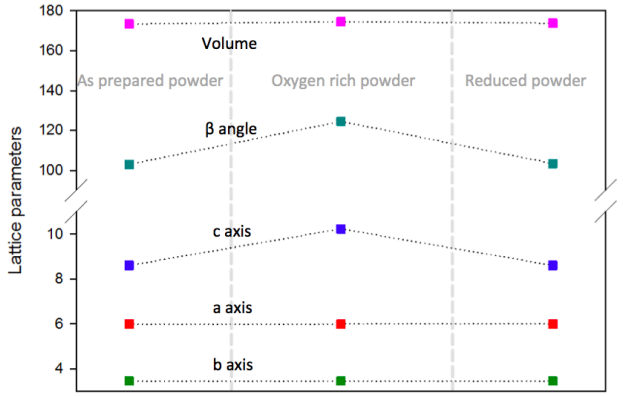

(c) Rietveld, Increase in c-axis and β in O_2

Figure 5.2: Three different results indicating the presence of oxygen interstitials being implemented in $YbFe_2O_4$ when the material is heat treated in O_2 atmosphere. (a) The increase in mass found from TGA when the material was heated in O_2 atmosphere, calculated in terms of oxygen excess, δ. (b) The increase in conductivity observed when changing from N_2 to O_2 atmosphere. (c) The large increase in the c axis parameter and β angle obtained from Rietveld refinement after heat treatment in O_2 atmosphere.

5.5.2 Possible position of an oxygen interstitial

The heat treatment of $YbFe_2O_4$ in oxygen atmosphere, is observed to increase the oxygen content in the material and result in an oxygen rich phase $YbFe_2O_{4.5}$ according to the results obtained from the TGA measurements displayed in Figure 5.2(a). The implementation of an oxygen interstitial is expected to alter the structure of the material significantly, in consistence with the results displayed in Figure 4.5, where a significant change in structure after heat treatment in oxygen atmosphere is observed. Where an oxygen interstitial is most likely to be positioned in the structure can not be predicted without performing DFT calculations gaining insight into where the unit cell obtains its energy minima when an oxygen interstitial is present in the structure. Despite this, there are some positions in the structure that are more probable than others. If an oxygen interstitial is to be implemented in the structure, the excess negative charge introduced must be compensated. This charge compensation is most likely to result from an oxidation of Fe^{2+} to Fe^{3+} assuming that a completely stoichiometric compound is present from start. The oxygen interstitial is also likely to go into a sterically favorable position in the structure where there is room for an excess oxygen atom. Considering these aspects, a possible position of the oxygen interstitial is given in Figure 5.3. The oxygen interstitial is indicated by the green atom. As can be seen in this figure, the postulated position is in the Fe layer. At the position indicated, the oxygen is in close vicinity to the iron atoms, while there is enough space around it to make it fit into the structure. By introducing the oxygen at this position, the iron atoms can bond to the oxygen interstitial, charge compensate it, and form FeO_6 octahedra instead of FeO_5 bipyramids. This will lead to a change in the crystal field splitting of the d-orbitals of iron in accordance with Figure 5.4. The oxidation of Fe^{2+} to Fe^{3+} changes the electronic configuration from d^6 to d^5, and the transition to FeO_6 octahedra from FeO_5 bipyramids will lower the total energy by lowering the energy of the d_{z^2} orbital.

A large oxygen increase at unusually low temperatures ranging from 200-400°C in $Dy_{1-x}Y_xMnO_{3+\delta}$ within the hexagonal $P6_3cm$ space group has been reported by Remsen et al. [9] and Abughayada et al. [10], indicating the presence of oxygen interstitials being implemented in the structure. Although these materials belong to a different crystal structure and an other space group

than $YbFe_2O_4$, some clear similarities between the two structures exists. They are both layered structures, and contain BO_5 trigonal bipyramids where B = Mn for $YMnO_3$ and Fe for $YbFe_2O_4$, and where B has the ability to obtain different valence states (Mn: Mn^{2+}, Mn^{3+}, Mn^{4+}, Fe: Fe^{2+}, Fe^{3+}). Preliminary studies performed within the ceramic research group at NTNU have indicated the presence of oxygen interstitials in the Mn layer of the $YMnO_3$ structure, and the possibility of obtaining oxygen interstitials at the same position, within the iron layers of $YbFe_2O_4$, might therefore also be present considering the above mentioned aspects.

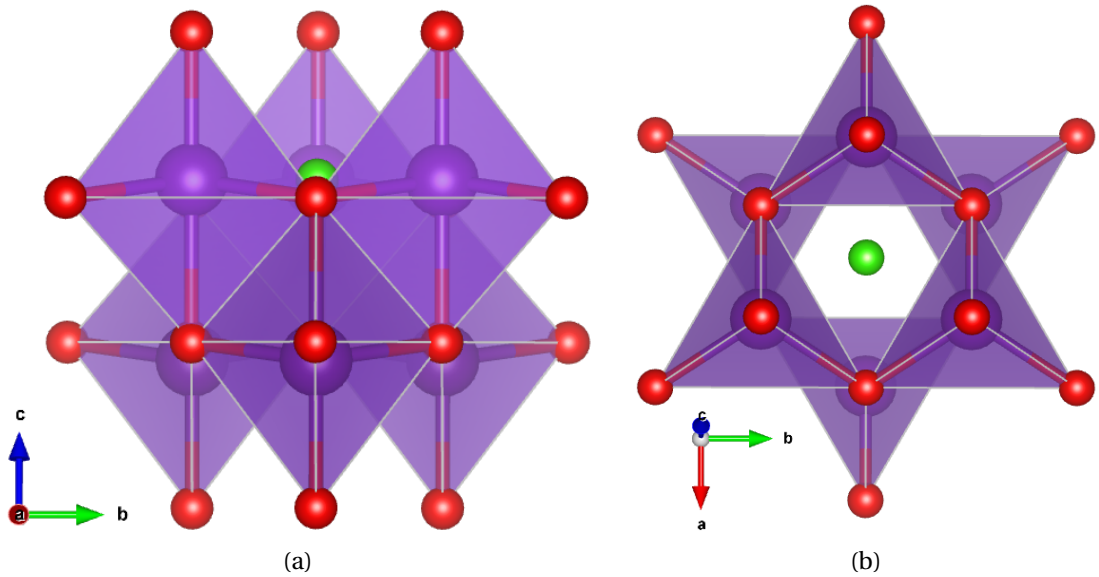

(a) (b)

Figure 5.3: A possible position for an oxygen interstitial in the $YbFe_2O_4$ material inside the $C2/m$ space group, where the oxygen is positioned inside one of the iron layers. The oxygen interstitial is indicated by the green atom, while the iron layer is given by the purple atoms. (a) The structure with the oxygen interstitial implemented, seen along the a axis, (b) the position indicated from a top view. [22].

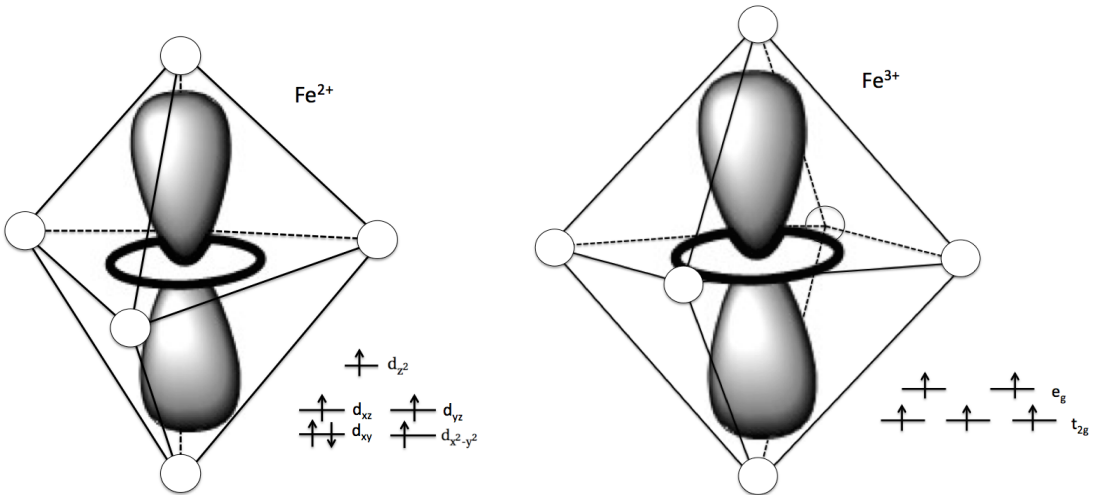

(a) (b)

Figure 5.4: A representation of the change in electronic configuration of iron when oxidized from Fe^{2+} to Fe^{3+}. By implementing an oxygen interstitial in the $YbFe_2O_4$ structure, iron can bond to the new oxygen becoming six coordinated instead of five coordinated. This is expected to result in an overall decrease in the energy of the system as the repulsion between the d_{z^2} orbital and the oxygen atoms positioned in the z-direction, is lowered.

The implementation of an oxygen interstitial at this position may also explain the increase in the c-axis and β angle observed after heat treatment of the material in O_2 atmosphere. In general, two competing interactions are expected when an oxygen interstitial is introduced at this position. The first is the reduction in ionic radii of iron when an oxygen interstitial is introduced in the structure which, intuitively is expected to result in a contraction of the structure because the ionic radii of iron will decrease when an oxidation from Fe^{2+} to Fe^{3+} occurs. The other interaction expected to influence the structure is the electrostatic repulsion between the oxygen interstitial introduced, and the other oxygen atoms in the structure. Of these two interactions, the electrostatic repulsion is expected to be the dominating one when an excess oxygen ion is introduced carrying a net negative charge. By looking at the structure, the ab-plane seem more rigid than the c-direction, because there are more atoms positioned in close vicinity to each other. The charge compensating ions are also positioned in this plane, and expected to remain in close vicinity to the interstitial oxygen, and may thereby hinder an expansion in the ab-plane. An elongation in the c-direction, where other oxygen atoms are positioned closer to the interstitial than the positive Yb ions, might therefore release some of the negative repulsion obtained inside the unit cell. The increase in the β-angle, as dis-

played in Figure 5.5, is also assumed to result from the electrostatic repulsion, trying to push the oxygen layers further apart. The small increase in volume observed after heat treatment in O_2 atmosphere might therefore originate from the increase in the c-direction and β angle caused by the electrostatic repulsion, while the a and b lattice parameters remain almost unchanged. A representation of the change in c-axis and β-angle observed after oxidation of the as prepared powder is given in Figure 5.5 where the structure prior to the oxidation is shown in Figure 5.5(a), while the oxygen rich structure with an excess oxygen atom present is given in Figure 5.5(b).

An understanding of how the formation of oxygen vacancies and transport of these through a material influences the structure, has in resent years been explored due to an increased interest for use of many of these materials in oxygen permeable membranes. As reported in section 2.1, the chemical expansion in $La_{1-x}Sr_xMnO_{3+\delta}$, reported by Grande et al. [18] was found to be larger when the material was heat treated in N_2 than O_2 atmosphere assuming to originate from the creation of oxygen vacancies. An investigation of how oxygen interstitials influences a structure has not been investigated to the same extent, since the interest in materials that can transport oxygen through oxygen interstitials instead of vacancies has emerged just recently. The understanding of how the materials behave under these conditions is complex, and more research into this field is therefore required.

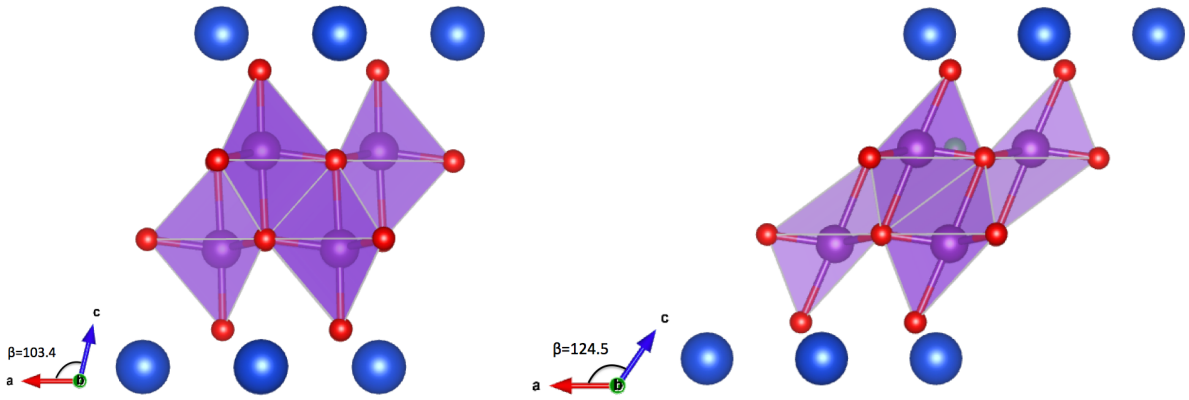

(a) Stoichiometric stucture

(b) Oxygen rich structure

Figure 5.5: A representation of the change in structure after heat treatment of the as prepared powder obtained from solid state synthesis, in oxygen atmosphere. An elongation of the c-axis and an increase in the β angle is observed. This is expected to originate from an oxygen interstitial being implemented in the structure. (a) A representation of the stoichiometric structure prior to the heat treatment. (b) The structure after heat treatment in oxygen atmosphere where an oxygen interstitial is implemented in the structure, indicated by the green atom seen in the background. [22]

5.5.3 Potential cycling ability, $YbFe_2O_{4\pm\delta}$

The results given in Figure 4.5 indicates, in addition to a significant structural change when the material is heat treated in different atmospheres, also a cycling ability of the material. A transition into an oxygen rich phase takes place when the material is heated in oxygen atmosphere, while a reduction back to the original stoichiometric structure follows when the material is heated in a 10 %H_2/Ar atmosphere. These results are also consistent with the results reported by Hervieu et al. [12]. As can be seen in Figure 2.9(b), a cycling ability is reported and quantified in five cycles for $LuFe_2O_4$. Since the experiment reported for $YbFe_2O_4$ was done ex. situ, a quantification of the oxygen storage and release was not obtained, but a combination of the XRD results and the TGA data combined, indicate a possible cycling ability also for $YbFe_2O_4$.

5.6 P-type conductivity

The results obtained in the conductivity measurement with changes in atmosphere given in Figure 4.15 and Figure 4.16 show a clear decrease in the conductivity of the material when changing from O_2 to N_2 atmosphere, and a clear increase in conductivity when changing from N_2 to O_2 atmosphere. Both the reduction and the increase in conductivity is seen to go through a plateau in the middle of the process as can be seen in Figure 4.16 (a) and (b). A decrease in temperature is observed during the decrease in conductivity when changing from oxygen to nitrogen atmosphere. This is assumed to be caused by the reduction of the material taking place when nitrogen is introduced into the chamber. A reduction is an endoderm reaction, and is therefore assumed to cause the observed decrease in temperature when changing from oxygen to nitrogen atmosphere. The same reasoning is used to explain the increase in temperature taking place when oxygen is introduced into the chamber when switching from N_2 to O_2 atmosphere. An oxidation of the material takes place when oxygen enters the chamber. The oxidation is an exothermic reaction expected to cause an increase in temperature as observed in Figure 4.16(b).

Due to the instabilities observed during the measurements, as reported in Figure B.1, the results obtained from the conductivity measurement can not be interpreted quantitatively. But a qualitative investigation of the conductivity can be performed. The data given in Figure 4.16 clearly indicates that the material is a p-type conductor. The conductivity decreases rapidly when a change in atmosphere from oxygen to nitrogen is performed, and increases rapidly again when the atmosphere is changed back to oxygen. The reduction and oxidation of the material is observed to happened fast, during a time span of approximately ten minutes for each of the processes. A p-type conductivity in the material was expected due to the increase in oxygen content observed during the TGA measurement and the large change in structure observed after heat treatment of the stoichiometric solid state synthesis powder in oxygen atmosphere. The p-type conductivity is assumed to originate from the implementation of oxygen interstitials in the material by oxidation of the Fe^{2+} ions into Fe^{3+} in accordance with equation 5.3, where the creation of an Fe^{3+} can be represented as an Fe^{2+} plus a hole in accordance with equation 5.4.

$$\frac{O_2}{2} + 2Fe^{x}_{Fe^{2+}} \rightarrow O_i^{"} + 2Fe^{\bullet}_{Fe^{2+}} \tag{5.3}$$

$$Fe^{\bullet}_{Fe^{2+}} \rightarrow Fe^{x}_{Fe^{2+}} + h^{\bullet} \tag{5.4}$$

5.7 Preparation of porous support

In the preparation of a porous support, as reported in section 3.4, the 30mm pellets obtained were heat treated in air and later sintered in N_2 atmosphere. The structure obtained after sintering in N_2 atmosphere was found to be $Yb_3Fe_5O_{12}$ as reported in Figure 4.17. Preparation of the desired $YbFe_2O_4$ phase was not obtained. In order to obtain the $YbFe_2O_4$ phase after the first heat treatment in air, a plateau should be added in the sintering process of the material in N_2 atmosphere. When the supports are heat treated in air, the oxygen rich structure $Yb_2Fe_4O_9$ is expected to form although this could not be investigated due to the porous support still being a green body and not sufficiently strong for an investigation by XRD. A plateau imple-

mented at 500°C with a holding time of 5 hours might be sufficient to reduce the material back to the original structure before the sintering of the material is performed. If this reduction can not be performed under inert conditions, a second step should be implemented in the heat treatment process, where the material is heat treated in a H_2/Ar atmosphere after the heat treatment performed in air, where the material is held at 500°C in H_2/Ar atmosphere until the original stoichiometric sample is obtained. A subsequent sintering in N_2 atmosphere should then result in a porous support containing the desired $YbFe_2O_4$ phase.

5.8 Future prospects for $YbFe_2O_4$, and rare earth ferrites in general

The new and simpler powder preparation routes presented in this study, significantly increases the potential for the use of $YbFe_2O_4$, and possibly also rare earth ferrites in general, in a further study into preferable properties. This include studies with respect to oxygen storage ability and the use of these materials in oxygen permeable membranes, and for a further investigation into the reported multiferroic properties of these materials and the potential for use in sensors and catalysts.

The combination of an oxygen increase taking place at a relatively low temperature, and a cycling ability observed when the material is heat treated under different atmospheres makes $YbFe_2O_4$ promising in terms of oxygen separation by the use of oxygen permeable membranes. The possibility of this material to transport oxygen at 500°C may improve many of the major challenges associated with high temperature performance of these membranes as indicated in Figure 2.3 and discussed in section 2.1 including high temperature sealing, cationic demixing and thermal expansion. But although these results are promising, there are still many material properties that need to be investigated before a conclusion of the potential of $YbFe_2O_4$ in terms of oxygen separation can be made.

5.8.1 Further optimization of the synthesis route for preparation of powder with enhanced properties

Two possible ways of improving the solid state powder preparation route has been discussed previously. As a continuation of the work presented in this study, attempts of preparing completely phase pure powder of $YbFe_2O_4$ by implementing a standardization step of the precursors in the sol-gel preparation route, should be performed. In order to investigate in what temperature range the $YbFe_2O_4$ phase is stable, the raw powder prepared in the sol-gel preparation route should be heat treated at different temperatures. This may reveal the maximum and minimum temperature for preparation of completely phase pure powder of $YbFe_2O_4$. Heat treatment of raw powder at different temperatures should also be performed in order to obtain both bulk and nanocrystalline powders to study if the different crystallite sizes influences the properties of the material. An increase in the sintering ability of the material is expected if the crystallite size is decreased since small crystallites have a higher surface to volume ratio and therefore are more reactive, and the low sintering ability observed in the dilatometry measurement in this study, may therefore be significantly improved. An investigation of the possibility of preparing YFe_2O_4 should also be performed. YFe_2O_4 was not obtained when a solid state synthesis route of the material was tested in this study, but the preparation of $YbFe_2O_4$ from a sol-gel synthesis route opens the possibility for preparation of other rare earth ferrites from the same preparation route. A replacement of Yb with Y in this compound would significantly increase the potential for up scale production of the material due to the decrease in the material cost of Y compared to Yb.

5.8.2 Quantification of oxygen storage and release during cycling

In order to obtain a better insight into the oxygen storage ability of $YbFe_2O_4$, a quantification of the oxygen increase and decrease in the material during cycling should be performed by in situ TGA. This can be performed by heating as prepared powder to 500°C in oxygen atmosphere, and switching to reducing atmosphere while keeping the temperature at 500°C. TGA should also be performed on both bulk and nanocrystalline powder to investigate how the different crystallite sizes influences both the oxygen storage ability of the material, and how

fast the oxygen increase and decrease takes place in the different materials.

5.8.3 Enhanced understanding of the conductivity of $YbFe_2O_4$

The results obtain in this study concerning the conductivity of $YbFe_2O_4$ was influenced by the heavy noise obtained in the data output from the van der Pauw measurement. In the continuation of this work, the conductivity of $YbFe_2O_4$ should therefore be studied in more detail, and a quantification of the conductivity obtained. Since contact problems were a reoccurring issue in the van der Pauw measurement, a preferable alternative can be to perform the conductivity measurement with another setup, for example a four point measurement which can hopefully improve the signal and result in less noise in the data. Measurements where heating and cooling in both N_2 and O_2 atmosphere of the material should also be performed, as well as alternating changes between H_2 and O_2 atmosphere at elevated temperatures.

5.8.4 Oxygen permeable membrane prototype

In order to investigate the potential of $YbFe_2O_4$ for use in oxygen permeable membranes, an asymmetric membrane should be prepared, and permeation measurements of the oxygen transport ability of this membrane performed. The asymmetric membrane should be made from the preparation of a porous support and a thin film, where either dip coating or spray coating is used in the preparation, in accordance with the methods described by Gurauskis et al. [39] and Lein et al. [40], respectively. The stability of the membrane in terms of chemical and thermal stability as well as cationic demixing and mechanical strength should also be investigated.

5.8.5 Possible position of oxygen interstitial

In order to investigate where in the $YbFe_2O_{4+\delta}$ structure an oxygen interstitial is most likely to be positioned, DFT calculation should be performed. The most preferable position in terms of electrostatics can be obtained in this calculation, and thereby a better understanding of the changes in the ionic and electronic structure that results after heat treatment of the as prepared powder in oxygen atmosphere.

6 Conclusion

In this study, phase pure powder of the rare earth ferrite, $YbFe_2O_4$, has been prepared from a conventional solid state synthesis route by the use of Yb_2O_3, Fe_2O_3 and FeO as precursor powders, and the raw powder obtained, annealed at 1300°C in N_2 atmosphere. Strong indications of the possibility of obtaining the same material from a sol-gel synthesis route by the use of a modified Pechini process is also reported, where the precursors were $Yb(NO_3)_3$ and $Fe(NO_3)_3$, and the raw powder obtained, annealed in N_2 atmosphere at 900°C.

Heat treatment of as prepared powder obtained from solid state synthesis in oxygen atmosphere resulting in an oxygen rich phase, $YbFe_2O_{4.5}$, was quantified from in situ TGA measurements, while an ex. situ heat treatment performed under oxidizing and reducing conditions strongly indicates a good cycling ability of the material. A huge change in structure was observed when the material was heated to 500°C in oxygen atmosphere, and the original stoichiometric sample retained after a subsequent heat treatment at 500°C in 10%H_2/Ar atmosphere. A significant change in the c-axis and β angle of the structure related to excess oxygen was observed by an investigation of the different structure parameters by Rietveld refinement, while the a and b-axes and the unit cell volume was found to remain relatively constant. A clear indication of a p-type conductivity of the material was found in a conductivity measurement performed by a van der Pauw setup.

The sintering ability of the material was found to be relatively poor from the results obtained in the dilatometry measurement, and a density of 72.1 % of theoretical density was found for pellets annealed at 1300°C for 12 hours in N_2 atmosphere. The reported potential of preparing phase pure $YbFe_2O_4$ from a sol-gel synthesis route, introduces the possibility of preparing powder containing smaller crystallite sizes which is likely to increase the sintering ability of these materials. The increase is expected to be caused by the increased surface potential of these particles, originating from the decrease in crystallite size that can be obtained from the sol-gel preparation route.

Bibliography

[1] A. C. Bose. *Inorganic Membranes for Energy and Environmental Applications*. Springer-Verlag New York, 2009.

[2] S. M. Hashim, A. R. Mohamed, and S. Bhatia. Current status of ceramic-based membranes for oxygen separation from air. *Adv. Colloid Interface Sci.*, 160(1-2):88–100, 2010.

[3] P. V. Hendriksen, P. H. Larsen, M. Mogensen, F. W. Poulsen, and K. Wiik. Prospects and problems of dense oxygen permeable membranes. *Catal. Today*, 56(1-3):283–295, 2000.

[4] X. Dong, W. Jin, N. Xu, and K. Li. Dense ceramic catalytic membranes and membrane reactors for energy and environmental applications. *Chem. Commun.*, 47(39):10886–10902, 2011.

[5] V. L. Kozhevnikov, I. A. Leonidov, and M. V. Patrakeev. Ceramic membranes with mixed conductivity and their application. *Rus. Chem. Rev.*, 82(8):772–782, 2013.

[6] J. Sunarso, S. Baumann, J. M. Serra, W. A. Meulenberg, S. Liu, Y. S. Lin, and J. C. D. da Costa. Mixed ionic-electronic conducting (MIEC) ceramic-based membranes for oxygen separation. *J. Membr. Sci.*, 320(1-2):13–41, 2008.

[7] H. L. Lein, K. Wiik, and T. Grande. Thermal and chemical expansion of mixed conducting $La_{0.5}Sr_{0.5}Fe_{1-x}Co_xo_{3-\delta}$ materials. *Solid State Ionics*, 177(19-25):1795–1798, 2006.

[8] Hermann Schmalzried. *Chemical kinetics of solids*. VCH, Weinheim.

[9] S. Remsen and B. Dabrowski. Synthesis and Oxygen Storage Capacities of Hexagonal $Dy_{1-x}Y_xMnO_{3+\delta}$. *Chem. Mater.*, 23(17):3818–3827, 2011.

[10] C. Abughayada, B. Dabrowski, M. Avdeev, S. Kolesnik, S. Remsen, and O. Chmaissem. Structural, magnetic, and oxygen storage properties of hexagonal $Dy_{1-x}Y_xMnO_{3+\delta}$. *J. Solid State Chem.*, (0).

[11] S. M. Selbach, A. N. Lovik, K. Bergum, J. R. Tolchard, M. Einarsrud, and T. Grande. Crystal structure, chemical expansion and phase stability of $HoMnO_3$ at high temperature. *J. Solid State Chem.*, 196:528–535, 2012.

[12] M. Hervieu, A. Guesdon, J. Bourgeois, E. Elkaim, M. Poienar, F. Damay, J. Rouquette, A. Maignan, and C. Martin. Oxygen storage capacity and structural flexibility of $LuFe_2O_{4+x}$ ($0 \leq x \leq 0.5$). *Nature Mater.*, 13(1):74–80, 2014.

[13] R. D. Shannon. Revised effective ionic-radii and systematic studies of interatomic distances in halides and chalcogenides. *Acta Crystallogr. Sect. A*, 32(SEP1):751–767, 1976.

[14] V. Sadykov, V. Zarubina, S. Pavlova, T. Krieger, G. Alikina, A. Lukashevich, V. Muzykantov, E. Sadovskaya, N. Mezentseva, E. Zevak, V. Belyaev, and O. Smorygo. Design of asymmetric multilayer membranes based on mixed ionic-electronic conducting composites supported on Ni-Al foam substrate. *Catal. Today*, 156(3-4):173–180, 2010.

[15] F. Liang, H. Jiang, H. Luo, R. Kriegel, and J. Caro. High-purity oxygen production by a dead-end $Ba_{0.5}Sr_{0.5}Co_{0.8}Fe_{0.2}O_{3-\delta}$ tube membrane. *Catal. Today*, 193(1):95–100, 2012.

[16] S. B. Adler. Chemical expansivity of electrochemical ceramics. *J. Am. Ceram. Soc.*, 84(9):2117–2119, 2001.

[17] H. L. Lein. *Mechanical Properties and Phase Stability of Oxygen Permeable Membranes $La_{0.5}Sr_{0.5}Fe_{1-x}Co_xO_{3-\delta}$*. PhD thesis, Norwegian University of Science and Technology, Department of Materials Technology, 2005.

[18] T. Grande, J. R. Tolchard, and S. M. Selbach. Anisotropic Thermal and Chemical Expansion in Sr-Substituted $LaMnO_{3+\delta}$: Implications for Chemical Strain Relaxation. *Chem. Mater.*, 24(2):338–345, 2012.

[19] N. Ikeda, H. Ohsumi, K. Ohwada, K. Ishii, T. Inami, K. Kakurai, Y. Murakami, K. Yoshii, S. Mori, Y. Horibe, and H. Kito. Ferroelectricity from iron valence ordering in the charge-frustrated system $LuFe_2O_4$. *Nature*, 436(7054):1136–1138, 2005.

[20] Y. Horibe, N. Ikeda, K. Yoshii, and S. Mori. Direct observation of low-temperature superstructure in spin-and charge-frustrated ferrite $YFe_2O_{4-\delta}$. *Phys. Rev. B*, 82(18), 2010.

[21] M. Isobe, N. Kimizuka, J. Iida, and S. Takekawa. Structures of $LuFeCoO_4$ and $LuFe_2O_4$. *Acta Crystallogr. Sect. C*, 46:1917–1918, 1990.

[22] F. Izumi K. Momma. *J. Appl. Crystallogr.*, (41), 2008.

[23] J. Bourgeois. *Les ferrites du type RFe_2O_4 à valence mixte*. PhD thesis, Universite de Caen, 2012.

[24] S. Stølen and T. Grande. *Chemical thermodynamics of materials: macroscopic and microscopic aspects*. Wiley, Chichester, 2004.

[25] A. Muan and E. Osborn. *Phase equilibria among oxides in steelmaking*. Addison-Wesley, Reading, Mass., 1965.

[26] N. Kimizuka, A. Takenaka, Y. Sasada, and T. Katsura. Series of new compounds $A^{3+}Fe_2O_4$ (A=Ho, Er, Tm, Yb, and Lu). *Solid State Commun.*, 15(8):1321–1323, 1974.

[27] N. Kimizuka and T. Katsura. Standard free-energy of formation of $YbFe_2O_4$, $Yb_2Fe_3O_7$, $YbFeO_3$, and $Yb_3Fe_5O_{12}$ at 1200 °c. *J. Solid State Chem.*, 15(2):151–157, 1975.

[28] Y. Qin, X. Q. Liu, Y. J. Wu, and X. M. Chen. Preparation, Dielectric, and Magnetic Characteristics of $LuFe_2O_4$ Ceramics. *J. Am. Ceram Soc.*, 96(8):2506–2509, 2013.

[29] D. S. F. Viana, D. Garcia, Jose A. Eiras, M. Olzon-Dionysio, S. D. Souza, D. Z. Montanher, L. F. Cotica, I. A. Santos, A. A. Coelho, and R. A. M. Gotardo. Magnetic states and valence fluctuations in charge frustrated polycrystalline lutetium ferrite samples. *Scripta Mater.*, 69(9):670–673, 2013.

[30] T. Maruyama, Y. Murakami, D. Shindo, N. Abe, and T. Arima. Observations of charge-ordered and magnetic domains in $LuFe_2O_4$ using transmission electron microscopy. *Phys. Rev. B*, 86(5), 2012.

[31] A. Ruff, S. Krohns, F. Schrettle, V. Tsurkan, P. Lunkenheimer, and A. Loidl. Absence of polar order in $LuFe_2O_4$. *Eur. Phys. J. B*, 85(8), 2012.

[32] A. R. West. *Basic solid state chemistry*. Wiley, Chichester, 1999. 2nd ed.

[33] Y. Qin, X. M. Chen, and X. Q. Liu. Dielectric, Ferroelectric, and Magnetic Characteristics of $LuFeCuO_4$ ceramics. *J. Am. Ceram. Soc.*, 95(3):977–981, 2012.

[34] M. Nespolo, M. Isobe, J. Iida, and N. Kimizuka. Crystal structure and charge distribution of $YbFeMnO_4$. *Acta Crystallogr. Sect. B*, 56:805–810, 2000.

[35] L. Smart and E. Moore. *Solid state chemistry: an introduction.* CRC Press, Boca Raton, Fla., 2012. 4th ed.

[36] D. W. Richerson. *Modern ceramic engineering: properties, processing, and use in design.* CRC Press, 2006.

[37] T. Schleid and G. Meyer. Single-crystals of rare-earth oxides from reducing halide melts. *J. Less Common Met.*, 149(1-2):73–80, 1989.

[38] M. Karppinen, H. Okamoto, H. Fjellvag, T. Motohashi, and H. Yamauchi. Oxygen and cation ordered perovskite, $Ba_2Y_2Mn_4O_{11}$. *J. Solid State Chem.*, 177(6):2122–2128, 2004.

[39] J. Gurauskis, O. F. Lohne, H. L. Lein, and K. Wiik. Processing of thin film ceramic membranes for oxygen separation. *J. Eur. Ceram. Soc.*, 32(3):649–655, 2012.

[40] H. L. Lein, T. Tezuka, T. Grande, and M. Einarsrud. Asymmetric proton conducting oxide membranes and fuel cells prepared by aqueous tape casting. *Solid State Ionics*, 179(21-26):1146–1150, 2008.

A Powder preparation

A.1 The attempt of preparing YFe_2O_4 and $ScFe_2O_4$ from solid state synthesis

A.1.1 Preparation of YFe_2O_4

In preparation route 1, the raw powder obtained was heated to three different temperatures as indicated in Figure 3.3. For YFe_2O_4, the raw powder decomposed when it was heated to 1500°C, while the XRD diffractogram obtained for heat treatment at 1450 was found to have obtained a structure consistent of $YFeO_3$, $Y_3Fe_5O_{12}$ and Fe_3O_4, by comparison to the DIFFRAC.EVA V3.0 PDF cards (04-010-6423), (04-009-8391) and (04-007-2412), respectively, indicating that the conditions were not reducing enough to obtain a 1:1 ratio of Fe^{2+} : Fe^{3+}. When the material was heated in both 3%H_2/Ar and 5%H_2/Ar atmosphere, the XRD diffractogram was found to contain metallic iron, indicating too reducing conditions. When the powder obtained from route 2 was heat treated in N_2 atmosphere at 1275 and 1300 °C, the material decomposed, while heat treatment at 100 °C resulted in a structure consistent of $YFeO_3$ and only small traces of YFe_2O_4. The diffractograms were compared with the PDF cards (04-010-6423) and (01-079-2435), respectively.

A.1.2 Preparation of $ScFe_2O_4$

The attempt of making $ScFe_2O_4$ from the two different preparation routes proved difficult. None of the heat treatments of the powders obtained from either of the two preparation routes resulted in a diffractogram that indicated traces of obtaining the right structure.

B Conductivity by van der Pauw

B.1 Conductivity

An overview of the results obtained in the conductivity measurement performed with a van der Pauw setup with changes in O_2 and N_2 atmosphere, as described in section 3.7, is given in Figure B.1. The data obtained can be observed to contain heavy noise during different stages of the measurement. The noise is expected to result from contact problems between the pellet and the four platinum electrodes, as displayed in Figure 3.12.

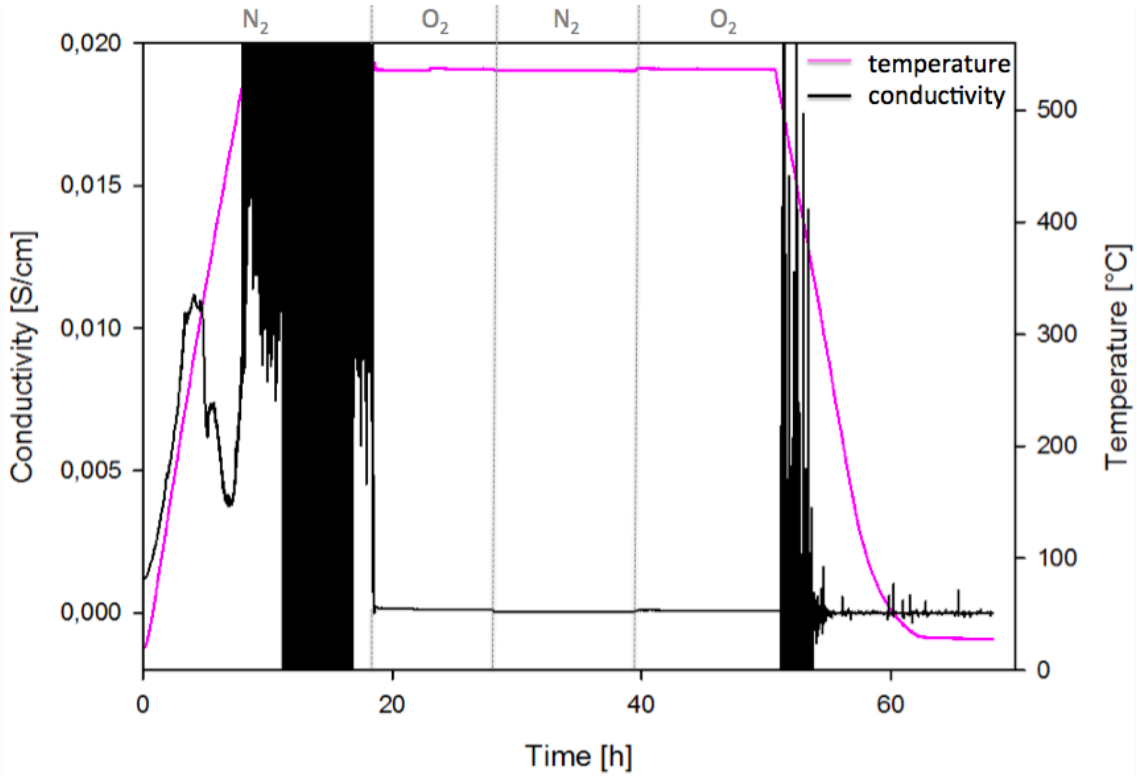

Figure B.1: An overview of the total data response obtained during the conductivity measurement performed in alternating N_2 and O_2 atmosphere with a van der pauw setup. The measurement was influenced by heavy noise.

C Dilatometry

The phase purity of the powder used in the dilatometry measurement with a secondary phase present is given in Figure C.1. The secondary phase was observed to be $Yb_2Fe_3O_7$ from the DIFFRAC.EVA V3.0 software.

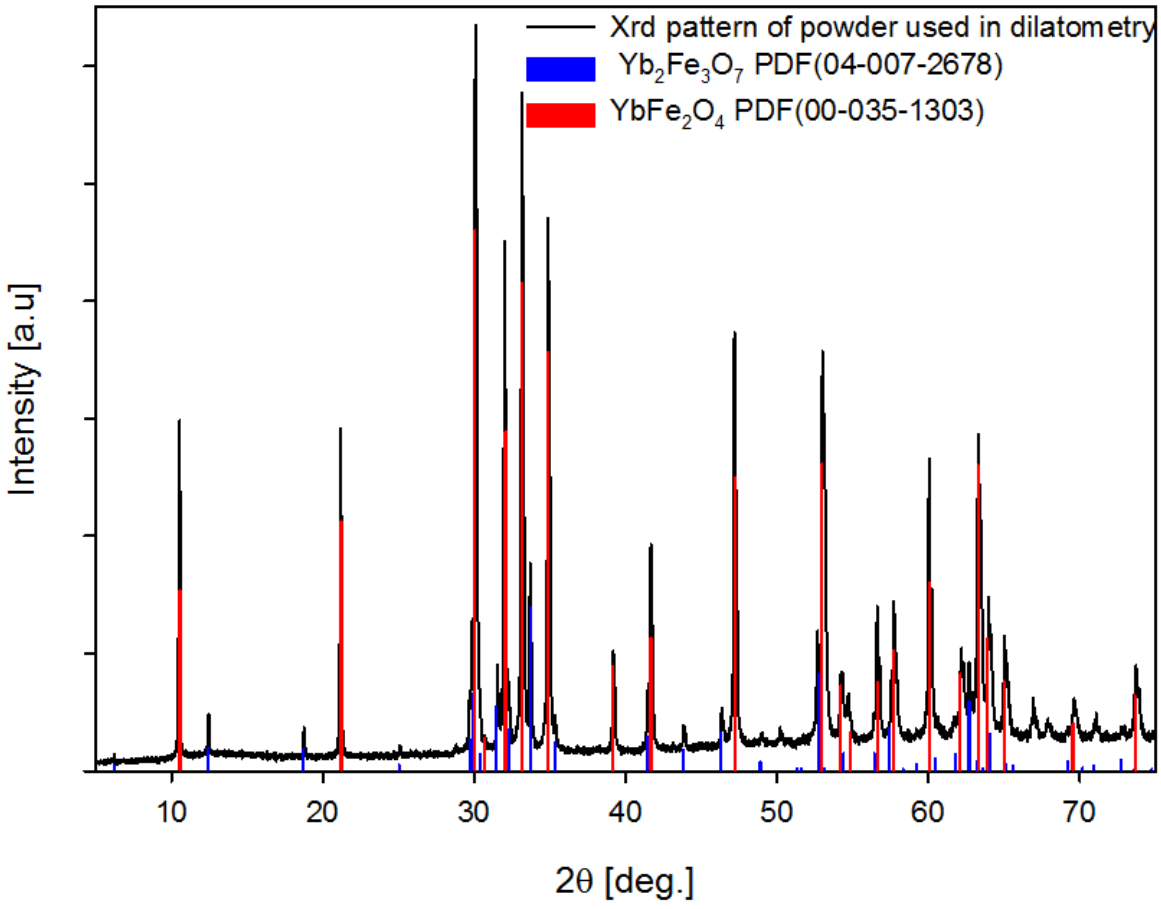

Figure C.1: The phase purity of the $YbFe_2O_4$ powder prepared from solid state synthesis used in the dilatometry experiment, with a secondary phase of $Yb_2Fe_3O_7$ present.